FOOTWEAR AND SOFT GROUND INTERACTION

Rachael Pisani

Research Institute of Advanced Engineering
School of Aeronautical, Mechanical and Civil Engineering
University of Salford
Salford
UK

Submitted for Degree of Doctor of Philosophy
April 2002

Table of Contents

List of Figures

List of Tables

Acknowledgements

I am very grateful to David Howard, who as my supervisor at Salford University provided invaluable help and support throughout the study of many new topics unfamiliar to us both. His reviews and useful comments have helped to shape the thesis. I would like to thank Phil Walker for his assistance in constructing the slip-rig.

I am also grateful to DCTA who funded the research in conjunction with EPSERC. DCTA provided much support, particularly during the early stages of the research and have continued to support the project by continuing to fund further research in this area.

I would also like to thank Phil, who has continued to encourage and support me even though he has been somewhat neglected whilst I have spent so much time writing this thesis.

Notation List

b	Width of cleat or wheel
B	Width of footing; modulus of deformation
b_1	Width of top of cleat
b_2	Width of top of gap between cleats
b_3	Width of bottom of cleat
b_4 , x	Width of bottom of gap between cleats
b_a	Width of top of gap between cleats in active zone
b_p	Width of top of gap between cleats in passive zone
b_{xa}	Width of bottom of gap between cleats in active zone
b_{xp}	Width of bottom of gap between cleats in passive zone
C_c , C_{c1} , C_{c2}	Adhesive shear force
c_c	Adhesive shear stress between retaining wall or cleat surface and soil
C_{cf} , C_{cr}	Adhesive shear force
C_s	Cohesive shear force
c_s	Cohesive shear stress between soil particles
C_{sa}	Active zone cohesive shear force
C_{sp}	Passive zone cohesive shear force
d	Standard unit of length (45mm)
F_b	Applied vertical force due to body weight
F_{ba}	Applied vertical force to active zone
F_{bp}	Applied vertical force to passive zone
$f_t, f_e, f_H, f_T f_{b,,}$	Degrees of freedom
$F_t, F_e, F_H, F_T,$	Variance ratio
h	Height of cleat
H, h	Height of retaining wall or cleat
H_1, H_2	Height of quadrilateral zone sides
k	Coefficient of proportionality
K_a , K_{ac}	Coefficient of active earth pressure
k_c, k_ϕ	Soil parameters
K_o	Coefficient of earth pressure at rest

K_p , K_{pc}	Coefficient of passive earth pressure
L	Length of footing
l	Length of cleat or wheel
n	Exponent corresponding to soil type for pressure (p) - sinkage relationship; number of trials
N_γ, N_c and N_q	Bearing capacity factors
p	Pressure
P_a , P_{at}	Active earth force
p_a	Active earth pressure
P_o	Earth force at rest
P_p , P_{pt}	Passive earth force
p_p	Passive earth pressure
P_t,P_e,P_H,P_T,	Percentage contributions
q	Uniform vertical load
q_0	Surcharge
q_f	Ultimate bearing capacity
r	Number of trial repetitions
R	Reaction force
R_a	Active zone resultant force beneath soil
r_c	Resultant of friction stress and stress normal to the wall or cleat, σ_c
R_c	Resultant force beneath cleat
R_p	Passive zone resultant force beneath cleat
R_s	Resultant force beneath soil
r_s	Resultant of friction stress and stress normal to the soil shear line, σ_s
s_γ, s_c and s_q	Shape factors (bearing capacity)
S'_b,S'_e,S'_H, S'_T	Pure sums of squares
S_b, S_e, S_H, S_T,	Sums of squares
T	Traction force
u	Pore water pressure
V_b, V_e,V_H,V_T	Mean square (variance)
W	Weight of soil wedge; vertical load
W_a	Weight of soil for active shear zone
W_p	Weight of soil for passive shear zone

z	Depth; sinkage
α	Angle of failure plane
$\alpha_a, \alpha_{at}\ \alpha_{aq}$	Active zone angle of failure plane
$\alpha_p, \alpha_{pt}\ \alpha_{pq}$	Passive zone angle of failure plane
β	Angle of incline of soil surface to the horizontal
γ	Unit weight of soil
δ	Friction angle for the wall or cleat and soil
θ	Angle of taper for cleats or angle of incline of retaining wall from the horizontal
σ	Applied stress
σ'	Effective stress
σ_1, σ_3	Principle stresses
σ_c	Stress normal to the wall or cleat
σ_s	Stress normal to the soil shear line
σ_z	Total vertical stress
σ_{xa}'	Horizontal stress of the active Mohr's circle
σ_{xp}'	Horizontal stress of the passive Mohr's circle
σ_z'	Effective vertical stress
τ_c	Shear stress between soil and retaining wall or cleat
τ_s	Shear strength of soil
ϕ	Friction angle for soil
ω	Angle of shear plane for Mohr's circle

Abstract

The aim of the research reported in this thesis was to improve the understanding of footwear and soft ground interaction and, in particular, its mathematical modelling. The work was undertaken for the Military Footwear Section of the MOD's Defence Clothing and Textiles Agency (DCTA) who funded the research is conjunction with the Engineering and Physical Sciences Research Council (EPSERC). Although research has been carried out on the interaction of footwear on firm surfaces, minimal work has previously been carried out on softer surfaces often encountered in combat situations and little effort has been applied to its mathematical modelling. The research programme included the development of mathematical models using soil mechanics theory, and experimental work using a soft-ground slip-rig.

The prototype soft-ground footwear slip-rig that has been developed is a manually operated device based on simple mechanical mechanisms using weights and pulleys. The rig enables the measurement of traction and sinkage for different soil types, sole materials and tread geometry, at various angles of heel contact and applied vertical load. All experimental work has been carried out with the use of scaled up cleats to obtain measurable results.

An investigation into three dimensional end effects has determined at what cleat length the problem becomes two dimensional. The experimental results have shown the effects of cleat geometry on total cleat traction for sand, and in particular the geometric characteristics that promote and reduce traction. These results have been analysed using Taguchi's Analysis of Variance technique. Traction distribution experiments have determined the proportion of traction obtained from different cleat areas.

Soil mechanics theory, and in particular Coulomb's retaining wall theory, has been applied in the theoretical modelling of footwear and soft ground interaction. A two dimensional total traction model has been developed using MATLAB software and experimental and theoretical results have been compared. The traction versus cleat geometry trends for both the experimental and theoretical results were in good agreement.

PAGE NUMBERING AS ORIGINAL

2. Literature Review

2.1. Introduction

Prior to the start of the research it was known that little work existed on the topic of foot interaction with soft, natural surfaces. Therefore, the aim of the literature review was to investigate existing works on foot interaction with both hard and soft surfaces and assess if any of the literature was relevant to the study. The literature review was also the starting point for the research and an opportunity to gain an understanding of the related subjects.

In the initial background literature study, it was necessary to gain an understanding of unfamiliar topics such as biomechanics with particular emphasis on the foot, gait analysis, footwear design, foot and ground interaction and soil mechanics. During this initial study a number of texts were found to be very useful. For the study of biomechanics and gait analysis the following texts were most valuable: Inman et al [1], Rose and Gamble [2], Whittle [3] and Rogers [4] where an understanding of the basic principles of human walking and foot function was gained. For the study of footwear and ground interaction the texts that were found to be most helpful were Cavanagh [5], Frederick [6] and Nigg [7] where the effects of shoe design and characteristics of playing and running surfaces in sport were analysed. The texts that have been most helpful in understanding soil mechanics include those by Craig [8], Smith and Smith [9], Spangler and Handy [10] and Whitlow [11].

Having completed the initial background literature study, and established an understanding of the basic concepts required for the research, it was decided that the two main topics for literature investigation were foot and ground interaction and soil mechanics, the findings of which are now discussed.

2.2. Foot-Ground Interaction

There are many different aspects to foot-ground interaction such as ground reaction force analysis, traction, gait analysis and interaction modelling to enhance sporting performance, analyse pathological disorders or reduce accidents and injury for example. For this research the traction aspect is of greatest importance.

Studies of walking on different terrains, including sand and snow, have been carried out to investigate its effect on walking speed, gait and energy expenditure [12,13,14,15]. Terrain coefficients were then developed to correct for the type of surface traversed in energy expenditure analysis.

Many personal injuries occur from slipping and falling each year. Research on the causes of slip and fall accidents is made difficult due to little information being available on the number of injuries and the circumstances that cause them. Manning et al [16] estimate that there must be more than one million injuries per annum from slipping in the UK alone, there were 13.6 million recorded in the United States. Many factors contribute to circumstances surrounding these incidents such as activity at the time, age and physical condition of the person involved, the surface on which the slip occurred, the type of footwear worn and other environmental factors for example contamination or extreme temperature. Research and testing has therefore been carried out to measure the coefficient of friction of floor and walkway surfaces, sport playing surfaces, shoe soling materials and the effect of different tread patterns. The effect of contamination on friction has also been explored. This review of foot-ground interaction is separated into two sections, the first being hard surfaces which has been well studied and the second being soft, natural surfaces which is much less documented.

As part of the review an investigation into walking machines was carried out to find out how they interacted with different terrain surfaces and in particular how it was modelled. Unfortunately this was unsuccessful due to very limited research having been done in this area. Very few models were found and they were based on either trajectory planning or a "go" and "no-go" stability algorithm [17,18,19],

therefore this study was not continued. It also emphasises the need for further work in that particular area which might be aided by this research.

2.2.1. Hard Surfaces

Much work has been carried out to investigate the interaction of footwear with hard surfaces encountered in every day situations. Wilson and Russel [20] reviewed slip resistance assessment discussing both footwear and floor surfaces. Friction tests were divided into three types: subjective tests, biomechanically based machine tests and simple machine tests. The subjective tests although valuable are time consuming and may be influenced by the individual subject, however, for some research requirements there is perhaps no alternative. Biomechanical machine tests aim to reproduce the slip conditions when walking, like the test equipment used at SATRA, which simulate heel and toe slip. The simple machine tests are mostly employed to test floorings and are only capable of measuring the friction coefficient between floor and soling materials.

Studies of testing equipment to measure the friction coefficient of floor surfaces include that of Brough, Malkin & Harrison [21,22] who designed a small portable machine for use in situ. It was developed from earlier research using an adaptation of the Eldridge machine, a slider of various shapes and materials mounted on a small trolley to determine friction coefficients of samples and floors, suggested by Childs and Tabor [23]. They observed that slip actions occur from the heel slipping forwards on heel-ground contact, the toe slipping backwards at toe-off when pushing the body forwards and, during turning, slipping of the ball of the outer foot. Heel slip was of most concern due to the severity of possible injury, therefore examination of foot contact with the floor was carried out. This suggested that the friction of the contact area of the heel is probably more important than friction properties of the sole.

Harper, Warlow and Clarke [24,25] concluded from abrasion and slipperiness testing that, for safety, the coefficient of friction between floor finishes and shoe soling materials should not be less than 0.4, this is supported by the work of

SATRA [26,27], and that the risk of slipping on stairs is much less than on the level. This however may be due to extra precautions taken during walking on stairs because the consequences of slipping are much greater. Pooley [27] compared several friction testing devices using a variety of soling materials and floor surfaces before selecting the James machine invented in 1945 by Dr. Sydney James. The James machine was selected to fulfil the need for a commercially available machine to measure comparative static coefficients of friction of shoe sole and heel materials and the effect of contamination.

Wilson [25,26] reports testing using the SATRA Friction Tester including results of studies on the relationship between soling material hardness and measured friction. For example, smooth PVC soling friction decreases with increasing hardness on a dry surface but increases to a certain level on a wet surface whilst vulcanised rubber tests indicated hardness was less significant. A tread pattern, however, reverses the hardness effect on the wet surface, giving results comparable with smooth PVC in the dry. Other results show the significant effects of abrasion of solings and floor surfaces on slip resistance and the key contribution of surface roughness to wet friction, for example, PVC wears to a polished finish, whilst others feather or roughen. The work of SATRA also illustrated good tread pattern design characteristics, also supported by the work of Shuh-Technik [29], stating the importance of cleats wearing to produce a flat profile, to maximise contact area, the influence of material type and hardness on the effectiveness of the tread pattern and the effect of surface texture.

Manning, Jones & Bruce [16] discuss their research on the cause of slipping, slip resistance and the effects of contamination and abrasion. The aim of the study was to confirm that certain footwear materials carry a greater risk of slipping and to find the most suitable footwear for the environment taking into account both slip resistance and durability. Testing of different soling materials was carried out using subjects working at a factory with oil and water contaminated floors. Tests were performed on issue of the footwear and at fortnightly intervals thereafter. The test rig consisted of a polished steel plate on which the subject stood that could be tilted. The plate was wiped in oil and the plate tilted until the subject slipped.

Forward and backward angles of slip were measured. The tests were repeated having wiped the boots with paper to remove loose dirt and swarf. During the three and a half year experiment over 1000 measurements of slipping angles were taken, using a variety of boots with different solings and amounts of wear.

Perkins [30] also suggests slip is most likely to occur during the landing phase of gait, and presents a technique for measuring slip under normal walking conditions. Subjects were asked to walk along a high friction surface onto a low friction surface mounted on a force platform. Subjects that slipped were restrained by a safety harness. The force exerted between the shoe and the ground was measured using a multi component Force Measuring Platform (Kistler Type 9261A) and angular and positional foot movement was measured using multiple-image, light-interrupted photography. Slip was examined whilst subjects wore a variety shoes with different soling materials and wear on different floor surfaces.

A coefficient of friction of 0.3 to 0.4 [26,27] is used to assess many types of footwear as this corresponds with the highest ratio of horizontal to vertical force, normally recorded in gait studies. This means that a coefficient of friction between a shoe and a surface below 0.3 indicates slipping is likely to occur, the risk of slip occurring increasing as the coefficient of friction decreases. When the coefficient of friction is greater than 0.3 to 0.4, the risk of slipping reduces. In sports, mountaineering and other alpine activities and industrial applications, friction becomes even more important due to the high reaction forces generated. The coefficient of friction values are therefore required to be much higher than those of everyday footwear. Due to so little information available about the interaction of footwear with the alpine environment, the required values of the coefficient of friction are not defined, and therefore require considerable research. In sports, however, great attempts have been made to analyse the friction between playing surfaces and footwear and the ground reaction forces generated relating to the aetiology of sports injury and enhancement of performance.

Footwear used in sports necessitates the need to develop high traction forces to stop and start, accelerate and decelerate quickly, run fast, turn and cut and jump. The

two main types of friction are translational and rotational which are well defined by Frederick [31]. A good example of a foot and hard surface interface is in basketball where too little traction will affect a player's performance and slip may occur, and too much traction could result in injury by inducing excessive torque. Therefore, in the design of a basketball shoe outsole, a compromise must be made between the performance of the player and the protection from injury.

Valiant [32] assessed a variety of sole patterns by testing translational and rotational traction with a device that could resemble actual loading conditions. Friction was shown to be dependent on material and surface area in contact with the playing surface. The study aids the development of a shoe sole design that maximises translational friction but minimises rotational friction. This work is complemented by Rheinstein et al [33] who investigated the effects on traction of basketball shoe outsole composition and hardness on three types of playing surfaces (clean hardwood, dusty hardwood and artificial gymnasium flooring). It was concluded that traction was dependent on player weight, playing surface, outsole material and outsole hardness and that further investigation was required.

Frederick [31] concluded many sport playing surfaces have greater friction than required for effective sports performance and that sports shoes should have a translational friction coefficient of 0.8 on the typical surface for which it is used and exhibit minimal rotational friction. Also, torque significantly exceeding 10 to 12 Nm increases the risk of injury due to excessive torsional strain. This may be compared to an optimal friction value of 0.5 for a clay surface in tennis, determined by Nigg and Segesser [34].

2.2.2. Soft Surfaces

The interaction of footwear on a soft surface must be considered separately from that on hard surfaces. Torg and Quedenfeld [35] were amongst the first to study knee and ankle injuries in football. They found that the frequency and severity of injuries was higher for players using conventional football shoes with seven 19mm long cleats of diameter 9.5mm than players using shoes with fourteen 9.5mm long

cleats of diameter 12.5mm. The cause of such injuries is excessive frictional forces due to foot fixation, especially in contact sport; this has been widely reported.

One of the possible ways to reduce translational and rotational friction is to increase the number of cleats [33]. The amount of friction generated by the shoe and the surface has been found to be dependent on contact area for natural turf and artificial turf, Van Gheluwe [36], Schlaepfer et al [37] Bonstingl et al [38], and Nigg and Yeadon [39] and Smith et al (40). This however violates classical friction theory, which states that friction is linearly related to normal load and is independent of contact area.

Both Van Gheluwe and Bonstingl et al tested a variety of tread patterns from metal studs to multi-cleated moulded soles to hard court un-cleated shoes on natural turf (Bonstingl only) and artificial turfs. Both tested with the shoe in the flat position and with only the stud tips in contact with the surface using a weighted artificial limb fitted with a sports shoe impacted by a weighted pendulum to produce instantaneous torque. The turf was mounted on a force platform, artificial turf using adhesive onto backing boards and natural turf encased in wooden pallets, and strain gauges were mounted on the limb. The static load on the leg, the foot stance (weight on ball of the foot, the weight on heel and equal distribution of weight on both the ball and heel), the energy of impact, shoe type and sole design (including cleat design and configuration) and the playing surface were all investigated.

In Van Gheluwe's study the largest number of small rubber studs showed the most traction on artificial turf while metal studs showed the least. In Bonstingl's study metal studs produced the greatest torque on natural turf for which they were designed. The multi-cleated shoe generated approximately the same amount of torque on natural and artificial turf. Non-cleated shoes produced minimal torque on all surfaces tested. Both studies concluded friction was dependent on shoe type, playing surface, contact area and load.

It is apparent from these studies and that of Torg and Quedenfeld [35] and Valiant [41] that friction increases with cleat height. Obviously, friction and foot fixation

increases with increased cleat penetration into the surface. This has been further discussed by Milburn and Barry [42] with regards to the reduction of injury in rugby union. Injury in rugby is caused by poor technique and corrective movement, also discussed by Frederick [43], as well as foot fixation during contact. In rugby union limits to cleat dimensions and wear are necessary to prevent injury to other players but should also be required for reduction in injury to the user. In their work the difficulty of recommending optimal footwear types, stud dimensions and configurations is highlighted due to the nature of the natural playing surface which has so many variables. The field surface can even change during a game. Therefore detachable studs of varying lengths have been recommended in the study. This will also eliminate the problem of different field positions that have different footwear requirements.

This study in particular illustrates many similarities with the military footwear requirements where different military personnel will have different footwear needs which can vary depending on surface and ground hardness, weather, load carriage etc. The work also discusses comfort, shoe construction, foot function and orthopaedic demands.

The desire to reduce the influence of external factors on natural playing surfaces as well as make maintenance easier and cheaper has led to the construction of artificial surfaces. This is well documented, but in turn has created its own new problems with regards to injury, Ekstrand and Nigg [44], Heidt Jr. et al [45] and Bowers Jr. and Martin [46]. Valiant [47] investigated ground reaction forces on artificial turf to determine minimum traction requirements. Subjective tests were carried out with the same pair of football shoes, the right shoe of each subject was also tested using a traction device as described in Valiant [32]. It was concluded that translational friction properties should be reduced thereby reducing rotational friction also. The rotational friction should be minimised which has been stated so often in previous works.

The recent work of Barry and Miburn in traction of footwear on natural surfaces is the most relevant work to this study. The need for soil mechanics since the classical

laws of friction do not apply to footwear interacting with natural surfaces has been discussed [48]. Soil is described as a mass of discrete particles that are not strongly bonded together and are relatively free to move with respect to each other. It is usually subjected to rain so pore spaces between soil particles can be partly filled with water and the rest of the space with air, depending upon saturation. As load is applied to the soil via the outsole and cleats, the soil particles respond by deforming, whether it be by compression, bending or sliding. Sliding has the most significant effect, and is non-linear and irreversible.

Barry and Milburn discuss friction and traction characteristics at a molecular level, including the following effects:

Adhesion- the formation and rupture of bonds

Ploughing- harder asperities plough through softer surfaces (contributing to wear)

Deformation- rigid plastic theory

Static friction

The failure criterion of Coulomb and failure zones were also discussed. External forces that cause sliding within soils are resisted by friction and bonding forces between particles. If applied loads become sufficiently large, soil failure occurs along an undefined slip plane and the soil slides as a failure wedge.

A device to measure traction load-deformation properties at the footwear-surface interface was introduced. Results for three surfaces tested were typically non-linear and provided the interface parameters, traction force, displacement and interface material stiffness. Sliding was found to be dependent upon soil behaviour and shoe sole deformation. Regarding soil failure with studs, a slip plane was observed during testing. Rear studs were seen to initiate the slip plane in sand, and front studs were seen to 'piggyback' the wedge of sand created by the soil shear. Plastic equilibrium theory was used to estimate the failure load. However, during tests with turf, there was no visual slip plane. It was also difficult to test with turf because of the different types and variable conditions. The traction function of turf was considered to be dependent upon the substrate, however, traction force was found to continually increase rather than reach a maximum. Failure of soil was also initiated at the rear cleats. Testing with clay has so far been unsuccessful.

Barry and Milburn have also presented a computer controlled footwear traction testing device [49] that measures the translational force (up to a maximum of 3000N) or rotational torque (up to a maximum of 100Nm) developed between footwear and natural or artificial surfaces. The device was designed at the Nike Sports Research Laboratory [32]. It is based on the direct shear test used for measuring soil properties. Traction measurements made from carefully designed mechanical devices are preferred to human subjects because of reduced variability in results. The device enables slide rate (0.1-80 mm/s range) and displacement of footwear to be precisely controlled in either translation or rotation. A vertical load of up to 150kg may be applied but 40kg is used. Vertical displacement of the boot is also measured (to within 0.1mm) as it passes over the test surface. The traction data was fitted by a non-linear regression analysis technique using an exponential model. Exponential functions are used by Wong, 1989 [50] to study traction performance of vehicles in terramechanics and by Barry and Milburn [51] to obtain maximum traction force and other boot – surface interface parameters. The results of a test provide traction force-displacement curves for an interface material, which provide particular interface parameters: maximum traction force, displacements versus corresponding traction forces and overall interface material stiffness. Each footwear-surface combination has unique interaction properties so it is therefore necessary to understand these properties. Barry and Milburn have carried out approximately 2000 tests using sand ('ACI sports 40' specification), Netlon mesh reinforced turf and natural river loam turf. For tests with sand, traction was found to increase with moisture content. For tests with Netlon and loam turf, data with respect to variable moisture content is obtained. Generally, traction was found to vary between boots, slide directions and surfaces. To study cleat/stud configuration an outsole with slots is used so that different cleats may be inserted into slots to vary cleat configuration, cleat sizes and cleat shapes. The traction device enables flat foot sliding, toe slip, heel slip and medial/lateral slip to be tested.

This research was discussed further when four rugby football boot types were tested using the footwear traction testing device (51). A combination of tests were carried out using the three surfaces mentioned previously, the four boot types,

variable moisture contents (nine with sand and five with turf) and boot orientations to obtain braking, acceleration and sideways traction forces.

The exponential model fitted the data for sand, but for the Netlon and loam data the model was limited. For sand, traction was seen to increase with moisture content but for turf, no obvious relationship was seen. Traction was found to vary with each boot type, boot orientation and surface.

It may be concluded that Barry and Milburn use soil mechanics theory to descriptively explain footwear traction on natural field surfaces. Their research focuses on the effect of cleat and stud configuration on traction on different playing surfaces, with the aim of matching cleat/stud configuration to a particular playing surface and field position to maximise performance and minimise injury. Their work uses an experimental approach, measuring traction of various football boot types of different orientations on various surfaces. The work reported in this thesis, however, has used soil mechanics theory to develop mathematical models to investigate the effects of cleat geometry on traction on soft surfaces. The mathematical modelling results are verified using the experimental results obtained from the soft ground test rig.

The foot-ground interaction literature to date has demonstrated that hard surface interaction has been well researched but soft surface interaction has received far less attention. The work with soil and turf has aimed to maximise performance but minimise injury in contact sport by optimising cleat configurations. It may therefore be concluded from the literature found that there is little to base this research on, and that it is necessary to investigate alternative areas.

2.3. Soil Mechanics

Since the study of foot-ground interaction has shown little suitable research on soft surfaces it was necessary to investigate other fields, terramechanics for example. Terramechanics is the study of the performance of a machine in relation to its environment, the terrain, pioneered by M.G. Bekker in the 1950's. Terramechanics

can be divided into two main branches, terrain–vehicle mechanics and terrain-implement mechanics, Wong [52].

In 1956, Bekker stated "The biped type of locomotion is substituted for by some sort of geometric pattern. The only pattern of this kind which would be close enough to the mechanics of a walk appears to be the rolling of a polygon, in which the centre of gravity is consecutively dropped and lifted up" [53]. He also stated that the smaller the steps, the more sides to the polygon, and the closer it approaches a circle. It may therefore be concluded that biped locomotion approximates the motion created by a wheel. Walking may be likened to the rolling of a rimless wheel, the spokes supporting the load. It has also been shown by Bejune et al [54], that walking may be simulated by rolling. Therefore the branch of terramechanics of most interest is terrain–vehicle mechanics, which deals with tractive performance of a vehicle over unprepared terrain whereas terrain-implement mechanics deals with the performance of soil working machinery used in agriculture for example.

Much research has been carried out on the interaction between soil and wheels, particularly by Wong and Reece [55,56,57] and Onafeko and Reece [58]. Wong and Reece studied the behaviour of soils beneath rigid wheels, further developing the work of Bekker, and were able to predict the performance of the rigid wheel based on this analysis. They investigated the effect of thin and wide wheels on sand and clay and were able to show that the behaviour of soil beneath a rolling wheel conforms to the basic principles of soil mechanics as developed by Coulomb [59], Terzaghi [60,61,62] and others. The analysis of soil stress and deformation beneath rigid wheels carried out by Onafeko and Reece takes into consideration soil flow whereas Bekker's theory does not. Bekker's theory, applicable to all soils, was based on two simple tests and semi-empirical equations. Muro [63] has presented a new method for better prediction of the tractive performance of a rigid wheel on soft ground by taking into account the effects of the rolling locus of the wheel. Further work was carried out to investigate tyre-soil interaction to predict tractive performance by Foda [64] using a tribology model. Baladi and Rohani [65] derived a mathematical model of the interaction of tyre and soil, and Mahmoud and Dwyer

[66] developed two dimensional models of different interface shapes to take into account both soil and tyre deformation. The works that have been mentioned here and many others are examined by Plackett [67] in a historic progression of tyre-soil force prediction methods. Other particularly useful studies include the appraisal of terrain characterisation techniques by Shoop [68] for vehicle traction studies concentrating on field measurement of strength related properties of soil, snow, muskeg and vegetation. Dwyer et al [69] studied the tractive performance of an experimental rubber track unit compared to a tractor tyre in various conditions and with different track tread patterns. Okello et al [70] completed a comprehensive review of soil strength characterisation techniques for the prediction of terrain vehicle performance.

Since the underlying soil theory of Bekker [53,71] used in terramechanics was actually based upon the soil mechanics work of Terzaghi [60] used in civil engineering, it was therefore appropriate to use the original civil engineering soil theory for this research. For this reason, theoretical soil mechanics is reviewed in detail in chapter 3.

3. A Review of Theoretical Soil Mechanics

3.1. Introduction

Since the study of foot-ground interaction has included very little research on soft surfaces it has therefore been necessary to investigate other fields, terramechanics for example. Terramechanics is the study of the performance of a machine in relation to its environment, the terrain, pioneered by M.G. Bekker in the 1950's. Terramechanics can be divided into two main branches, terrain-vehicle mechanics and terrain-implement mechanics. Of most interest is the terrain-vehicle mechanics, which deals with tractive performance of a vehicle over unprepared terrain. It was found that the underlying soil theory of Bekker [53,71] used in terramechanics is based upon the soil mechanics work of Terzaghi [60] used in civil engineering. It was therefore appropriate to use the original civil engineering soil theory for this research.

This chapter reviews the existing soil mechanics theory, which was used as a modelling base and adapted for foot-ground interaction as reported in chapter 4. The passive earth force, P_p, is defined as the resistance of soil against the forces which tend to displace it at the point of plastic failure. Whereas passive earth force is the resistance to displacement, the active earth force, P_a, is the thrust of soil in expansion; as a retaining wall is moved away from a mass of soil, expansion of the soil will occur. From a civil engineering point of view, passive earth pressure is utilised as a support for structures which have horizontal and vertical forces acting on them, for example, retaining walls and support footings for buildings. In the vertical direction, whether support footings for a building or cleats on a boot sole, if the load exceeds the ultimate bearing capacity of the soil, sinkage will occur. The stability of almost any lateral earth support and the bearing capacity of shallow foundations is dependent to some extent on passive earth pressure. By evaluating the magnitude and location of these forces, it was expected that the prediction of "slip or stick" for different boot treads would be possible for different terrain conditions.

3.2. Shear Strength

Throughout this research, drained soil has been considered, and therefore the effects of pore water pressure, u, have not been discussed. The stress considered within the soil mechanics theory and the mathematical modelling is referred to as *effective stress*, σ', defined by Terzaghi in 1943 [60]. Effective stress is the average stress transmitted through the soil via the inter-granular contacts only, i.e. the skeleton of soil particles. The total stress is equal to the effective stress via the soil plus the pore water pressure:

$$\sigma' = \sigma - u \tag{3.1}$$

If a soil is saturated, then the voids between the soil particles are full of water instead of air so when an external stress, σ, is applied to the soil, the pore water pressure would immediately increase. If the soil is drained, the water would then flow away and the pore pressure reduce to zero so that the applied stress would then be transferred entirely to the granular structure. If pore water pressure is zero, the effective stress, σ', is equal to the applied stress, σ.

Soils exhibit cohesive, adhesive and frictional properties. Cohesion, c_s, is the shear stress between soil particles irrespective of the normal pressure exerted by one particle upon another. Adhesion, c_c, is the shear stress between a retaining wall surface and the soil irrespective of the normal pressure exerted by one upon the other. Friction is the shear stress between soil particles or between a wall and soil, and is proportional to the normal pressure exerted. When soil shears, the resultant, r_s, of the friction stress and the stress normal to the soil shear line, σ_s, acts at an angle ϕ from the normal. When soil slides over a wall the resultant, r_c, of the friction stress and the stress normal to the wall, σ_c, acts at an angle δ from the normal. The friction component of the resultant, r, is $\sigma_s \tan\phi$ for soil and $\sigma_c \tan\delta$ for a wall where ϕ is the friction angle for soil and δ is the friction angle for the wall and soil.

To evaluate the stability of soil masses the shear strength of the soil is required. If at any point within the mass the shear stress becomes equal to the shear strength of the soil, failure will occur at that point. The state of stress may be represented by a Mohr circle, see figure 3.1. An infinite number of circles may satisfy the conditions for elastic equilibrium as long as they intersect the principal stress, σ_3, on the horizontal axis. A state of elastic equilibrium is when a small change in stress produces a corresponding reversible change in strain. The shear strength of a soil at a particular point and in a particular direction may be expressed by Coulomb's shear strength equation:

$$\tau_s = c_s + \sigma_s \tan\phi \tag{3.2}$$

where, c_s and ϕ (cohesion and the friction angle) are the shear strength parameters. Similarly the shear stress between the soil and the retaining wall or boot cleat may be represented by $\tau_c = c_c + \sigma_c \tan\delta$. In figure 3.1, Coulomb's equation (equation 3.2) is represented by the straight-line failure envelope. If the Mohr circle touches the failure envelope it represents plastic equilibrium and shear failure occurs. Plastic equilibrium is when irreversible strain occurs at constant stress. In this case,

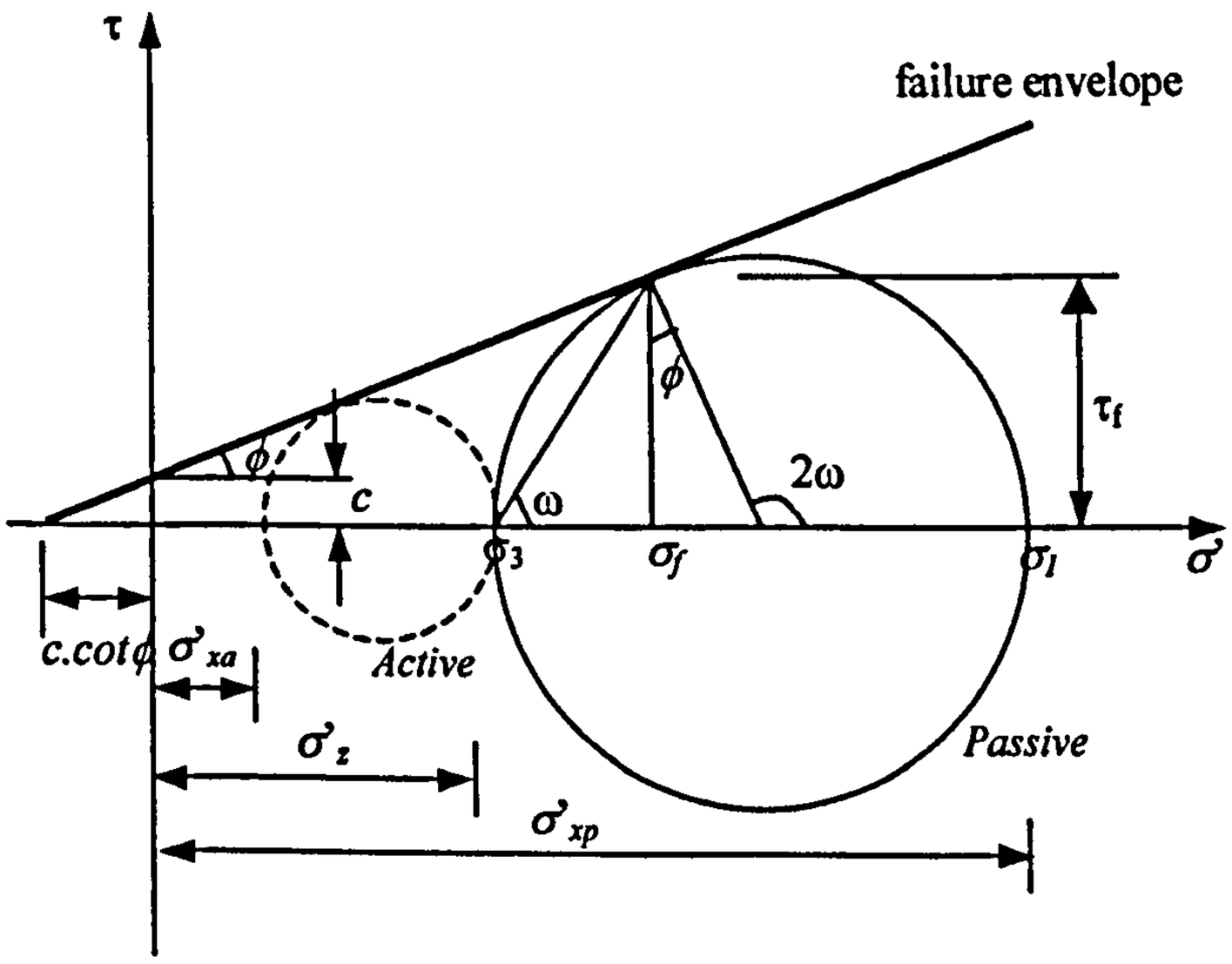

Fig. 3.1: The Mohr circle representing the state of stress at failure in a 2D element.

from the geometry of the circle and shear line in figure 3.1, expressions can be derived for the shear strength and the angle, ω, of the shear planes [8,11].

3.3. Rankine's Theory

Effective stress increases or decreases with the corresponding change in diameter of the Mohr circle. With lateral expansion, plastic equilibrium occurs at the minimum value of horizontal stress, σ_{xa}', of the circle; with lateral contraction, failure occurs at the maximum value, σ_{xp}', as illustrated by figure 3.1. Rankine referred to these as *active* and *passive* states respectively. The magnitude of, σ_{xa}' or σ_{xp}', depends only on the shear strength of the soil and the vertical stress, σ_z'.

Rankine's theory of passive and active earth pressure considers the state of stress in soil at the point of shear failure. For passive earth pressure as a vertical wall or cleat moves against a mass of soil, lateral compression of the soil will occur, thus the horizontal stress, σ_x, will increase until shear failure. At this point the Mohr's circle contacts the failure envelope, as shown in figure 3.1, σ_x is the major principle

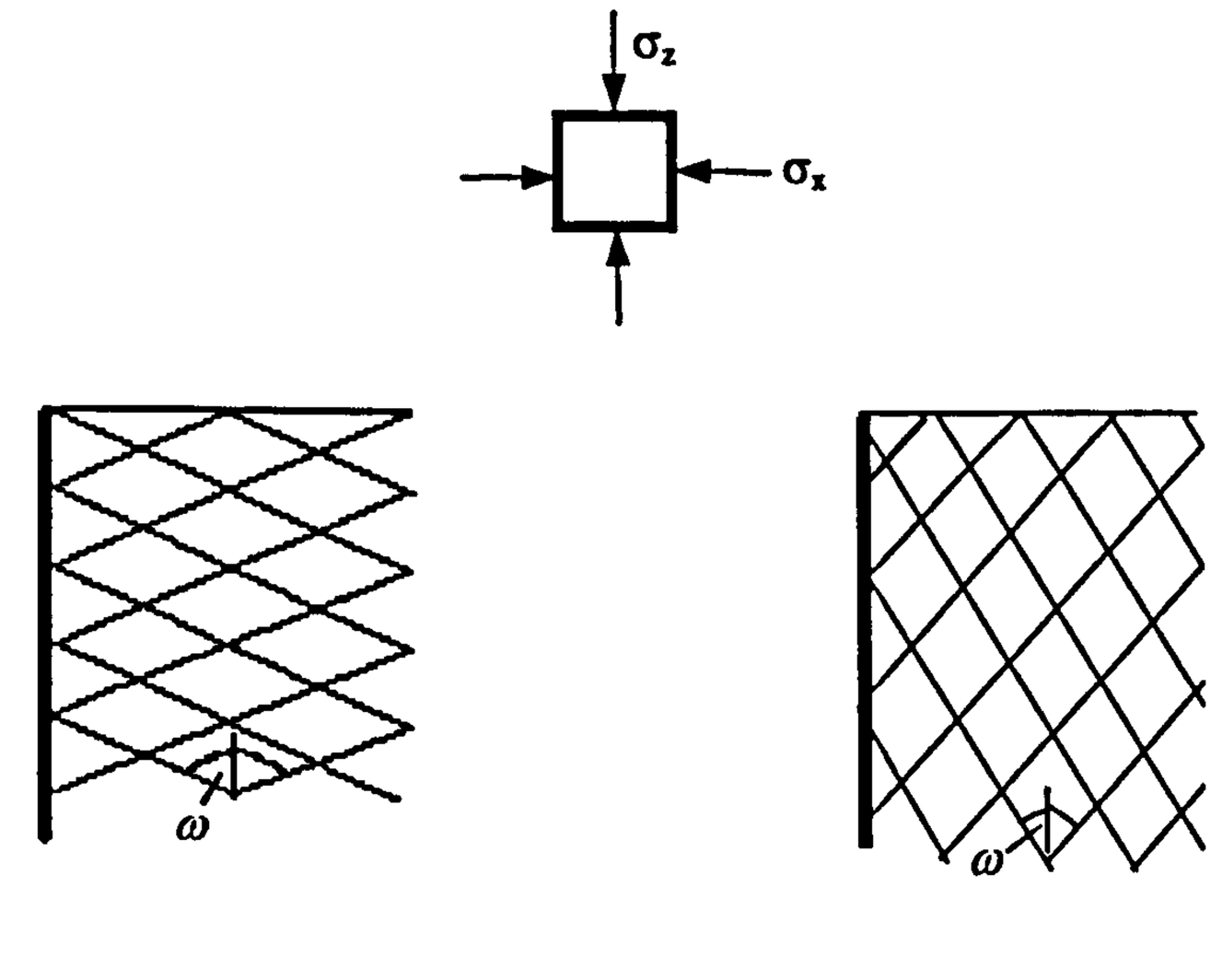

$\omega = 45 + \phi/2$ (a) Passive Rankine state

$\omega = 45 - \phi/2$ (b) Active Rankine state

Fig. 3.2: The passive and active Rankine states.

stress, σ_1, and $\sigma_z = \gamma z$ is the minor principle stress σ_3, where γ is the unit weight of the soil (N/mm^3). This condition is plastic equilibrium where the failure planes or slip lines are inclined to the principal planes by an angle ω as shown in figure 3.2.

In the case of a vertical wall, the passive earth pressure acting on the wall at failure is equal to:

$$p = \sigma_x = K_p \gamma z$$

(K_p = coefficient of passive earth pressure and γ = unit weight of soil)

In the case of a vertical wall, the active earth pressure acting on the wall at failure is equal to:

$$p = \sigma_x = K_a \gamma z$$

(K_a = coefficient of active earth pressure)

When the horizontal stress becomes equal to the passive pressure the soil is then said to be in the *passive Rankine state*, as shown in figure 3.2(a), where there are two sets of failure planes each inclined at $(45° + \phi/2)$ to the vertical. When the horizontal stress becomes equal to the active pressure the soil is then said to be in the *active Rankine state*, as shown in figure 3.2(b) where there the two failure planes are inclined at $(45° - \phi/2)$ to the vertical. The active and passive states are the two limiting states for the equilibrium of a soil. Every intermediate state, including the state of rest when elastic equilibrium with no lateral displacement occurs, is a state of elastic equilibrium.

If a uniform vertical load, q say, was applied to the surface it would be assumed that the vertical stress would increase by that amount:

At depth, z:

$$\sigma_z = \gamma z + q \quad \text{and} \quad \sigma_x = K_a(\gamma z + q)$$

Therefore horizontal stress is increased by either $K_a q$ or $K_p q$.

The Rankine theory originally dealt with granular soils only ($c_s = c_c = 0$), neglects wall friction, and it assumes a semi-infinite mass. However, in 1915, Bell based a solution on Rankine's approach to allow for a cohesion intercept on the shear axis (figure 3.1). Rankine's theory does provide analysis based on simple calculations but does impose limitations and consequentially, large errors. It is based on vertical retaining walls with a smooth surface, so does not consider the friction between the wall and the soil or the sloping of the wall. It also assumes that the yielding of the whole structure is like the yielding of a small element. With the limitations of the technique an overestimation of passive pressure occurs. Coulomb's theory overcomes some of these problems, by assuming a wedge of soil to move up or down the wall face and along a failure plane.

3.4. Coulomb's Retaining Wall Theory

3.4.1. Passive Case

Coulomb's theory of passive earth pressure considers the stability of a soil wedge between a retaining wall (or boot cleat) and a failure plane. The passive force between the wall and the wedge may be determined by consideration of the equilibrium of forces acting on the wedge on the point of sliding up the failure plane. Figure 3.3(a) shows the forces acting on the soil wedge between a wall surface AB, inclined at an angle θ to the horizontal, and a trial failure plane BC, at an angle α to the horizontal. The soil surface AC is inclined at an angle β to the horizontal. The Coulomb theory may be used for soils in which the soil shear parameter c_s (*cohesion)* and the wall adhesion parameter c_c may be equal to or greater than zero depending on soil type.

The failure condition implies the soil wedge is in equilibrium under its own weight (W), the passive earth resistance (P_p) between the soil and wall, the force due to the constant component of shearing resistance on the wall (adhesion C_c), the force on the failure plane due to the constant component of shear strength (cohesion C_s), and

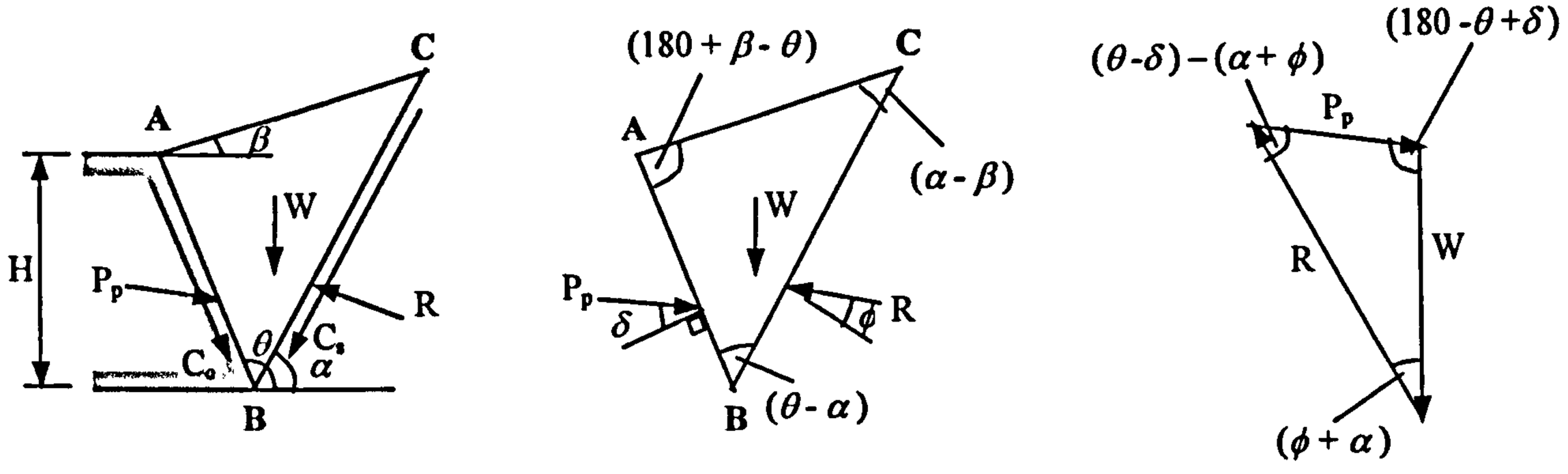

(a) Soil Section (b) Forces acting on wedge ABCD ($C_s = C_c = 0$) (c) Triangle of forces ($C_s = C_c = 0$)

Fig. 3.3: Coulomb's theory for passive earth force.

the reaction (R) on the failure plane. Because of friction, the passive earth force (P_p) acts at an angle δ above the normal to the wall surface and the reaction (R) at an angle ϕ above the normal to the failure plane. As shown by the triangle of forces in figure 3.3(c) the angle between W and P_p is ($180° - \theta + \delta$) and the angle between W and R is ($\alpha + \phi$). The angle between R and P_p is therefore equal to [($\theta - \delta$) – ($\alpha + \phi$)]. The passive earth resistance is equal to the minimum value of P_p since soil shears along the plane of minimum resistance, but for trial values of α, P_p may be calculated as follows.

The following example demonstrates the derivation of P_p when $c_s = c_c = 0$.

$$P_p = \tfrac{1}{2} K_p \gamma H^2 \qquad (3.3)$$

Where K_p is the passive earth force coefficient and γ is the unit weight of soil. This is shown as follows.

Referring to the triangle of forces (Figure 3.3c), and from the sine rule:

$$\frac{P_p}{sin(\alpha+\phi)} = \frac{\mathrm{W}}{\sin[(\theta-\delta)-(\alpha+\phi)]}$$

Therefore,

$$P_p = \frac{\mathrm{W}\sin(\alpha+\phi)}{\sin\left[(\theta-\delta)-(\alpha+\phi)\right]}$$

Also

$$W = ½\,\gamma\,\sin(180° + \beta - \theta).AB.AC$$

Or

$$W = ½\,\gamma\,\sin(\theta - \beta).AB.AC$$

And

$$AB = \frac{H}{\sin\theta} \qquad AC = \frac{H\sin(\theta-\alpha)}{\sin\theta\sin(\alpha-\beta)}$$

Then

$$W = ½\gamma\,sin(\theta-\beta).\frac{H\sin(\theta-\alpha)}{\sin\theta\sin(\alpha-\beta)}.\frac{H}{\sin\theta}$$

Therefore

$$P_p = ½\,K_p\gamma H^2 \tag{3.3}$$

Where

$$K_p = \frac{sin(\alpha+\phi)sin(\theta-\beta)sin(\theta-\alpha)}{sin[(\theta-\delta)-(\alpha+\phi)]\sin^2\theta\,sin(\alpha-\beta)}$$

The minimum value of P_p corresponds to a particular value of α given by $\partial P_p/\partial\alpha = 0$, which can be solved analytically [59]. When this value is substituted into equation (3.3) we obtain a coefficient of passive earth force corresponding to the value of α for minimum P_p:

$$K_p = \left(\frac{\sin(\theta + \phi) / \sin\theta}{\sqrt{[\sin(\theta - \delta)]} - \sqrt{\frac{\sin(\phi + \delta)\sin(\phi + \beta)}{\sin(\theta - \beta)}}} \right)^2 \qquad (3.4)$$

Although in this simple case the required value of α can be found analytically, in the author's work a numerical search method is used to adjust α and thereby find the minimum P_p. However, since Coulomb's equation assumes plane failure when realistically the failure surface is curved, the above equation for K_p, equation (3.4), does in fact overestimate the passive resistance. The error increases with roughness of the wall or cleat surface, i.e. for the higher values of δ, so for smooth rubber and plastic surfaces it will be small. For this reason it has been suggested in soil mechanics texts that passive pressure coefficients derived by Caquot and Kerisel [72] or Sokolovski [73] be used. Caquot and Kerisel derived both active and passive pressure coefficients by integrating the differential equations of equilibrium where the failure surface was taken to be a logarithmic spiral. Sokolovski, however, obtained coefficients by numerical integration. To use these derived coefficients the values of some soil parameters are required.

In general, irrespective of the method used to obtain K_p, the passive pressure at a depth z below the soil surface (*when* ϕ, δ, c_c *and* $c_s > 0$) may be expressed as [8]:

$$p = K_p \gamma z + K_{pc} c_s \qquad (3.5)$$

Where,

$$K_{pc} = 2\sqrt{K_p\left(1 + \frac{c_c}{c_s}\right)}$$

The total passive earth resistance, (*when* ϕ, δ, c_c *and* $c_s > 0$) using Coulomb's theory [11]:

$$P_p = \tfrac{1}{2} K_p \gamma H^2 + c_s H K_{pc} \qquad (3.6)$$

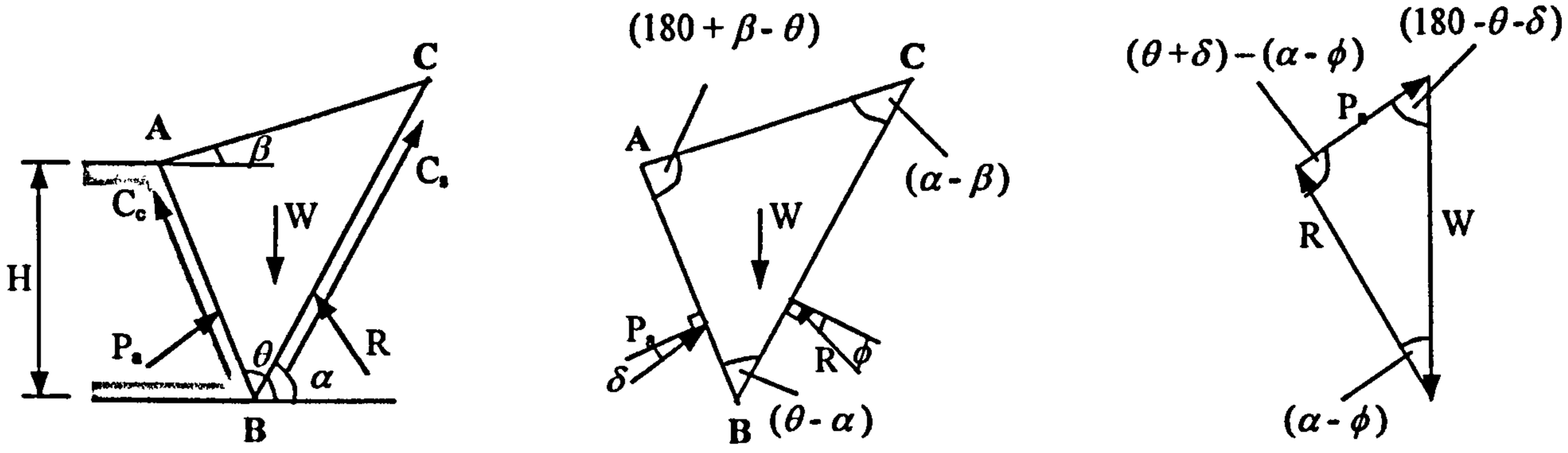

(a) Soil Section (b) Forces acting on wedge ABCD $(C_c = C_s = 0)$ (c) Triangle of forces $(C_c = C_s = 0)$

Fig. 3.4: Coulomb's theory for active earth force.

3.4.2. Active Case

In the active case, the wedge is on the point of sliding down the failure plane. The active earth force P_a acts at an angle δ below the normal to the wall surface and the reaction R at an angle ϕ below the normal to the failure plane. In the triangle of forces (Figure 4c) the angle between W and P_a is $(180° - \theta - \delta)$ and the angle between W and R is $(\alpha - \phi)$. Following a similar derivation to that for the passive case, the active earth force is equal to the maximum value of P_a since the soil will fail at the earliest opportunity as P_a reduces, and is given by:

$$P_a = \tfrac{1}{2} K_a \gamma H^2 \qquad (3.7)$$

where K_a is the passive earth force coefficient and γ is the unit weight of soil. This is shown as follows.

Referring to the triangle of forces (Figure 3.4c), and from the sine rule:

$$\frac{P_a}{\sin(\alpha-\phi)} = \frac{W}{\sin[(\theta+\delta)-(\alpha-\phi)]}$$

Therefore,

$$P_a = \frac{W \sin(\alpha - \phi)}{\sin[(\theta + \delta) - (\alpha - \phi)]}$$

Therefore,

$$P_a = \tfrac{1}{2} K_p \gamma H^2 \tag{3.7}$$

Where

$$K_a = \frac{\sin(\alpha - \phi)\sin(\theta - \beta)\sin(\theta - \alpha)}{\sin[(\theta + \delta) - (\alpha - \phi)]\sin^2\theta \sin(\alpha - \beta)}$$

The maximum value of P_a corresponds to a particular value of α given by $\partial P_a/\partial\alpha = 0$. When this value is substituted into equation (3.7) we obtain a coefficient of active earth force corresponding to the value of α for maximum P_a:

$$K_a = \left(\frac{\sin(\theta - \phi)/\sin\theta}{\sqrt{[\sin(\theta + \delta)] - \sqrt{\dfrac{\sin(-\phi - \delta)\sin(\beta - \phi)}{\sin(\theta - \beta)}}}} \right)^2$$

In general, irrespective of the method used to obtain K_a, the active pressure at a depth z below the soil surface (*when* ϕ, δ, c_c *and* $c_s > 0$) may be expressed as [8]:

$$p = K_a \gamma z - K_{ac} c_s \tag{3.8}$$

Where,

$$K_{ac} = 2\sqrt{K_a\left(1 + \frac{c_c}{c_s}\right)}$$

3.5. Bearing Capacity of Soil

The ultimate bearing capacity (q_f) of a soil is defined as the lowest pressure, which would cause shear failure of the supporting soil beneath an applied load. From a civil engineering point of view this would be applicable to foundations and footings etc., but could be applied to the sinkage of footwear in the ground at a cleat scale and a complete sole scale. There are three distinct modes of failure, which are general shear failure, local shear failure and punching shear failure. In the case of general shear, as the pressure beneath the load increases towards the value q_f, continuous failure surfaces develop which spread outwards and downwards until a state of plastic equilibrium is developed throughout the soil. This causes the soil to erupt above the ground surface, i.e. heaving, around the load until slip occurs. This type of failure occurs usually in low compressibility soils, which are dense and stiff, and is assumed in most texts. In local shear there is significant compression beneath the load and only partial development of plastic equilibrium therefore there is little sign of heaving. Local shear usually occurs with soils of high compressibility. Punching shear occurs where there is high compression beneath the load and shearing in the vertical direction around the edges of the load. No heaving will occur and the failure depends on the compressibility of the soil and the ratio of length to width of the load. This type of shear is most likely to occur where there is long term drainage or at greater depths where there may be softer layers of soil. Due to the small scale of the cleat/sole modelling problem to define the nature of shear failure only adds to the complication. General shear failure is suitable for undrained, low compressibility soils and exhibits a failure zone shape as illustrated by figure 3.5, this same shape is generally used to illustrate all bearing capacity problems.

3.5.1 Shallow Strip Footings

Consider a shallow strip footing, or in fact a boot cleat, of width B greater than or equal to its depth D, and length L much greater than B. The weightless footing will apply a uniform applied pressure, q, say, onto the surface of the soil, which is assumed to be homogeneous and isotropic. The shear parameters of the soil are c and ϕ and the unit weight is assumed to be zero. When the applied pressure, q_f,

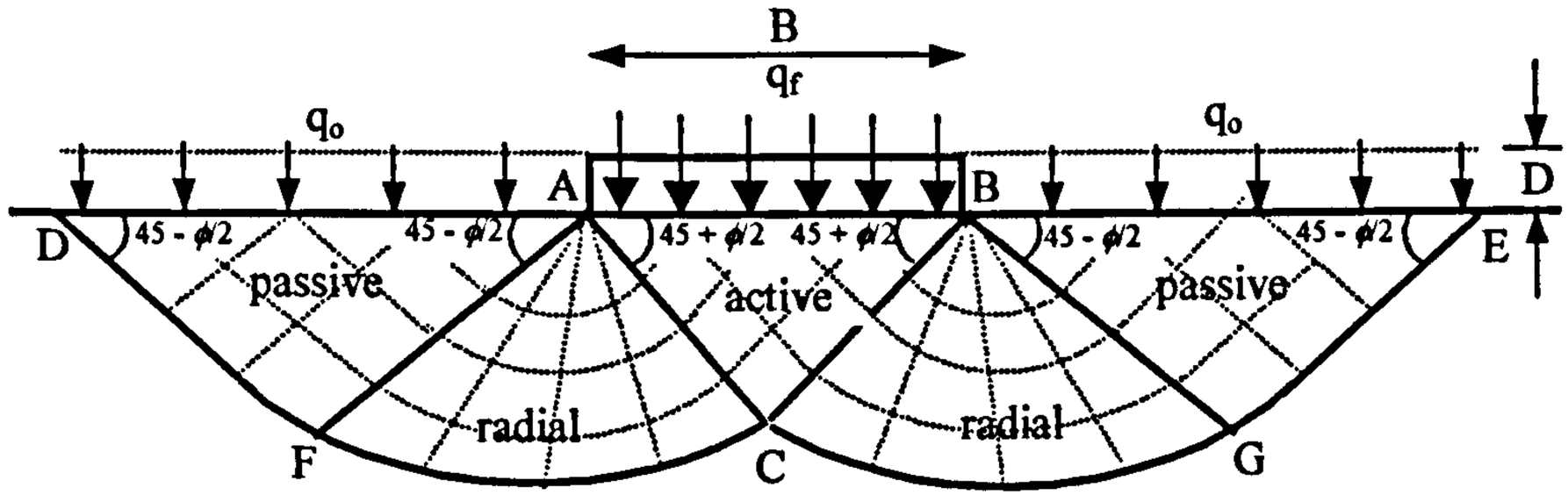

Fig. 3.5: General shear in drained conditions.

becomes equal to the bearing capacity the cleat will push downwards into the soil producing a state of plastic equilibrium in the form of an active Rankine zone below the footing as shown by figure 3.5. In the active state the major principle stress is vertical and the minor principle stress is horizontal. The downward movement of the soil wedge ABC forces the adjoining soil sideways producing lateral forces. Passive Rankine zones ADF and BGE are therefore formed next to the wedge ABC. In the passive state the minor principle stress is vertical and the major principle stress is horizontal. The *active* wedge angles ABC and BAC are $(45° + \phi/2)$ and the *passive* sector angles FAD and GBE are $(45° - \phi/2)$. The footing or cleat cannot penetrate the ground until the pressure exerted by the load exceeds the passive earth pressure. The transition between downwards movement of the wedge ABC and the lateral movement of the wedges ADF and BGE is carried out through radial shear zones ACF and BCG, the surfaces CF and CG being logarithmic spirals (drained) or circular arcs (undrained). BC and FD or AC and GE are tangential to these arcs. For shallow footings the shear strength between the surface and the depth D of the footing or cleat is neglected, the soil is only considered as a surcharge imposing a uniform pressure $q_0 = \gamma D$.

The ultimate bearing capacity of the soil under a shallow strip footing can be expressed using Terzaghi's general equation [61]:

$$q_f = \tfrac{1}{2}\gamma B N_\gamma + c N_c + \gamma D N_q \qquad (3.12)$$

width + cohesion + surcharge

where N_γ, N_c and N_q are bearing capacity factors (based upon theoretical solutions) depending only on the value of soil shear parameter ϕ.

$$N_q = exp\,(\pi \tan\phi)\, \tan^2\,(45^\circ + \phi/2)$$

$$N_c = (N_q - 1)\cot\phi$$

$$N_\gamma = 1.80(N_q - 1)\tan\phi \quad \text{(Brinch Hansen)}$$

$$N_\gamma = (N_q - 1)\tan(1.4\phi) \quad \text{(Meyerhof)}$$

The most widely used values of the factor N_γ are those obtained by Brinch Hansen [74] and Meyerhof [75] since there has been no agreement of empirical values for N_γ.

3.5.2. Shape Factors

The ultimate bearing capacities of square, rectangular and circular footings are determined by means of semi-empirical shape factors applied to the strip footing solution. The bearing capacity factors N_γ, N_c and N_q are multiplied by respective shape factors s_γ, s_c and s_q. The shape factors proposed by Terzaghi and Peck [62] are widely used in practise although they are considered to give conservative values of ultimate bearing capacity for high values of ϕ. These factors are $s_\gamma = 0.8$ for a square footing or 0.6 for a circular footing, $s_c = 1.2$ and $s_q = 1$. Therefore equation (3.12) becomes, for a square footing:

$$q_f = 0.4\gamma B N_\gamma + 1.2cN_c + \gamma D N_q \qquad (3.13)$$

and for a circular footing:

$$q_f = 0.3\gamma B N_\gamma + 1.2cN_c + \gamma D N_q \qquad (3.14)$$

For a rectangular footing of width B and length L, the shape factors are obtained by linear interpolation between the values for a strip footing *(B/L = 0)* and a square footing ($B/L = 1$), e.g. $s_\gamma = (1 - 0.2B/L)$.

3.5.3. Sinkage

The calculation of the bearing capacity of a soil indicates the pressure at which a footing or a boot cleat will sink on a particular soil, it does not indicate the amount to which it will sink. The cleats themselves may only sink to a maximum of their height but there is no limit to what sinkage can occur for the boot as a whole. To determine sinkage the corresponding stress strain relationship must be investigated. Bekker [71] assumes a straight-line relationship between sinkage z and pressure p, which considers the soil to be elastic:

$$p = kz \tag{3.15}$$

where k is a coefficient of proportionality. For hard soil, k will be large and the sinkage z will be small and for a soft soil, k will be small and z will be large. A more general form of the equation was proposed by Letoshnev, Goriatchkin et al [76] who describe the relationship between static sinkage z and pressure p as:

$$p = kz^n \tag{3.16}$$

where n is the exponent corresponding to different soil types. Values of n were determined by Bernstein and Klein for average conditions *(n = ½)* and by Gerstner, Shultz, Goriatchkin and Grandvoinet for snow *(n = 1)*. However, $n = ½$ is the most frequently accepted value. In civil engineering soil mechanics, it is sometimes assumed that a small deformation z of the ground beneath a unit load p of a structure having width b (smaller dimension) may be expressed by the straight-line equation [71]:

$$p = \left(\frac{B}{b} + C\right)z \tag{3.17}$$

where B is a modulus of deformation due to the cohesive component of soil shear while C is a similar modulus due to the friction component. Both moduli are practically independent of the size or form of the load, but equation (3.17) is only valid for very small sinkage where z is small in comparison to b. Bekker therefore introduced exponent n to this equation assuming parameters B and C remain unchanged irrespective of the size of the load:

$$p = \left(\frac{kc}{b} + k\phi\right) z^n \tag{3.18}$$

where $k_c = B$, $k_\phi = C$ and b is the smaller dimension of the loading area, i.e. track or tread width. Tests performed by the Land Locomotion Laboratory show that equation (3.18) predicts load-sinkage with reasonable accuracy and may be used for the prediction of ground deformation in extensive sinkage. To define the relationship between sinkage and load, the soil parameters k_c, k_ϕ and n have to be measured. Apparatus to obtain such measurements are described by Bekker [71].

A phenomenon which should also be considered, and is not discussed in the literature, is the sinkage that takes place in addition to static sinkage z. Experimental evidence reported in this thesis has indicated that the initial static sinkage caused by a vertical load W is accompanied by additional dynamic sinkage due to the build up of the horizontal traction force T on the slipping boot cleat, which would not have existed when the cleat was initially loaded by vertical force W.

An alternative to the theoretical sinkage models described above, is to undertake sinkage measurement experiments using cleats and to develop an empirical model from the data. A similar approach was taken by Burland and Burbridge [77], for the settlement of foundations on sand and gravel.

4. Mathematical Modelling

4.1. Introduction

For walking or running on a surface, the compressive and shear forces that are applied to the ground, via the foot, may be modelled mathematically. For hard surfaces the interaction between the foot and the ground may be modelled by a coefficient of friction but for soft surfaces the interaction is dependent upon soil properties, water content, sinkage, sole material properties and tread geometry for different terrains. The relationship between cleat geometry, sinkage and traction has to be utilised, for example, a fell running shoe has small square cleats with large spacing to optimise cleat sinkage to gain grip in slippery conditions as well as optimise mud shedding. The soft sole compound enhances these properties. Traction is affected by the magnitude of F_b, the vertical force due to body mass, which will vary according to the size of the soldier, the amount of load being carried and the gait cycle. At heel strike this vertical force may increase to three times body weight and at another part of the cycle it may be less than body weight. The horizontal tractive force T also changes with respect to the gait cycle.

A series of two dimensional mathematical models of boot cleats on soil have been developed to investigate the effect of tread geometry, material properties, and soil conditions on traction performance. Although it would be ideal to use three dimensional models due to the nature of soils, confidence in two dimensional models may be gained by the two-dimensional work of Coulomb [59] and Bekker [53,71]. Bekker demonstrated that beneath a narrow wheel, soil was displaced sideways and longitudinally, creating a three-dimensional problem. However, beneath wide wheels, the soil displacement was primarily longitudinal, creating a two dimensional problem. This approach has been taken in both the theoretical and experimental work.

The models are based on simple tread geometry as illustrated by figure 4.1. They enable cleat dimensions to be varied, for example, cleat taper, cleat depth, cleat

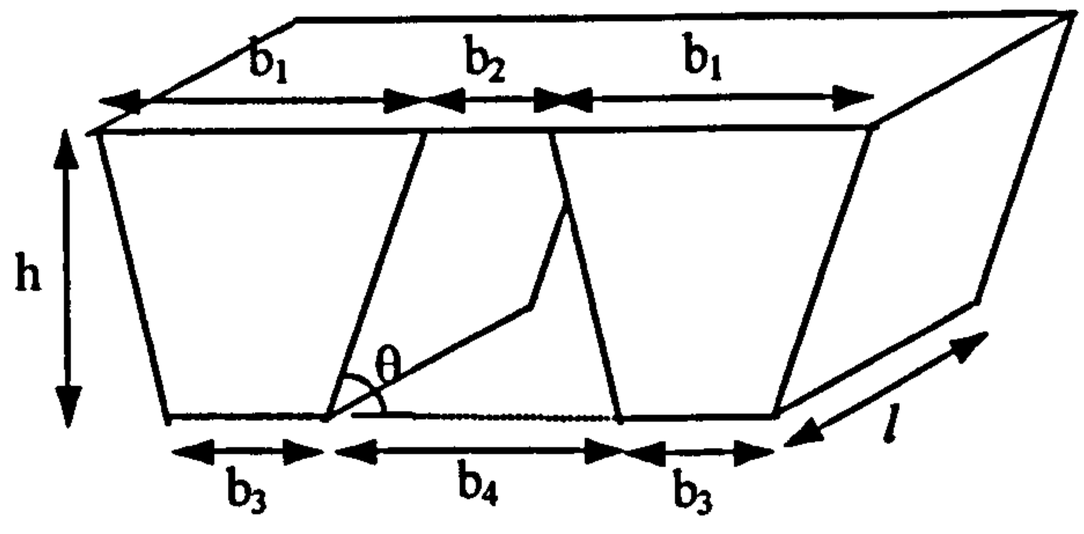

Figure 4.1: Cleat geometry (including taper)

width and cleat spacing. The models are applicable to different terrains such as cohesive or granular soils and allow for deformation of the soil between the cleats, hence changing the shape of the shear zones with different soil and sinkage conditions. Cohesion increases the shear strength of the soil and adhesion increases the friction between soil and cleat. If the soil is too sticky then mud shedding is seemingly impossible, resulting in the clogging up of cleats so that they are unable to function properly. Due to the changes in soil properties and water content over different terrains, variations in cleat sinkage and sole traction will occur. The different soil consistencies affecting the sinkage, create different soil-cleat interactions and contact areas. For this reason different models corresponding to different sinkage conditions have been considered. They show how the shear zones and application of forces change with respect to sinkage.

A front cleat and rear cleat, as illustrated by figure 4.1, the soil in between the two cleats, the soil in front of the leading cleat and the soil behind the trailing cleat are modelled. The cleat length, *l*, is assumed to be large compared to the other cleat dimensions and therefore soil flow is approximately two dimensional. Therefore, two dimensional soil flow is assumed in the mathematical models of the cleat and soil behaviour. The long cleat length produces a rib like cleat pattern much like a traditional tread design.

Figure 4.2 illustrates the external forces acting upon the front and rear cleats (per unit length) during horizontal slip after sinkage has occurred. The front and rear

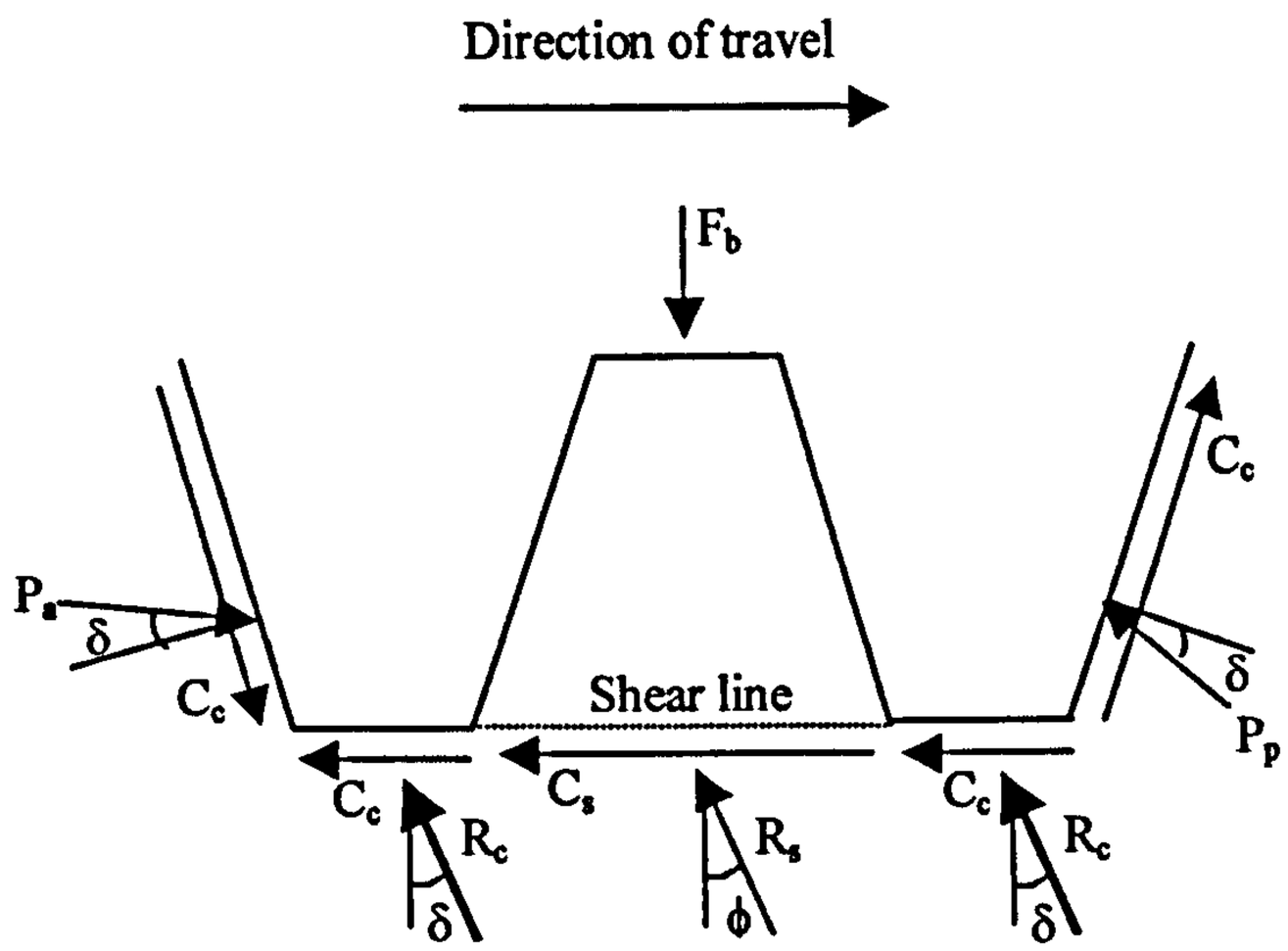

Figure 4.2: A free body diagram of cleats full of soil

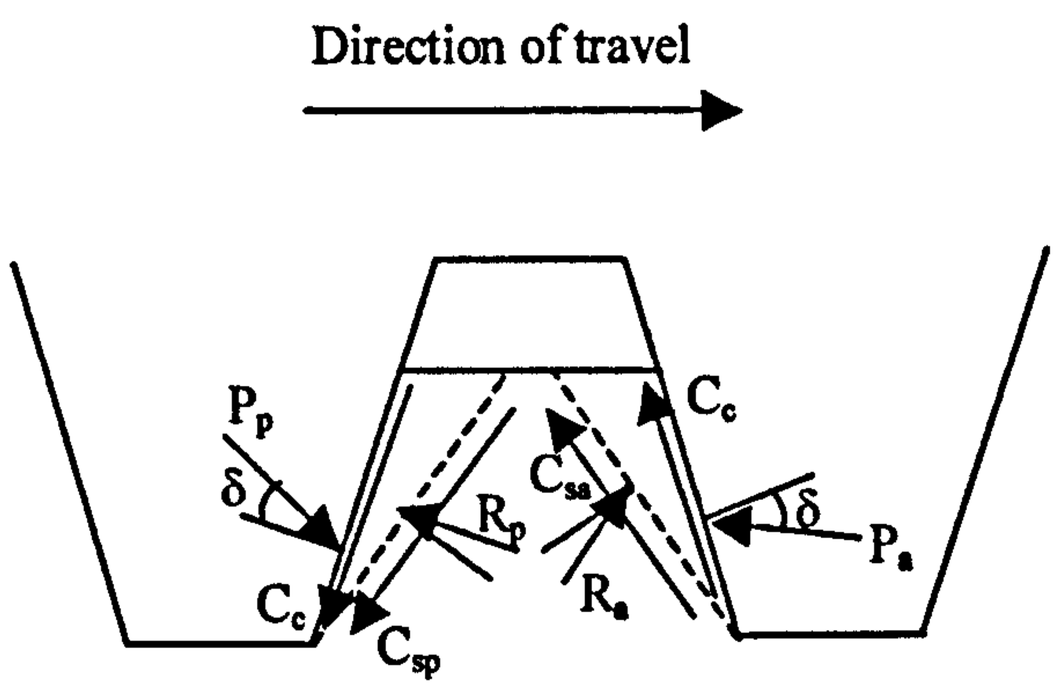

Figure 4.3: A passive and active triangular shear zone

cleat, including the soil in between, may be considered as one body in this instance. During the occurrence of slip, adhesive forces, C_c, are generated on the cleat surfaces, and a cohesive force, C_s, as the soil between the cleats shears along a shear plane. An active thrust, P_a, acts at an angle δ above the normal to the rear cleat surface as the cleats slip. A passive resistance to slip, P_p, also occurs at an angle δ below the normal to the front cleat surface. Resultant forces beneath the cleats and the soil in between are also developed, R_c and R_s, respectively. R_c acts at angle δ to the normal, where δ is the friction angle for cleats and soil, and R_s acts at angle ϕ to the normal, where ϕ is the friction angle of soil. The resultant forces are

generated from a vertical stress component, σ_c, and a horizontal friction component, $\sigma_c tan\delta$, beneath the cleats, and similarly $\sigma_s tan\phi$ and σ_s beneath the soil.

In this example the soil shear line, between the cleats, is assumed to be horizontal and the cleats full, however, the soil shear between the cleats could be more complicated. For example, there could be two triangular shear zones, one active and one passive, their shape being determined by the amount of sinkage and the shear angles. The forces acting on these zones are shown in figure 4.3. These forces include cleat-soil adhesive forces, C_c, and soil cohesion forces, C_{sp} and C_{sa}. Only when the cleats are full is a vertical load, F_b, applied to the soil within the cleats. The weight of the active and passive soil shear zones are W_a and W_p respectively. Resultant forces R_a and R_p act at an angle ϕ to the normal as shown by figure 4.3. Passive and active earth forces are applied to the soil shear zones at an angle δ above and below the normal as shown above. The standard soil mechanics theory that has been presented in chapter 3 was applied to cleats where the soil shear zones were considered to be triangular, however, it was also necessary to consider quadrilateral shear zones.

The shear zones between the cleats were first considered to be triangular, in which case the standard soil mechanics 'retaining wall' theory applied. Therefore, to calculate the total tractive force of the cleats, the passive and active earth forces could be derived using standard formulae for triangular shear zones. The required values of α_p and α_a could be found by putting the derivatives of K_p and K_a with respect to α equal to zero as seen in standard texts, or more easily by using a numerical approach as seen in this research.

The models based on standard soil mechanics theory are for triangular shear zones only. However, the models have to allow for change in shape of the shear zones, due to sinkage conditions and the restricted movement of the soil between the cleats. It was therefore required to adapt the retaining wall theory of Coulomb, the equations for the passive and active earth pressure coefficients K_p and K_a, and the total earth resistance accordingly.

Computer programs were developed using MATLAB to enable calculation of the minimum passive earth pressure and the maximum active earth pressure. Throughout this chapter it can be seen how the modelling developed from the simple application of standard soil theory using triangular shear zones, to use of quadrilateral shear zones, and then the modelling of passive and active shear zone interaction. At first, the models considered passive and active shear forces separately for simplicity but realistically they both co-exist so it was necessary to model their interaction.

4.1.1 The Sinkage Conditions

For the purpose of modelling horizontal slip three sinkage conditions have been assumed:

i Cleats partially full of soil

ii Cleats full of soil

iii No sinkage of cleats

These different sinkage conditions and the corresponding shapes of shear zones will now be introduced.

4.1.1.1. Cleats partially full of soil

Referring to figure 4.4, when the tread is not full due to partial sinkage, soil is able to move vertically and laterally between the cleats shearing at angles α_p and α_a. If α_p and α_a are large enough, two triangular shear zones will be formed, with the passive zone moving up into the air gap and the active zone moving down (see figure 4.4 (a)). However, if α_p and α_a are too small, the two zones will interact and therefore become two quadrilateral zones (see figure 4.4 (b)). In this case soil can transfer directly from the passive to the active zone as well as moving up into the air gap. There will be no vertical compression of the soil between the cleats due to the gap between the soil and the sole. Body weight will only be distributed over the cleat area resulting in increased pressure and friction beneath the cleats.

(a)

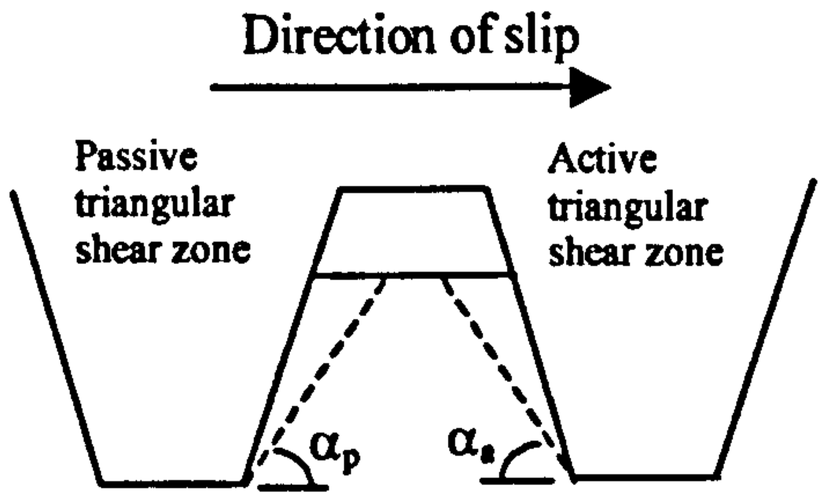

(b)

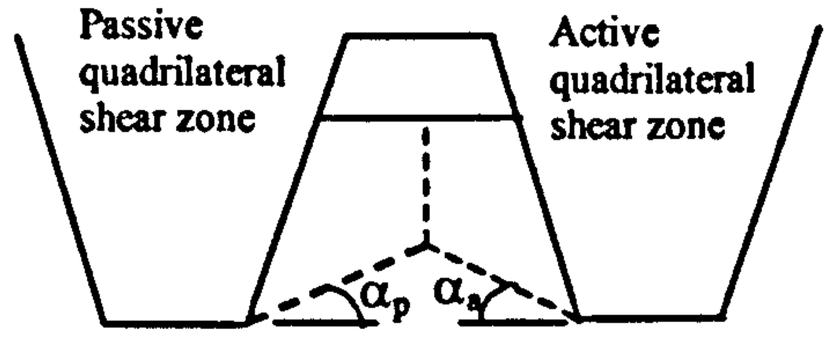

Figure 4.4: (a) Triangular and (b) quadrilateral shear zones

4.1.1.2. Cleats full of soil

Again, referring to figure 4.4, there will be two shear planes at angles α_p and α_a. However, in this case there is no air gap for a triangular passive shear zone to move up into. It was therefore assumed that two interacting quadrilateral zones would occur with soil transferring directly from the passive to the active zone.

Without an accurate sinkage model, it is difficult to predict the vertical compression of the soil between the cleats. However, for our purposes, it has been assumed that the soil is fully compressed in the sense that body weight is evenly distributed over the whole sole. In other words the pressure between the cleats is the same as the pressure under the cleats. In this way, the partially full model and the full model represent the two extremes with respect to soil compression between the cleats.

4.1.1.3. No sinkage of cleats

When there is no sinkage of the tread into the soil (figure 4.5) the interaction problem then becomes one of simple friction between the cleat bottoms and the soil.

4.1.2. Model Development

In this chapter, the model development is described in the sequence in which it actually occurred including the intermediate stages that led to the final model. Initially, triangular shear zone models were developed and tested against standard textbook results. This work is reported in section 4.2. Following this, quadrilateral shear zone models were developed that neglected the interaction of adjacent passive and active zones. This work is reported in section 4.3. Then interacting passive and active shear zones, as shown in figure 4.4(b), were modelled. This work is reported in section 4.4. Finally, a full model of a two cleat test-piece (figure 4.1) was created, as described in section 4.5. In all cases the models developed have been implemented as MATLAB programs.

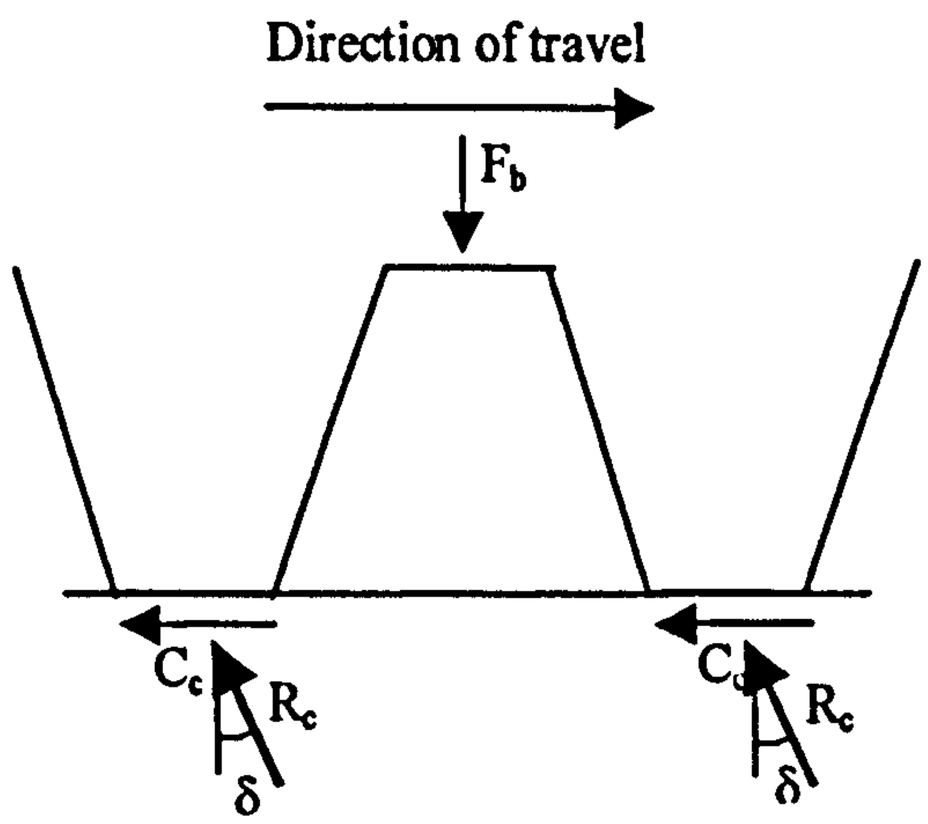

Figure 4.5: No sinkage of soil

4.2. Triangular Shear Zones

As previously discussed in the soil mechanics theory chapter, passive and active earth forces may be derived by standard formulae for triangular soil shear zones. The required value of shear angle α may be found by putting the derivatives of K_p and K_a with respect to α equal to zero as seen in standard texts. However, the author found the minimum passive earth force (or maximum active earth force) by a numerical search method where passive or active earth forces are calculated for a range of α. This was done in preparation for the modelling of quadrilateral zones.

4.2.1 Initial Model

An initial model was created to compare the results with existing retaining wall theory using triangular shear zones. Soil properties, cleat geometry and the range of α were entered into the MATLAB program enabling the area and mass of the soil segment to be calculated. The range of α was limited so that only a triangular soil segment could be formed. Then active and passive earth pressures were calculated and plotted for each value of α. From the curve, the program identifies the minimum value of P_p and the corresponding value of α, and similarly for the maximum value of P_a. The results were found to be consistent with soil testing data and existing theory. The programming could then be developed further for use with quadrilateral shear zones.

Example 1: Calculation of P_p (cohesion and adhesion = 0)

For triangular shear zones and the following inputs:

Unit weight of soil, $\gamma = 1.5 \times 10^{-6}$ N/mm^3

Incline of soil surface, $\beta = 0°$

Friction angle of soil, $\phi = 40°$

Friction angle of cleat, $\delta = 10°$

Angle of taper, $\theta = 90°$

Cleat height, H = 8mm

For a given α,

$$P_p = \frac{1}{2} K_p \gamma H^2 \tag{3.2}$$

Where,

$$K_p = \frac{\sin(\alpha+\phi)\sin(\theta-\beta)\sin(\theta+\alpha)}{\sin((\theta-\delta)-(\alpha+\phi))\sin^2\theta\sin(\alpha-\beta)}$$

Equation (3.2) for P_p and K_p was derived from the triangle of forces used in retaining wall theory, as discussed in chapter 3. The cleat geometry was then input into the computer model. From the MATLAB program, when α is equal to 19°, P_p is at a minimum and is equal to 0.35 x 10^{-3} N and K_p is equal to 7.3. From triaxial shear test data, K_p is equal to 6.5 for the same inputs [8]. Using Coulomb's theory, differentiating K_p with respect to α and putting it equal to zero, K_p also equals 7.3.

Example 2: Calculation of P_a (cohesion and adhesion = 0)

For triangular shear zones and the following inputs:

Unit weight of soil, $\gamma = 1.5 \times 10^{-6}$ N/mm^3

Incline of soil surface, $\beta = 0°$

Friction angle of soil, $\phi = 30°$

Friction angle of cleat, $\delta = 15°$

Angle of taper, $\theta = 90°$

Cleat height, H = 8mm

For a given α,

$$P_a = \frac{1}{2} K_a \gamma H^2 \tag{3.7}$$

Where,

$$K_a = \frac{\sin(\alpha-\phi)\sin(\theta-\beta)\sin(\theta+\alpha)}{\sin((\theta+\delta)-(\alpha-\phi))\sin^2\theta\sin(\alpha-\beta)}$$

From the MATLAB program, when α is equal to 65°, P_a is at a maximum and is equal to 1.49 x 10^{-5} N and K_a is equal to 0.31. Using Coulomb's theory, differentiating K_a with respect to α and putting it equal to zero, K_a also equals 0.31.

Since Coulomb's theory has been used in the modelling and programming work it has overestimated K_p as expected. What is significant is that the program results, using a numerical search method, are the same as those produced by the textbook differentiation method. This agreement of results has enabled the program to be further developed for quadrilateral shear zones.

The above examples consider cohesionless soil, but since existing and well proven soil mechanics theory for triangular shear zones is applied in the model, the same theory may be applied to cohesive soils:

$$P_p = \tfrac{1}{2} K_p \gamma H^2 + c_s H K_{pc} \tag{3.6}$$

Where,

$$K_{pc} = 2\sqrt{K_p(1+\frac{c_c}{c_s})}$$

And similarly for active earth force,

$$P_a = \tfrac{1}{2} K_a \gamma H^2 - c_s H K_{ac}$$

Where,

$$K_{ac} = 2\sqrt{K_a(1+\frac{c_c}{c_s})}$$

4.2.2. Model Development

Having established the initial program, the theory was applied to modelling the soil between cleats. Since the amount of sinkage depends on the terrain, the models include calculation of passive and active earth pressure for full cleats and partially full cleats.

For a cleat full of compressed soil, a proportion of the body weight will be transferred to the soil between the cleats. It has been assumed that the pressure is the same over the whole sole area. Therefore the percentage of the body weight

acting on the upper side of a triangular shear zone is equal to the percentage of the sole area that the upper side of the shear zone represents. In this case, using results from chapter 3, section 3.4, the passive and active earth forces, P_p and P_a, (when $\beta = 0$) are equal to:

$$P_p = \frac{(F_b + W)\sin(\alpha + \phi)}{\sin[(\theta - \delta) - (\alpha + \phi)]} \quad \text{(N)}$$

$$P_a = \frac{(F_b + W)\sin(\alpha - \phi)}{\sin[(\theta + \delta) - (\alpha - \phi)]} \quad \text{(N)}$$

Where F_b is the proportion of the body weight acting on the upper side of the triangular shear zone.

For a partially full cleat, body weight will not be transferred to the soil within the cleat i.e. $F_b = 0$, therefore (when $\beta = 0$):

$$P_p = \frac{W\sin(\alpha + \phi)}{\sin[(\theta - \delta) - (\alpha + \phi)]} \quad \text{(N)}$$

$$P_a = \frac{W\sin(\alpha - \phi)}{\sin[(\theta + \delta) - (\alpha - \phi)]} \quad \text{(N)}$$

4.3. Quadrilateral Shear Zones

The retaining wall model assumes a triangular shear zone for which the K_p and K_a equations, above, can be used. It also assumes that during shear failure the soil wedge is free to move up or down the failure plane. As discussed earlier, the soil between the cleats has restricted movement and it is likely that non-triangular zones will occur. At this time the accurate prediction of shear zone shapes is not possible. However, as discussed earlier, where the zones are not triangular they were assumed to be quadrilateral.

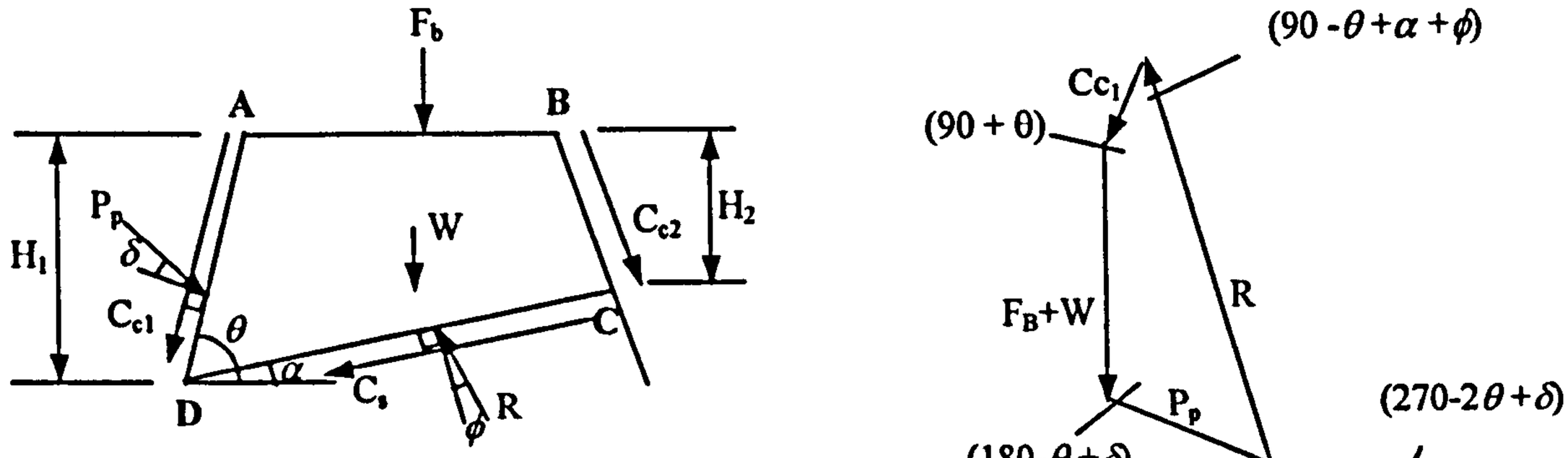

(a) Soil segment (c>0) (b) Polygon of forces (c>0)

Fig. 4.6: Adaptation of Coulomb's theory for a quadrilateral soil segment ABCD (passive case).

The MATLAB programs for quadrilateral shear zones were then developed by assuming that the zone is either active or passive but cannot be both. In other words, either a passive earth force is present or an active earth force, but not both.

It was therefore required to adapt Coulomb's theory, the equations for the passive and active earth pressure coefficients K_p and K_a, and the total earth resistance accordingly.

4.3.1 Passive Case

The quadrilateral shear zone ABCD, in figure 4.6, is acted upon by a passive earth force *(P_p)* at an angle δ to the normal, cohesion *(C_s)*, adhesion *(C_{c1})* and *(C_{c2})*, resultant *(R)* at angle ϕ to the normal and the vertical force due to body weight F_b. The weight W of the soil wedge itself is considered to be very small with respect to the vertical force due to body weight F_b. However, it has still been included. When considering the passive quadrilateral shear zone, it has been assumed that $P_a = 0$ and that shear will occur at minimum P_p.

The passive earth force P_p for a quadrilateral soil segment may be obtained by the consideration of the forces on the soil segment (figure 4.6a):

From figure 4.6a, resolving vertically↑

$$R\cos(\alpha+\phi)-F_b-W-P_p\cos(\theta-\delta)-C_{c1}\cos(90-\theta)-C_s\cos(90-\alpha)-C_{c2}\cos(90-\theta)=0$$

Therefore,

$$R=\frac{F_b+W}{\cos(\alpha+\phi)}+P_p\frac{\cos(\theta-\delta)}{\cos(\alpha+\phi)}+C_{c1}\frac{\cos(90-\theta)}{\cos(\alpha+\phi)}+C_s\frac{\cos(90-\alpha)}{\cos(\alpha+\phi)}+C_{c2}\frac{\cos(90-\theta)}{\cos(\alpha+\phi)} \quad (4.1)$$

From figure 4.6a, resolving horizontally⟶

$$-R\sin(\alpha+\phi)+P_p\sin(\theta-\delta)-C_{c1}\sin(90-\theta)-C_s\sin(90-\alpha)+C_{c2}\sin(90-\theta)=0$$

Therefore,

$$R=P_p\frac{\sin(\theta-\delta)}{\sin(\alpha+\phi)}-C_{c1}\frac{\sin(90-\theta)}{\sin(\alpha+\phi)}-C_s\frac{\sin(90-\alpha)}{\sin(\alpha+\phi)}+C_{c2}\frac{\sin(90-\theta)}{\sin(\alpha+\phi)} \quad (4.2)$$

Eliminating R by substitution,

$$P_p\left(\frac{\sin(\theta-\delta)}{\sin(\alpha+\phi)}-\frac{\cos(\theta-\delta)}{\cos(\alpha+\phi)}\right)=\frac{F_b+W}{\cos(\alpha+\phi)}+C_{c1}\left(\frac{\sin(90-\theta)}{\sin(\alpha+\phi)}+\frac{\cos(90-\theta)}{\cos(\alpha+\phi)}\right)$$
$$+C_s\left(\frac{\sin(90-\alpha)}{\sin(\alpha+\phi)}+\frac{\cos(90-\alpha)}{\cos(\alpha+\phi)}\right)$$
$$+C_{c2}\left(\frac{\cos(90-\theta)}{\cos(\alpha+\phi)}-\frac{\sin(90-\theta)}{\sin(\alpha+\phi)}\right)$$

$$P_p = \left(1\Big/\left(\frac{sin(\theta-\delta)}{sin(\alpha+\phi)} - \frac{cos(\theta-\delta)}{cos(\alpha+\phi)}\right)\right)\left(\frac{F_b+W}{cos(\alpha+\phi)} + C_{c1}\left(\frac{sin(90-\theta)}{sin(\alpha+\phi)} + \frac{cos(90-\theta)}{cos(\alpha+\phi)}\right)\right.$$
$$\left. + C_s\left(\frac{sin(90-\alpha)}{sin(\alpha+\phi)} + \frac{cos(90-\alpha)}{cos(\alpha+\phi)}\right) + C_{c2}\left(\frac{cos(90-\theta)}{cos(\alpha+\phi)} - \frac{sin(90-\theta)}{sin(\alpha+\phi)}\right)\right) \quad (4.3)$$

To find the position, α, of the shear line a MATLAB computer program is used to obtain the value of α corresponding to the minimum passive earth force. The program searches for the minimum value of P_P by inputting different values of α, over a given range, into equation (4.3) until the required value of α is found. The range of α is limited so that only a quadrilateral soil segment can be formed.

Cleat geometry (cleat height, cleat width, angle of taper and depth of cleat), soil properties (cohesion, adhesion, shear angles and unit weight of the soil), applied body weight for the cleat under consideration and sinkage are input into the program. The sinkage condition to be evaluated must also be input into the program. When full sinkage is under consideration, the pressure due to body weight is assumed to be the same over the whole sole and acts on the top side of the shear zone. When only partial sinkage is under consideration, body weight is not transferred to the soil between the cleats, therefore, $F_b = 0$, due to the air gap between the soil and the top of the cleat.

4.3.2. Active Case

The quadrilateral wedge ABCD, in figure 4.7, is acted upon by an active earth force *(P_a)* at an angle δ to the normal, cohesion *(C_s)*, adhesion *(C_{c1})* and *(C_{c2})*, resultant *(R)* at angle ϕ to the normal and the vertical force due to body weight F_b. When considering the active quadrilateral shear zone, it has been assumed that $P_p = 0$ and that shear will occur at maximum P_a.

Similarly, the active earth force P_a for a quadrilateral soil segment may be obtained by consideration of the forces (per unit length) on the soil segment (figure 4.7a):

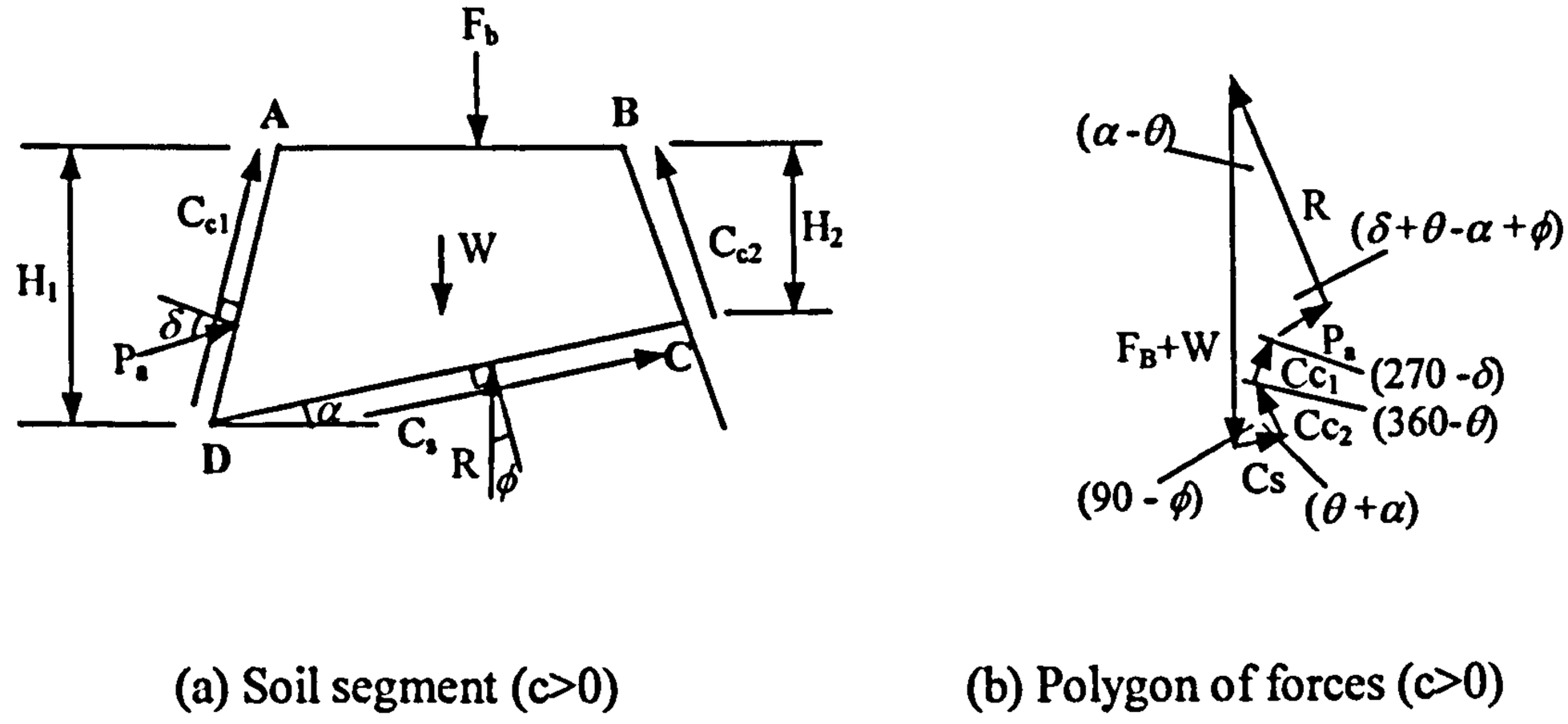

(a) Soil segment (c>0) (b) Polygon of forces (c>0)

Fig. 4.7: Adaptation of Coulomb's theory for a quadrilateral soil segment ABCD (active case).

From figure 4.7a, resolving vertically ↑

$$R\cos(\alpha-\phi)-F_b-W-P_a\cos(\theta+\delta)+C_{c1}\cos(90-\theta)+C_s\cos(90-\alpha)+C_{c2}\cos(90-\theta)=0$$

Therefore,

$$R=\frac{F_b+W}{\cos(\alpha-\phi)}+P_a\frac{\cos(\theta+\delta)}{\cos(\alpha-\phi)}-C_{c1}\frac{\cos(90-\theta)}{\cos(\alpha-\phi)}-C_s\frac{\cos(90-\alpha)}{\cos(\alpha-\phi)}-C_{c2}\frac{\cos(90-\theta)}{\cos(\alpha-\phi)} \quad (4.4)$$

From figure 4.7b, resolving horizontally ⟶

$$-R\sin(\alpha-\phi)+P_a\sin(\theta+\delta)+C_{c1}\sin(90-\theta)+C_s\sin(90-\alpha)-C_{c2}\sin(90-\theta)=0$$

Therefore,

$$R=P_a\frac{\sin(\theta+\delta)}{\sin(\alpha-\phi)}+C_{c1}\frac{\sin(90-\theta)}{\sin(\alpha-\phi)}+C_s\frac{\sin(90-\alpha)}{\sin(\alpha-\phi)}-C_{c2}\frac{\sin(90-\theta)}{\sin(\alpha-\phi)} \quad (4.5)$$

Eliminating R by substitution,

$$P_a\left(\frac{\sin(\theta+\delta)}{\sin(\alpha-\phi)}-\frac{\cos(\theta+\delta)}{\cos(\alpha-\phi)}\right)=\frac{F_b+W}{\cos(\alpha-\phi)}-C_{c1}\left(\frac{\sin(90-\theta)}{\sin(\alpha-\phi)}+\frac{\cos(90-\theta)}{\cos(\alpha-\phi)}\right)$$
$$-C_s\left(\frac{\sin(90-\alpha)}{\sin(\alpha-\phi)}+\frac{\cos(90-\alpha)}{\cos(\alpha-\phi)}\right)$$
$$-C_{c2}\left(\frac{\cos(90-\theta)}{\cos(\alpha-\phi)}-\frac{\sin(90-\theta)}{\sin(\alpha-\phi)}\right)$$

$$P_a=\left(1\Big/\left(\frac{\sin(\theta+\delta)}{\sin(\alpha-\phi)}-\frac{\cos(\theta+\delta)}{\cos(\alpha-\phi)}\right)\right)\left(\frac{F_b+W}{\cos(\alpha-\phi)}-C_{c1}\left(\frac{\sin(90-\theta)}{\sin(\alpha-\phi)}+\frac{\cos(90-\theta)}{\cos(\alpha-\phi)}\right)\right.$$
$$\left.-C_s\left(\frac{\sin(90-\alpha)}{\sin(\alpha-\phi)}+\frac{\cos(90-\alpha)}{\cos(\alpha-\phi)}\right)-C_{c2}\left(\frac{\cos(90-\theta)}{\cos(\alpha-\phi)}-\frac{\sin(90-\theta)}{\sin(\alpha-\phi)}\right)\right) \quad (4.6)$$

A MATLAB program has also been developed to obtain the value of the shear angle α corresponding to the maximum active earth force. Again, cleat geometry, soil properties, applied body weight and sinkage are input into the program. The program searches for the maximum value of P_a by substituting different values of α, over a given range, into equation (4.6) until the required value of α is found.

4.3.3. Testing the Models

It was deemed necessary to check the programs by carrying out hand calculations and graphical checks to make sure no mathematical errors were produced, although this was quite time consuming. The hand calculations were carried out to ensure there were no disagreements with MATLAB. Then passive and active force polygons were graphically constructed by hand, using the calculated magnitude of each force for specific values of α, to check that the forces did in fact form closed polygons. Hand calculations were found to agree with MATLAB and the polygons all joined quite accurately. These checks confirmed that the programs were working satisfactorily.

4.4. Passive and Active Shear Zone Interaction for Quadrilateral Shear Zones

The modelling then became more complex by consideration of passive and active shear zone interaction (figure 4.8), the models developed so far had only considered these earth forces and shear zones separately. As horizontal slip occurs it is assumed that soil at the rear of the cleat space, the passive shear zone, will move forwards and upwards along a shear line. The soil at the front of the cleat space, the active shear zone however, is expected to move down and forwards along another shear line as shown by figure 4.8. At some point within the whole soil mass, the passive and active shear zones will interact with zero lateral strain, the horizontal stress being only that due to body and soil weight. The author has assumed that this occurs on the vertical line drawn at the point where the two shear lines intersect. On this vertical interaction line, the horizontal force component of R, due to the absence of lateral strain, is considered as the passive earth force at rest, usually expressed in terms of effective stress P_o.

In general:

$$p_o = K_o \gamma' z \tag{4.7}$$

where, K_o is defined as the coefficient of earth pressure at rest and γ' is the effective unit weight of soil. K_o is equal to 0.5 for a medium density sand [8].

4.4.1. Modelling Passive and Active Earth Force Interaction

The modelling work to date has enabled the shear angles of the passive and active shear zones to be obtained separately with the use of MATLAB computer programs. To enable the shear angles to be obtained in this case it was necessary to consider combined active and passive force polygons to derive equations for P_p and P_a, illustrated by figure 4.10. The polygons share the common forces R and C_s, which act on the vertical interface between the passive and active shear zones. It was again necessary to limit the ranges of α_p and α_a to ensure only quadrilateral soil segments were formed, (see figure 4.9). Therefore, the following relationship was enforced:

$$H_1 \tan(90-\alpha_a) + H_1 \tan(90-\alpha_p) > x$$

It was also necessary to determine the geometric relationship between the passive and active soil wedges, as illustrated by figure 4.9 by solving the following equations:

$y = x_p \tan\alpha_p = x_a \tan\alpha_a$

$x = x_p + x_a$

When there is no taper, $b_2 = x$.

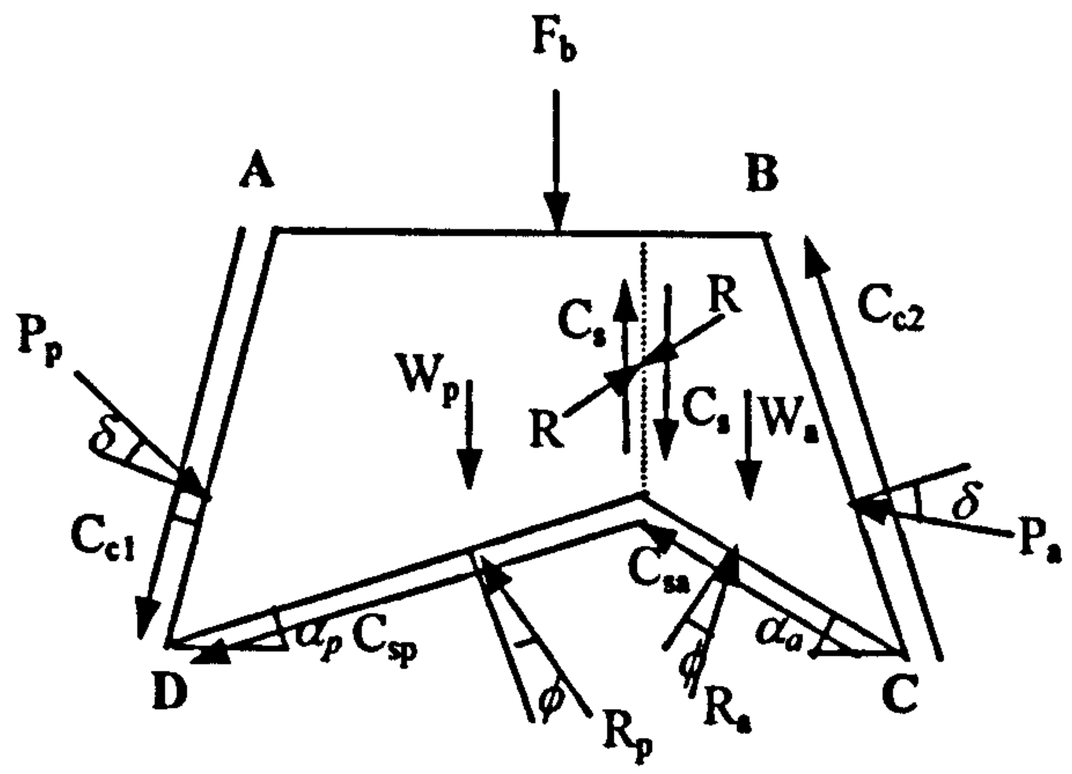

Fig. 4.8: Passive and active interaction

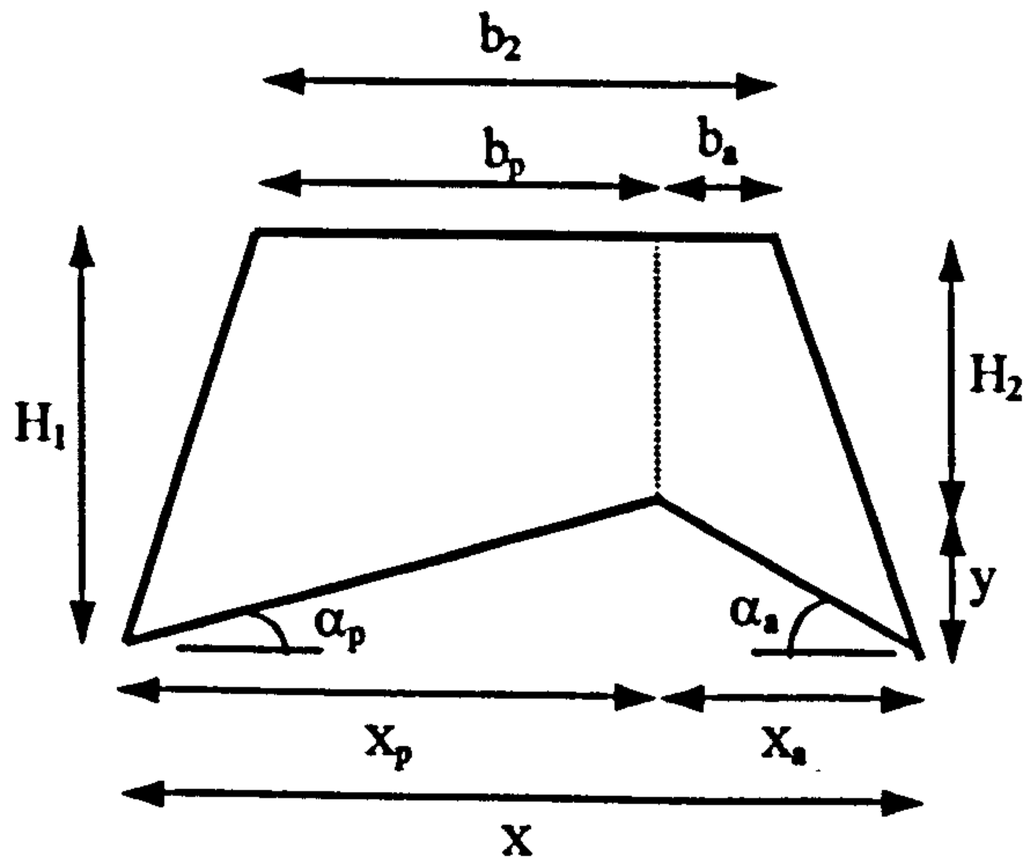

Fig. 4.9: Combined geometry

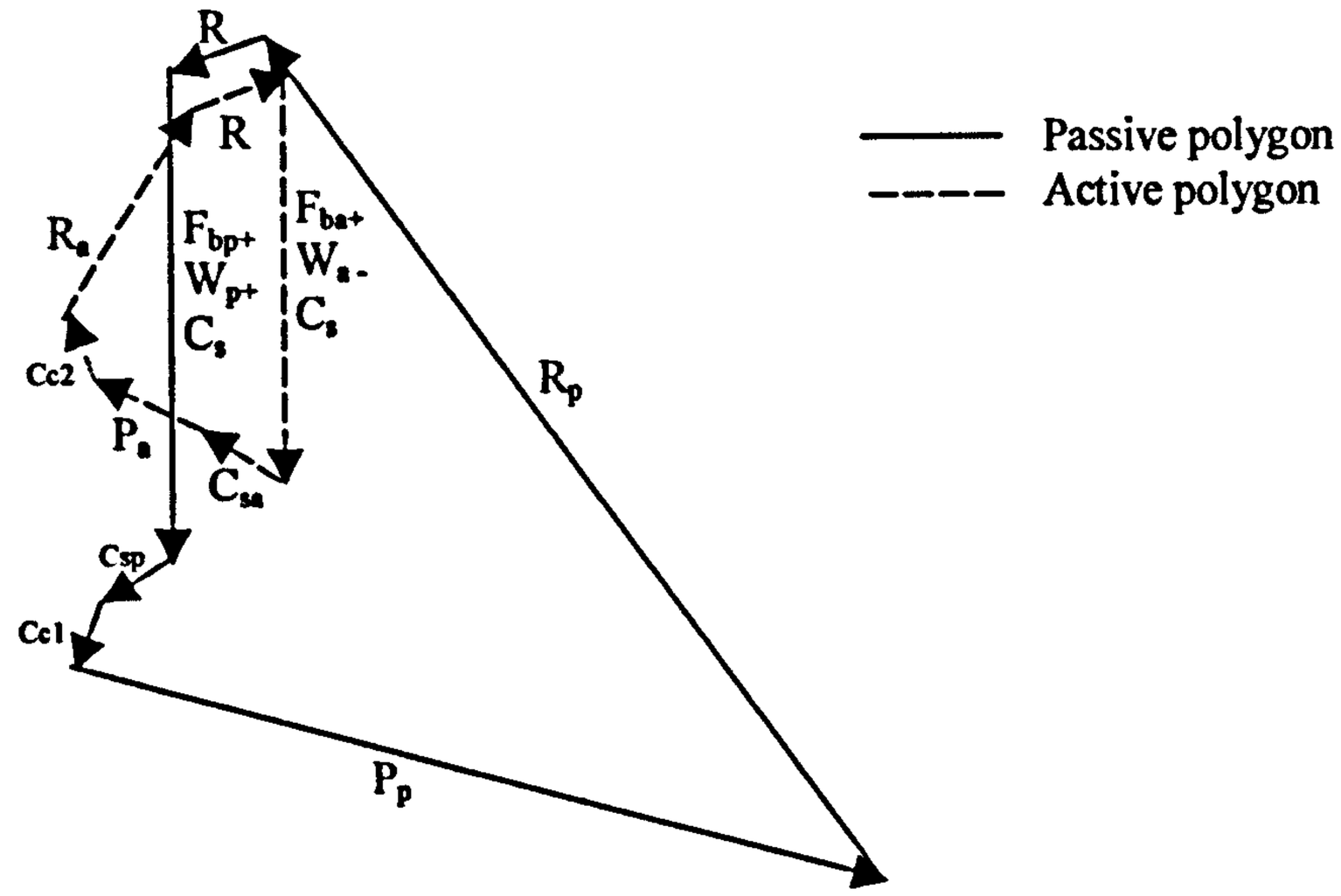

Fig. 4.10: Combined passive and active force polygons

C_s (common to both passive and active) = $c_s H_2$

$C_{c2} = C_{c1} = c_c H_1 / \cos(90-\theta)$

$C_{sp} = c_s(H_1-H_2)/ \sin\alpha_p$

$C_{sa} = c_s(H_1-H_2)/ \sin\alpha_a$

$F_{bp} = (F_b/ b_2)b_p$

$F_{ba} = (F_b/ b_2)b_a$

$W_p = area_p \gamma'$

$W_a = area_a \gamma'$

The passive earth force has been derived from the free body diagram (figure 4.11). The angle of taper has been limited to the range $45 < \theta < 90$ degrees.

From figure 4.11, resolving vertically↑

$$R_p \cos(\alpha_p + \phi) - F_{bp} - W_p - C_s - P_p \cos(\theta - \delta) - C_{c1} \sin\theta - C_{sp} \sin\alpha_p - R \sin\phi = 0$$

Therefore,

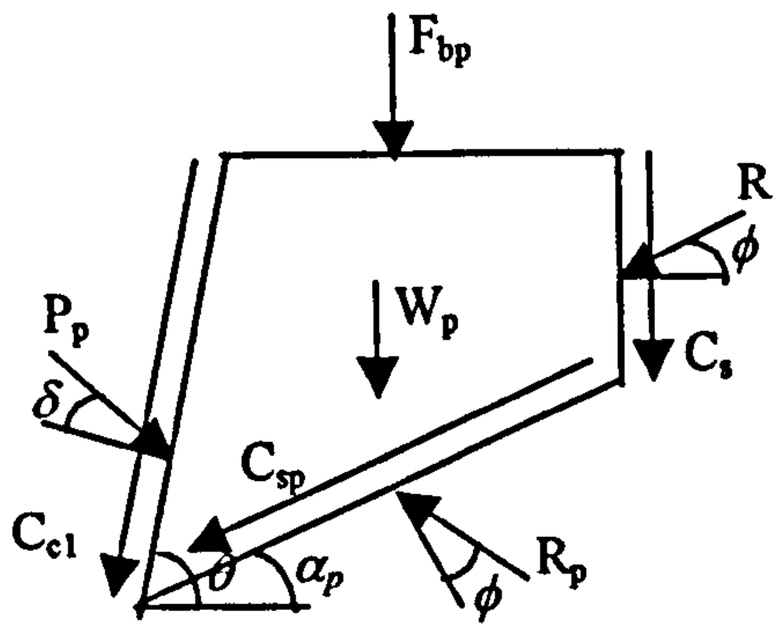

Figure 4.11: Passive segment

$$R_p = \frac{F_{bp} + W_p + C_s}{\cos(\alpha_p + \phi)} + P_p \frac{\cos(\theta - \delta)}{\cos(\alpha_p + \phi)} + C_{c1} \frac{\sin\theta}{\cos(\alpha_p + \phi)} + C_{sp} \frac{\sin\alpha_p}{\cos(\alpha_p + \phi)} + R \frac{\sin\phi}{\cos(\alpha_p + \phi)} \quad (4.8)$$

From figure 4.11, resolving horizontally⟶

$$-R_p \sin(\alpha_p + \phi) + P_p \sin(\theta - \delta) - C_{c1} \cos\theta - C_{sp} \cos\alpha_p - R\cos\phi = 0$$

Therefore,

$$R_p = P_p \frac{\sin(\theta - \delta)}{\sin(\alpha_p + \phi)} - C_{c1} \frac{\cos\theta}{\sin(\alpha_p + \phi)} - C_{sp} \frac{\cos\alpha_p}{\sin(\alpha_p + \phi)} - R \frac{\cos\phi}{\sin(\alpha_p + \phi)} \quad (4.9)$$

Eliminating R_p by substitution,

$$P_p \left(\frac{\sin(\theta - \delta)}{\sin(\alpha_p + \phi)} - \frac{\cos(\theta - \delta)}{\cos(\alpha_p + \phi)} \right) = \frac{F_{bp} + W_p + C_s}{\cos(\alpha_p + \phi)} + C_{c1} \left(\frac{\sin\theta}{\cos(\alpha_p + \phi)} + \frac{\cos\theta}{\sin(\alpha_p + \phi)} \right)$$
$$+ C_{sp} \left(\frac{\sin\alpha_p}{\cos(\alpha_p + \phi)} + \frac{\cos\alpha_p}{\sin(\alpha_p + \phi)} \right)$$
$$+ R \left(\frac{\sin\phi}{\cos(\alpha_p + \phi)} + \frac{\cos\phi}{\sin(\alpha_p + \phi)} \right)$$

$$P_p = \left(1\Big/\left(\frac{sin(\theta-\delta)}{sin(\alpha_p+\phi)} - \frac{cos(\theta-\delta)}{cos(\alpha_p+\phi)}\right)\right)\left(\frac{F_{bp}+W_p+C_s}{cos(\alpha_p+\phi)}\right.$$

$$+C_{c1}\left(\frac{sin\theta}{cos(\alpha_p+\phi)}+\frac{cos\theta}{sin(\alpha_p+\phi)}\right)+C_{sp}\left(\frac{sin\alpha_p}{cos(\alpha_p+\phi)}+\frac{cos\alpha_p}{sin(\alpha_p+\phi)}\right) \qquad (4.10)$$

$$\left.+R\left(\frac{sin\phi}{cos(\alpha_p+\phi)}+\frac{cos\phi}{sin(\alpha_p+\phi)}\right)\right)$$

Similarly, the active earth force has been derived from the free body diagram (figure 4.12). Again, the angle of taper has been limited to the range $45 < \theta < 90$ degrees.

From figure 4.12, resolving vertically↑

$$R_a\, cos(\phi-\alpha_a) - F_{ba} - W_a + C_s - P_a\, cos(\theta+\delta) + C_{c2}\, sin\theta + C_{sa}\, sin\alpha_a + R\, sin\phi = 0$$

Therefore,

$$R_a = \frac{F_{ba}+W_a-C_s}{cos(\phi-\alpha_a)} + P_a\frac{cos(\theta+\delta)}{cos(\phi-\alpha_a)} - C_{c2}\frac{sin\theta}{cos(\phi-\alpha_a)} - C_{sa}\frac{sin\alpha_a}{cos(\phi-\alpha_a)} - R\frac{sin\phi}{cos(\phi-\alpha_a)} \qquad (4.11)$$

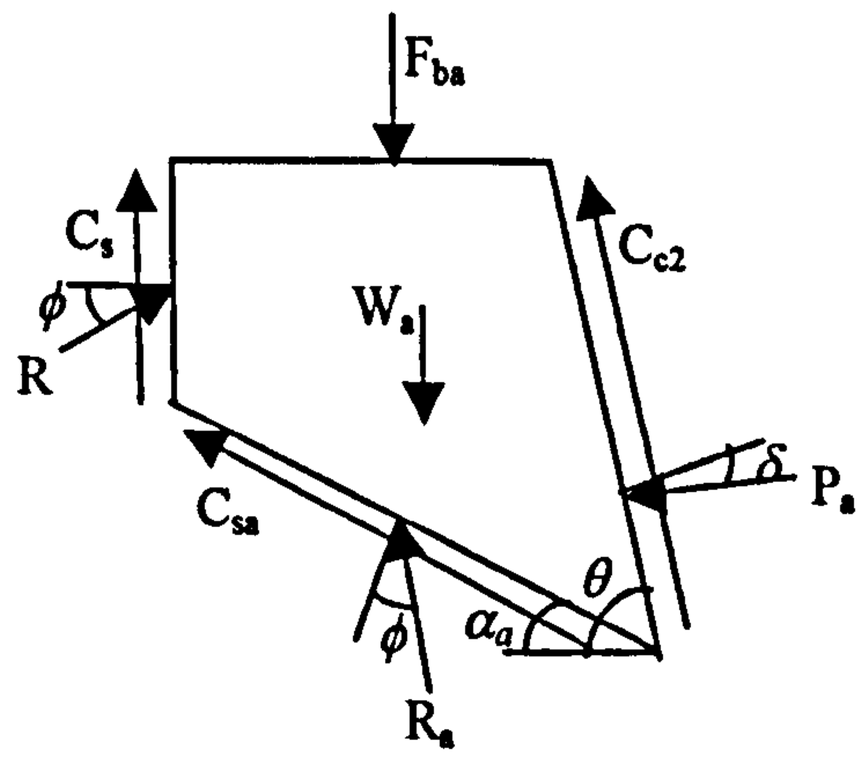

Figure 4.12: Active segment

From figure 4.12, solving horizontally ⟶

$$-R_a \sin(\phi-\alpha_a)-P_a \sin(\theta+\delta)-C_{c2}\cos\theta-C_{sa}\cos\alpha_a+R\cos\phi=0$$

Therefore,

$$R_a=-P_a\frac{\sin(\theta+\delta)}{\sin(\phi-\alpha_a)}-C_{c2}\frac{\cos\theta}{\sin(\phi-\alpha_a)}-C_{sa}\frac{\cos\alpha_a}{\sin(\phi-\alpha_a)}+R\frac{\cos\phi}{\sin(\phi-\alpha_a)} \qquad (4.12)$$

Eliminating R_a by substitution,

$$P_a\left(\frac{\sin(\theta+\delta)}{\sin(\phi-\alpha_a)}+\frac{\cos(\theta+\delta)}{\cos(\phi-\alpha_a)}\right)=R\left(\frac{\cos\phi}{\sin(\phi-\alpha_a)}+\frac{\sin\phi}{\cos(\phi-\alpha_a)}\right)-C_{c2}\left(\frac{\cos\theta}{\sin(\phi-\alpha_a)}-\frac{\sin\theta}{\cos(\phi-\alpha_a)}\right)$$
$$-C_{sa}\left(\frac{\cos\alpha_a}{\sin(\phi-\alpha_a)}-\frac{\sin\alpha_a}{\cos(\phi-\alpha_a)}\right)-\frac{F_{ba}+W_a-C_s}{\cos(\phi-\alpha_a)}$$

$$P_a=1\Bigg/\left(\frac{\sin(\theta+\delta)}{\sin(\phi-\alpha_a)}+\frac{\cos(\theta+\delta)}{\cos(\phi-\alpha_a)}\right)\left(R\left(\frac{\cos\phi}{\sin(\phi-\alpha_a)}+\frac{\sin\phi}{\cos(\phi-\alpha_a)}\right)-\left(\frac{F_{ba}+W_a-C_s}{\cos(\phi-\alpha_a)}\right)\right.$$
$$\left.-C_{c2}\left(\frac{\cos\theta}{\sin(\phi-\alpha_a)}-\frac{\sin\theta}{\cos(\phi-\alpha_a)}\right)-C_{sa}\left(\frac{\cos\alpha_a}{\sin(\phi-\alpha_a)}-\frac{\sin\alpha_a}{\cos(\phi-\alpha_a)}\right)\right)$$

(4.13)

Cohesive and adhesive forces have been considered within this model. If a granular soil is to be modelled, cohesion and adhesion may just be input as zero.

Cleat geometry (cleat height, cleat width, angle of taper and depth of cleat), soil properties (cohesion, adhesion, shear angles and unit weight of the soil), applied body weight for the cleat space under consideration and sinkage are input into the program to enable the geometry, area and weight of the soil segments to be calculated, and then all the forces to be calculated.

To find the position of the combined active and passive shear lines a MATLAB program has been developed to simultaneously obtain values of P_p and P_a, equations (4.10) and (4.13) respectively, for given ranges of α_p and α_a (see flow chart, Appendix III). It is the minimum combined earth resistance that is required, which is not necessarily the combination of the maximum active earth force and the minimum passive earth force. A three dimensional graph is constructed by the program to show α_p, α_a and the total earth resistance. The program is able to determine the minimum total earth resistance and the corresponding shear angles.

The model for combined active and passive earth pressure has been developed for both partially full and full cleats. When the cleats are partially full, there is an air gap, so the applied vertical load is not transferred to the ground via the soil in between the cleats. When the cleats are full, the applied load is transferred to the ground via the soil within the cleats so that the pressure beneath the cleats is the same as that beneath the space between the cleats.

4.4.2. Testing the Model

For this model, a series of checks have been done to ensure there have been no mathematical errors. First of all, some hand calculations were carried out to ensure there were no disagreements with MATLAB, and then force polygons were constructed by hand using the calculated magnitude of each force, to check that closed polygons were formed. Polygons were constructed for $\alpha_p = \alpha_a = 0.5$ and 45.° The value of 0.5° was considered to be the minimum shear angle since the program can produce errors when zero is used.

4.5. Total Traction Force

All of the models that have been presented so far have considered the soil between the cleats only. It is necessary to consider all of the horizontal forces on the boot, or cleats, to obtain a total traction force, T. The free body diagram in figure 4.13 shows the forces acting on the cleats and the soil in between. By resolving horizontally, the total traction force is given by:

$$T = P_{pt}\sin(\theta-\delta)+C_c-C_{cr}\cos\theta+R_c\sin\delta-P_{at}\sin(\theta+\delta)-C_{cf}\cos\theta+C_c$$
$$+R_c\sin\delta+C_{sp}\cos\alpha_p+R_p\sin(\alpha_p+\phi)+C_{sa}\cos\alpha_a-R_a\sin(\alpha_a-\phi) \qquad (4.14)$$

The forces acting on the soil between the cleats are obtained by using the interacting shear zones model described in section 4.4. The forces on the front of the front cleat and the rear of the rear cleat are obtained by assuming triangular shear zones (passive and active respectively). Simple adhesion and friction act on the undersides of the two cleats.

The minimum T is required since slip will occur at the plastic equilibrium point of minimum resistance. Therefore the sand at the front and rear of the cleats was modelled using the standard passive and active retaining wall theory since triangular shear zones have been assumed. The passive earth force at the front of the cleat, P_{pt}, was calculated for a range of shear angles, α_{pt}. The minimum passive earth force was determined with the corresponding value of α_{pt}. Similarly, the active earth force at the rear of the cleat, P_{at}, was calculated for a range of shear angles, α_{at}, and the maximum active earth force was determined with the corresponding value of α_{at}. These soil shear zones and corresponding passive and active earth forces are independent of each other and of the passive and active

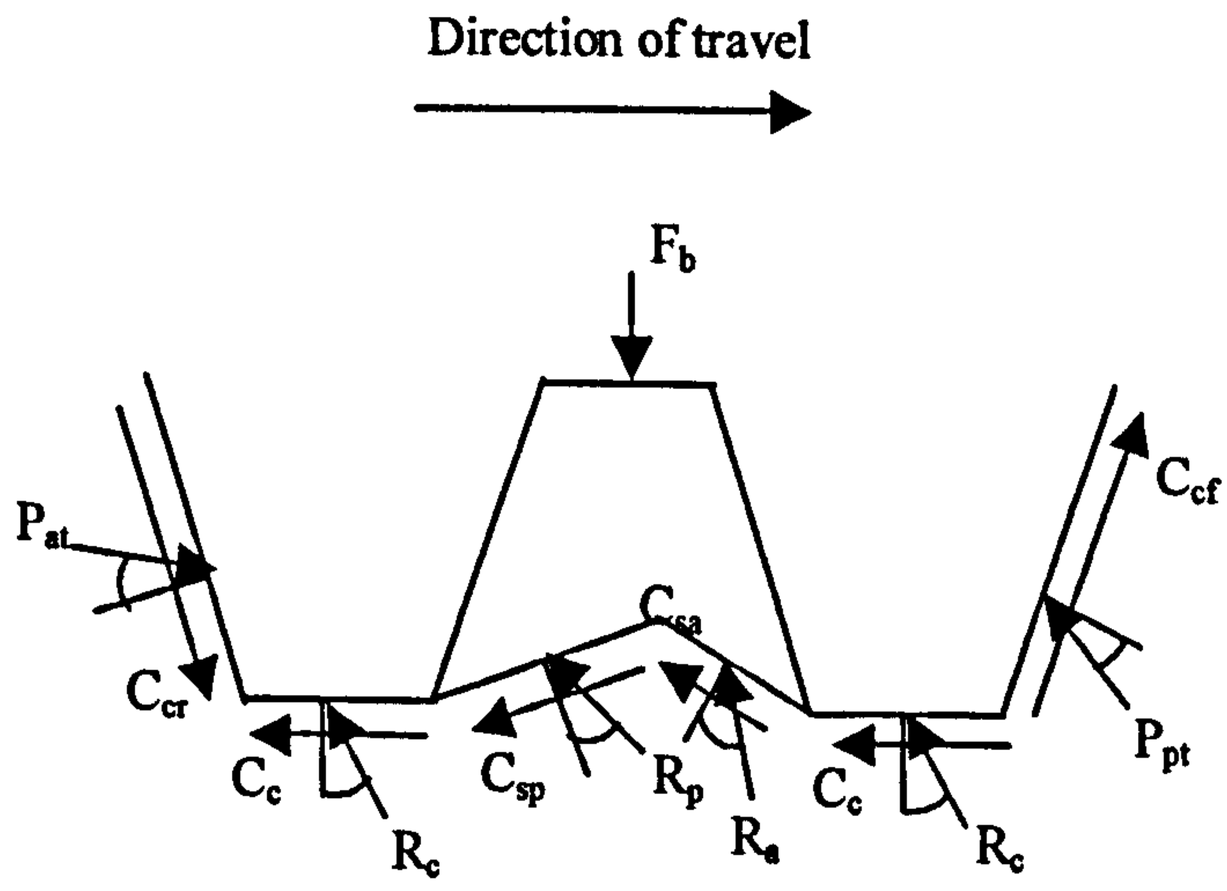

Figure 4.13: Free body diagram showing traction forces acting upon the cleats and soil in between.

interaction between the cleats. The model then considered the passive and active shear zone interaction between the cleats and the forces acting on the soil. The combined P_p and P_a was calculated for a range of passive and active shear angles, α_p and α_a respectively, different to those at the front and rear of the cleat for the triangular shear zones. The minimum combined horizontal force, in other words the minimum sum of the horizontal forces (R_p, R_a, C_{sp} and C_{sa}) was determined with the corresponding values of α_p and α_a, the values of which were input into equation 4.14.

The total traction, considering the forces between the cleats, beneath and in front of and behind the cleats was then calculated using the horizontal components of the minimum passive earth force P_{pl}, the maximum active earth force P_{al}, adhesion C_c, C_{cf} and C_{cr}, cohesion C_s, C_{sp} and C_{sa}, and reactive forces R_c, R_a and R_p as in equation 4.14.

4.6. Sinkage Modelling

The mathematical models for traction require a sinkage level input, it was therefore considered necessary to develop a separate sinkage model. The application of bearing capacity theory using shape factors would enable the prediction of when a cleat would sink, for both two dimensional and three dimensional cases, but would not be able to indicate the amount of sinkage.

Foundation settlement was then investigated [9,11], the methods of Terzaghi, Meyerof and Schmertmann were considered. Terzaghi's method, for immediate settlement, was developed as a design criterion to achieve 25mm settlement so was not considered appropriate. Meyerhof's method for a quick estimate of settlement required data from Dutch cone penetration tests, a technique that results in an empirical factor, which was not considered appropriate either because the cone shape did not represent that of cleats or boot sole and did not differentiate between different soil parameters. Schmertmann's method was considered far too complex for the requirements of this research and was designed for long term settlement prediction, again data from Dutch cone penetration tests was required.

The author decided to establish an empirical model based on cleat measurements. This approach was also taken by Burland and Burbridge [77] who carried out statistical analysis of foundation settlement on sands and gravels. Relationships were established between compressibility of soil (a_f), width of foundation (B), average penetration resistance (N) over depth of influence of the foundation.

Sinkage data was collected from the eight full factorial experiments carried out using different cleat shapes to enable relationships between sinkage, vertical load and geometry to be established. However, when the data was analysed it was not possible to determine any relationships because of the large amount of scatter.

5. The Soft Ground Slip-Rig

5.1 Introduction

Existing footwear slip-rigs, such as the PM144 rig [78,79] used at the Defence Clothing and Textiles Agency (DCTA) Colchester, Adidas, SATRA and Inter-Tech are designed for testing traction on hard surfaces such as steel decking, tarmacadam, clay tiles etc. Although the PM144 slip-rig and experimental procedures comply with British Standards, inconsistency in results between the different PM144 installations are seen even though most of the rigs have been calibrated by the same personnel. The walking simulator used at the Institute of Industrial Technology (TNO), Eindhoven and the walking simulator designed at Worchester Polytechnic Institute, Massachusetts could be used with a variety of soft and hard surfaces [80]. The rig at TNO was visited although it was not seen in operation. The rig could be used as a walking simulator through the cycle of heel strike to toe off where the impact of walking and the flexibility of the shoe can also be taken into account, or as a slip-rig where the foot does not roll. However, little is known about its results, experimental procedures and compliance with British and European Standards. It is known that European footwear testing standards vary considerably between each other and also with British Standards. Other rig designs, including that of Valiant (Nike) [32] and Barry and Milburn [49,51] were discovered during the literature study, however, little is known about their operation procedures and standards either.

Having reviewed existing slip rigs it became apparent that there were only two options, either to modify the PM144 rig at DCTA or to construct a new test rig since the walking simulator at TNO and other PM144 rigs were not available. After some consideration, it was deemed unrealistic to modify the PM144 rig at DCTA for work with soft materials such as sand or soil since it would only allow a depth of 35mm of soil. The rig would also have to be used in conjunction with hard surface testing by DCTA so any modifications would have to be temporary. It was therefore considered necessary to construct a prototype soft-ground slip-rig at Salford, Pisani and Howard [81].

The prototype soft-ground slip-rig is a manually operated device based on simple mechanical mechanisms using weights and pulleys. Equipment such as force transducers were not used due to cost and since calibration would be required, probably by the use of weights anyway. The preparation of the soil tray was considered the most important factor although the most time consuming, automation of the rig in any sense would not have affected soil preparation or made it any easier. Arguably, any increased sensitivity in applied force and sinkage measurement would have been deemed insignificant with respect to human error in manual soil preparation.

The test rig enables the measurement of tread traction and sinkage for different soil types and tread geometry at various angles of heel contact with an applied vertical load. It can also be used for observation of soil shear patterns by means of a viewing window. The latter is best achieved with the use of a scaled up tread pattern since soil shear observations would not be possible with normal scale cleats.

5.2. The Prototype Soft Ground Slip-Rig

The slip-rig is illustrated by figure 5.1. The test rig consists of a main frame (1) and rotational cross bar (2). The rotational cross bar is able to move from side to side to enable a number of slip runs in one tray of soil. It is held by locking screws (3) at both ends and is used to pre-set the angle of contact of the tread to the soil surface. A shoe last (4) to which footwear and cleat samples are attached is connected to a hardened steel pole (5) that slides through a bearing assembly located within the rotational bar. An anti-rotation device (6) has been fitted to the pole to maintain a forward direction of the cleats during testing and also to ensure no damage to the bearing assembly. The pole also has a loading platform (7) at its other end where the vertical load is applied using free weights. Having set the lateral position of the rotational bar and the contact angle of the tread, and having applied the vertical load using the weights, the position of the shoe last is determined. A soil tray (8) is mounted on a roller assembly (9) to eliminate tray and table surface friction and is pulled by weights and a pulley. Although a force meter (10) is available, the

horizontal force is determined by the weights applied. The tray has a Perspex viewing panel (11) on one of its sides so that observations may be made of soil shear during a slip run adjacent to the window. Engineering drawings for the test-rig are reproduced in appendix I.

5.3. Slip-Rig Development

The rig was constructed with a limited budget, therefore materials available within the department were used whenever possible. The soil tray was constructed from a shallow stainless steel tray, the sides of which were built up using plywood. A Perspex window was fitted into one of the side panels. One of the tray ends was strengthened with a steel plate on the inside to which two eye-hooks were secured. This enabled the tray to be pulled via a cord fastened

1. Main frame
2. Rotational crossbar
3. Locking screw
4. Shoe last/ cleat sample
5. Loading pole
6. Anti-rotation device
7. Loading platform
8. Soil tray
9. Roller assembly
10. Force meter
11. Perspex viewing panel

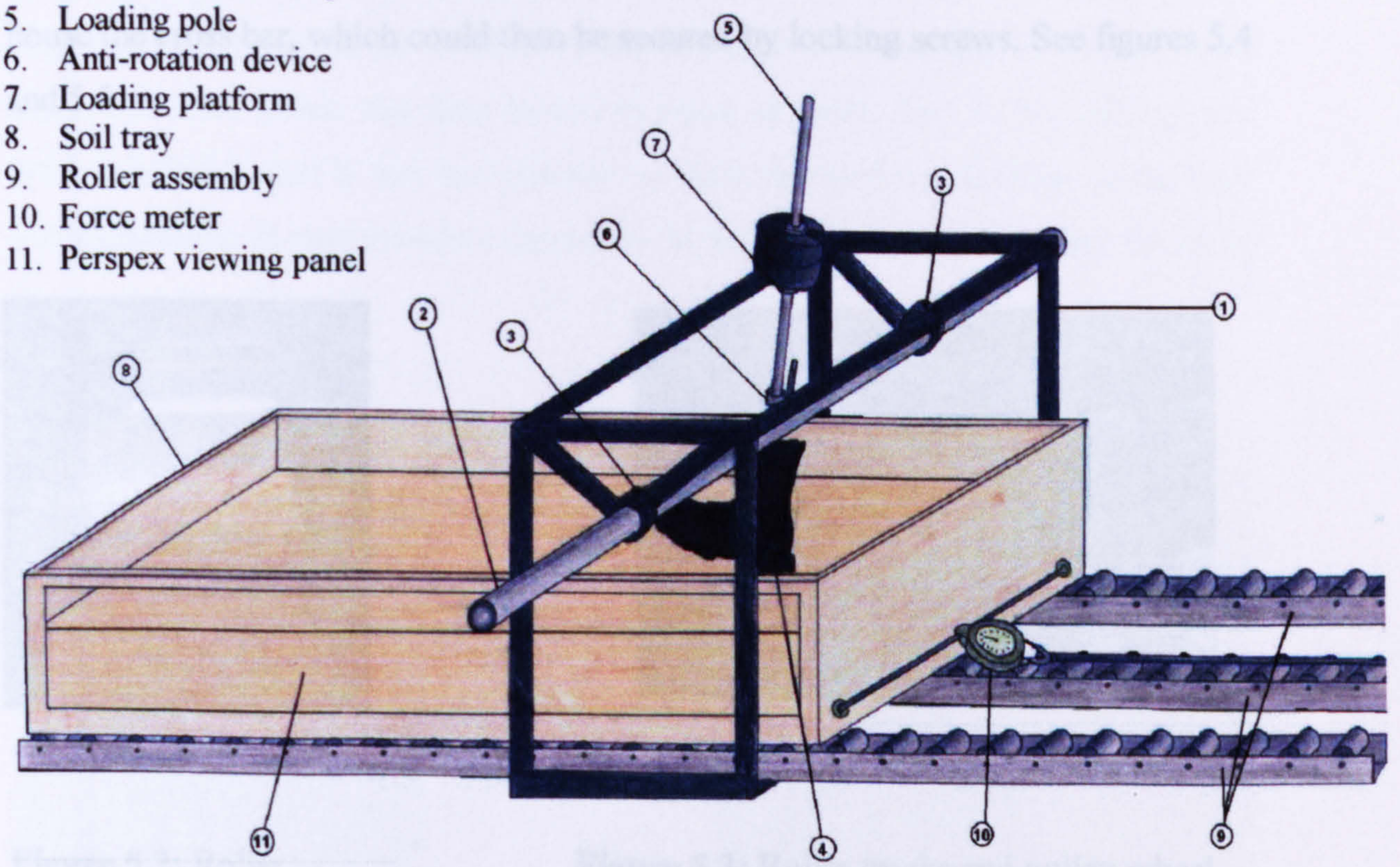

Figure 5.1: Prototype soil slip rig.

between the two hooks. The inside of the tray was then covered with fibreglass, and the window sealed to make it watertight.

To enable the soil tray to slide freely it was necessary to mount it on a roller system. An investigation into roller assemblies and bearings was then carried out and a pallet roller track system was selected. The tracks could be fitted with different types of rollers and wheels. Three, 3m lengths of steel roller track with 50mm diameter and 80mm length steel rollers with a ball bearing assembly were chosen, see figures 5.2 and 5.3. There was some doubt regarding the tray maintaining a forward direction on the rollers, however, this was found not to be a problem.

A suitable steel tube was then obtained from within the department for the cross bar and a main frame was then designed to fit it. The frame had to enable the cross bar tube to be rotated and moved horizontally within its supports. The main frame was constructed from lengths of square section steel tubing and joints. For added strength the joints were also welded. Two rings were welded to the main frame to house the cross bar, which could then be secured by locking screws. See figures 5.4 and 5.5.

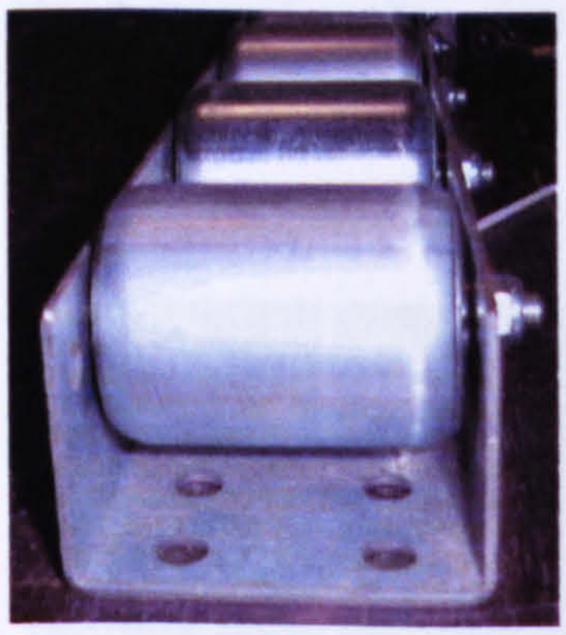

Figure 5.2: Roller.

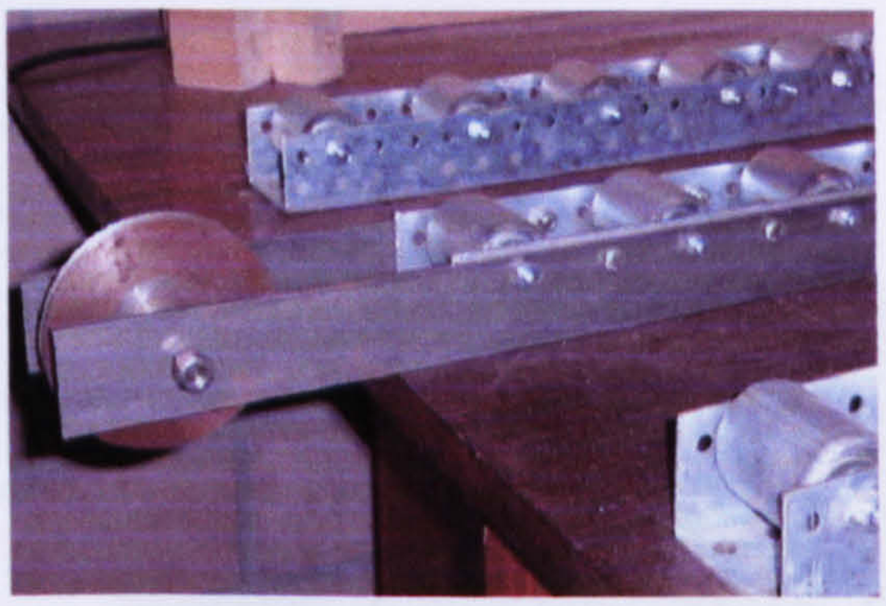

Figure 5.3: Roller tracks and pulley wheel.

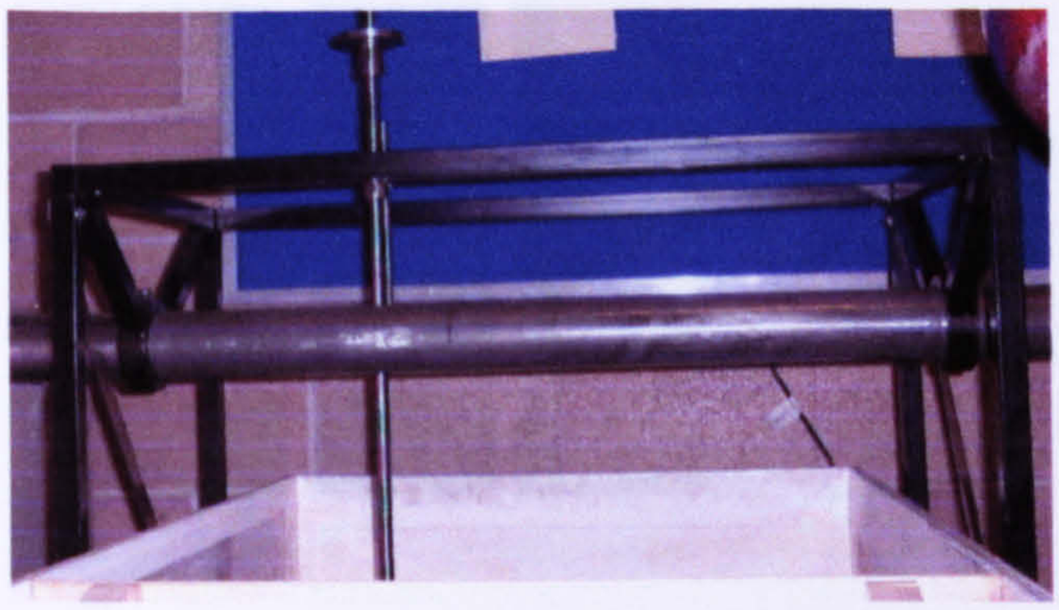

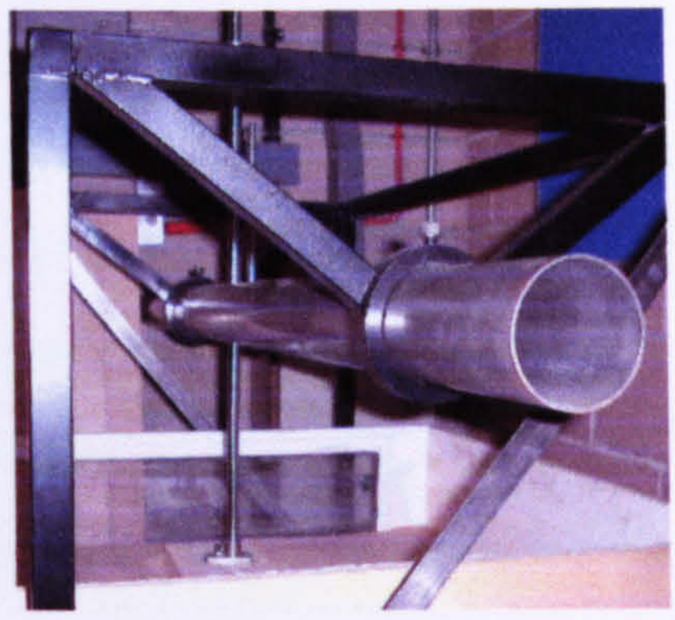

Figures 5.4 and 5.5: Main frame and horizontal cross bar

A loading platform, figure 5.6, and shoe last/cleat attachment, figure 5.7, mounted on a pole were required to slide through the cross bar. It was decided that a bearing assembly would be necessary to minimise sliding friction between the cross bar and loading platform pole. An investigation into suitable bearings was then carried out. Drawn cup re-circulating linear ball bearings were selected because they are designed especially for linear shaft guidance. A 16mm hardened steel shaft and two 16mm inner diameter linear bearings were used. To enable the bearings to be placed securely within the cross bar, the bearings were housed in a steel block inside the tube, which was then locked in place by bolts. Due to the loading pole being hardened steel it was not possible to weld the loading platform or the shoe last attachment. It was therefore necessary to design them such that they could be fixed using Loctite.

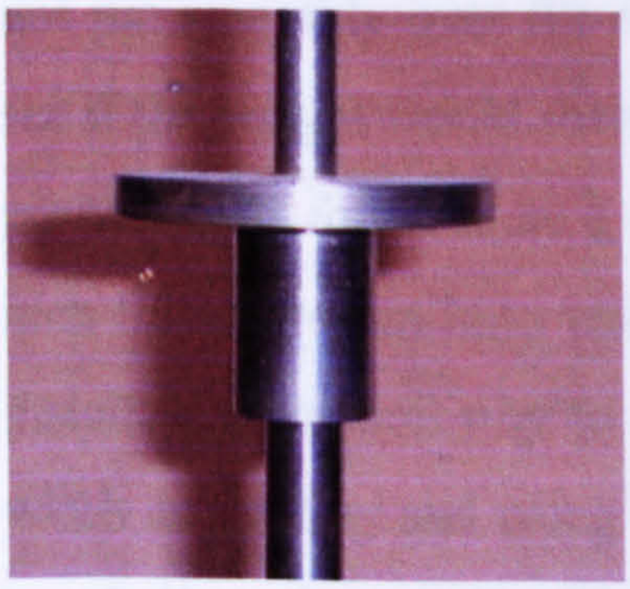

Figure 5.6: Loading platform

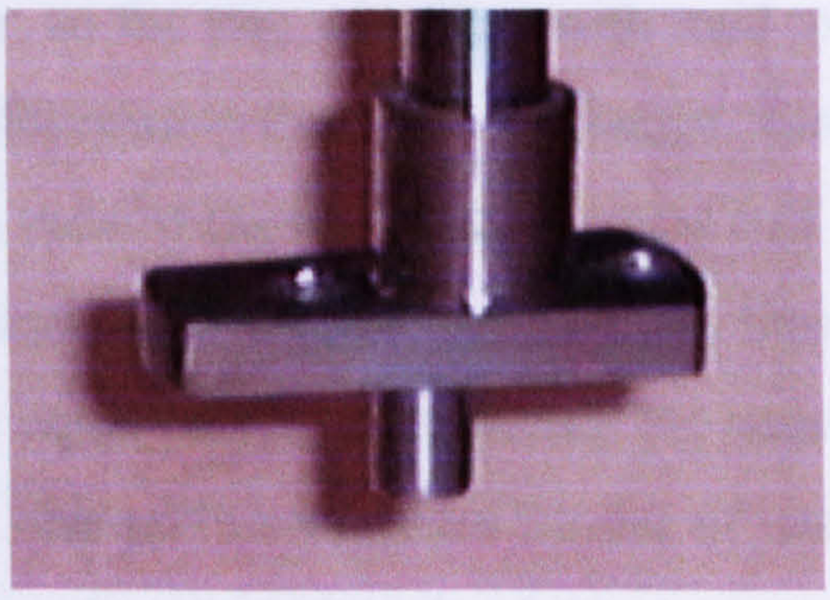

Figure 5.7: Shoe last/ cleat attachment

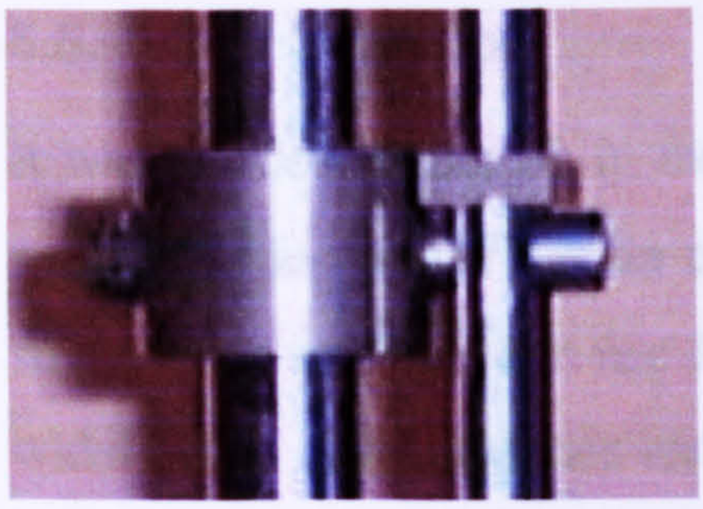

Figure 5.8: Anti-rotation device

To prevent the loading pole from rotating within the bearings an anti-rotation device was designed, figure 5.8. The device fits onto the shaft and is secured in position by a locking screw. It is guided by two shaft alignment rods, which have been secured to the horizontal cross bar. The shaft is then able to move vertically between the alignment rods but not able to rotate, maintaining the direction of the cleat attachment and preventing damage to the bearings. A rod spacer is placed above the anti-rotational device to maintain rod separation. The device and spacer drawings are also shown in appendix I.

5.4. Slip-Rig Commissioning

During initial tests with the slip-rig it was considered necessary to modify the main frame and the soil tray base. The main frame was pinned at each joint and mounted on a base, which is positioned beneath the roller assembly for added stability. Two diagonal braces were also added to the frame. It was noticed that the soil tray did not run smoothly over the rollers when empty, so the tray was filled with sand to see if the weight would solve the problem. Unfortunately there was no change. The problem was found to be a slight bow at both ends of the tray base so a new half-inch thick wooden base was attached to the tray. A removable partition was then installed in the soil tray to divide it into two equal halves, each having the same width as the tray and using half of its length. This partition enables the use of just one half, making soil preparation easier, since the whole length of the tray was found not to be required.

5.5. Soil Selection

It was decided earlier on in the research to begin testing with dry sand, since the soil properties would remain constant, also, wet and dry sand have similar shear strengths. It was hoped to use dry Leighton Buzzard sand to begin testing since it is widely used in laboratories and was also found to be used in testing tyre traction. Since Leighton Buzzard sand was used in the geotechnics laboratory within the Civil Engineering Department at Salford University, it was possible to carry out some initial tests with it, to look at its sieve sizing and range of density. Unfortunately, Leighton Buzzard sand was found to be unavailable, therefore it was decided to use kiln dried Congleton HST60 silica sand.

5.6. Shear and Sinkage Properties

Before the experimental work using the test rig could begin it was necessary to carry out tests with the silica sand to determine shear properties, maximum and minimum densities and the range of particle sizes within the sand sample.

Different shear tests were also investigated to enable the measurement of soil properties. Since dry sand was used for testing, ongoing measurement of soil properties was not required, which was one of the reasons for using dry sand.

5.6.1. Cone Penetrometer

The cone penetrometer is a device that is pushed into the ground. It combines all of the mechanical properties of soil into a single parameter called the Cone Index (CI). The CI may be described as the force/mm^2 required to push the penetrometer into the ground. The index contains components of shear, compressive strength and soil friction but the proportions of these components vary as moisture content varies The cone penetrometer does not enable measurement of individual soil properties and is not suitable for use with sand.

5.6.2. Bevameter

The Bevameter technique was pioneered by M.G. Bekker. It comprises of two tests, a plate sinkage test and a shear annulus test. The shear parameters, cohesion c and friction angle ϕ, and the sinkage parameters, exponent of deformation n and terrain constants k_c and k_ϕ, are then used in Bekker's analytical models. Although very effective when applying the results to Bekker's models [71], earlier work has shown that adaptation for other models is required and accuracy is doubtful.

5.6.3. Shear Vane Test

A vane is rotated at a constant angular velocity. The volume of soil contained within the blades is then sheared off. The shear strength of the soil is reflected in the torque required to rotate the device as the soil fails in a cylindrical shape around the circumference of the vane. The vane shear test is only suitable for clays and silts, and other equipment would be required to operate such a device.

5.6.4. Triaxial Shear Test

The triaxial shear test is a laboratory test requiring specialist equipment. The most common is the cylindrical compression test which consists of a pedestal on which the soil rests, a removable watertight cylinder enclosing the soil sample to which fluid may be added and a ram or load cell acting on top of the cylinder to provide applied stress. Due to having to import samples from the field unrepresentative results are to be expected.

5.6.5. Direct shear testing

The direct shear test is usually carried out in the field. It comprises of an open rectangular box, known as a shear box, separated into two equal halves. Porous plates may be placed above and below the soil sample to allow free drainage, if the sample is dry or drainage is not required, solid plates may be used. The hollow box is inserted into the terrain with one half resting on top of the other. However, it is possible to reproduce the required sand density within the shear box. A vertical load (N) is applied to the top half, keeping the lower half stationary, the top half is

then moved horizontally and the soil sample is then sheared off. The shear force (T) is measured together with the corresponding displacement (Δl). The change in thickness of the sample (Δh) may also be measured. When a number of samples are tested, each under different vertical loads, the value of shear stress at failure may be plotted against the normal stress for each test. The shear strength parameters, cohesion, c, and friction angle ϕ can be obtained directly from the line of best fit through the plotted points. The direct shear test procedure is also described in BS 1377: part 8: 1990 [82].

The direct shear test is simple to use, and soil properties may be obtained directly. The direct shear test method could also be used before each set of traction tests, to measure the soil properties used in the mathematical models. However, this was not considered necessary when using dry sand. This test may also be used to measure the friction and adhesion characteristics of sole materials by substitution of a sole sample for the soil sample in one half of the shear box, the other half of the box still containing soil.

5.7. Sieve Sizing

Although the particle size of the sand was specified by the supplier, it was still necessary to measure the particle size for classification assessment using the procedure described in 7.3 of BS 1377: part 1: 1990 [83]. The sieve test on a 500g sample of the silica sand showed 90% of the particles were retained on a 600 micron sieve. The sample was therefore classified as a medium grained cohesionless soil.

5.8. Maximum and Minimum Density Testing

It was necessary to carry out minimum and maximum density tests to find the full range and therefore the mid-density. The mid-density would then be reproduced during testing with the test rig.

The soil was prepared to 7.3 of BS 1377: part 1: 1990 [83] for compaction tests, which included soil classification and sieve sizing as discussed previously. Since the sand to be used was kiln dried it was not necessary to determine moisture content and dry the soil. A 6 inch (one litre) California Bearing Ratio (CBR) mould (figure 5.9) was used for compaction testing to determine maximum dry density and a glass measuring cylinder was used to determine the minimum dry density of cohesionless soils as described in 4 of BS 1377: part 4: 1990 [84]. The cylindrical corrosion resistant, metal mould has nominal internal diameter of 152 +/-0.5mm and a detachable base plate and extension collar (as shown).

Mass of mould (without collar)	5551g
Mass of mould with (collar)	7401g
Mass of collar	1851g
Mould dimensions (without collar): diameter, d:	152mm
Height, h:	127mm

Volume of mould (without collar), v: $\frac{\pi h d^2}{4} = 2.3 \times 10^6 \text{ mm}^3$

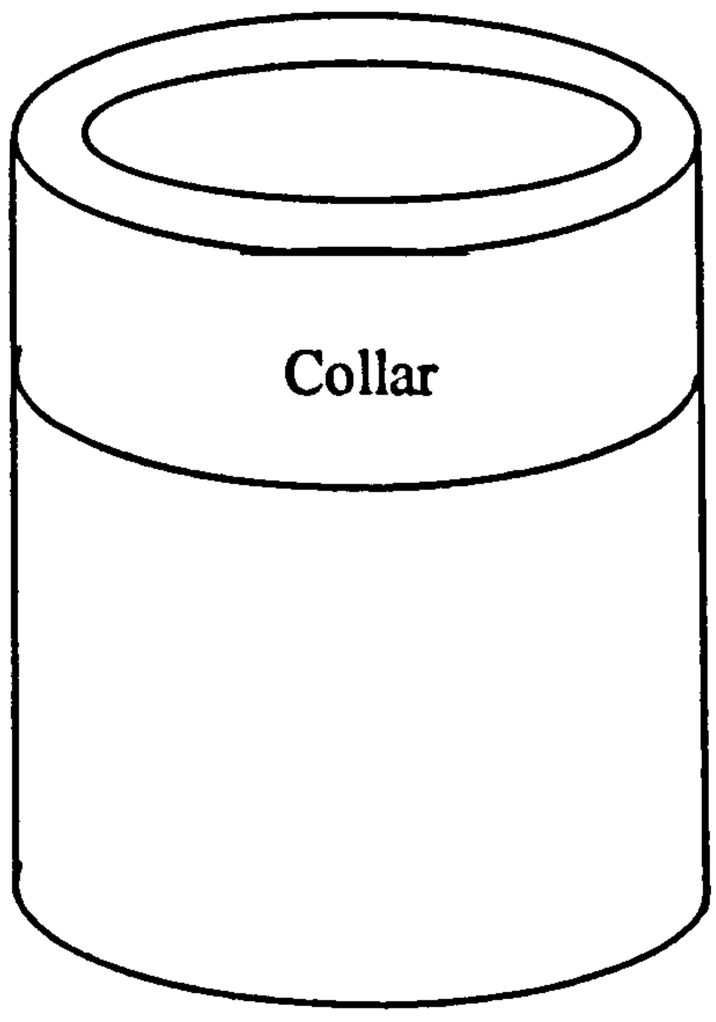

Figure 5.9: 6 inch California Bearing Ratio (CBR) mould

5.8.1. Minimum Density (ρ_{min})

For determination of the minimum density of the dry sand, a weighed sample of sand was shaken in a glass measuring cylinder with a fitted bung and allowed to fall freely thus enclosing the maximum possible volume of voids. The cylinder was turned upside down until the sand was at rest and then turned the right way up before standing the cylinder on a flat surface. The volume reading at the mean level was recorded. This was repeated several times and the average taken. The minimum dry density was then calculated, see below.

Mass of sand, W:	3564g (loose)
Average volume (maximum)	2.3×10^6 mm^3
Density of sand, (ρ_{min}):	$\frac{W}{V} = 1.55 \times 10^{-3}$ g/mm^3

5.8.2. Maximum Density (ρ_{max})

For determination of maximum density, the internal dimensions of the compaction mould were measured and the collar extension to the mould was attached. A quantity of sand was added to the mould so that when compacted the mould was one-third filled. A circular tamper was placed on the sand and compacted with the vibrating hammer as specified in [84], for 2 minutes with an applied downward force (including the mass of the hammer) of between 300N and 400N. This was repeated twice more to obtain three layers, the third layer was at least level with the mould body but no more than 6mm proud of it. The mould collar was removed carefully and the sand levelled with the top of the mould using a straight edge, any cavities left were refilled. The compacted sand was removed from the mould into a metal tray without loss of particles and the mass of sand determined. The internal volume of the mould and maximum dry density was calculated.

Mass of sand (minimum volume), W:	4060g (compressed)
Volume of mould (without collar),	2.3×10^6 mm^3

Density of sand, (ρ_{max}): $\frac{W}{V} = 1.76 \times 10^{-3}$ g/mm^3

After the test for maximum density had been completed, it could be seen that the sand particles had been crushed. Another sieve test was carried out using a 500g sample taken from the mould.

1.4g was retained on a 850 micron sieve,
35.1g was retained on a 600 micron sieve,
463.5g was retained in the pan,
i.e. 7.5% was retained on the 600 micron sieve.

Considering how destructive this test was using a percussion hammer and how unrealistic it is compared to the traction tests that were to be carried out it was decided to do another test. This test was to find the maximum density achievable by vibrating the mould. An electric sander was used to apply the vibration to the mould, which is also used to apply vibration to the sand during preparation in the sand tray.

5.8.3. Maximum Density Using Vibration Method (ρ_{maxv})

The mass of sand required to fill the mould and a third of the collar was taken and divided into three equal parts, to achieve three level equal layers within the mould. The first layer was established by pouring the first quantity of sand into the mould. The mould was then vibrated using the electric sander, which was firmly held on top for one minute. The second quantity was then poured into the mould on top of the first layer and the mould vibrated for a further minute. This was repeated for the third layer. The collar was then removed and a blade was used to remove excess sand, producing a flush surface with the surface of the mould. The mass of the sand within the mould was measured. This test was repeated once and the average taken as shown below.

Mass of sand (maximum volume), test 1: 3970g (compressed)

Mass of sand (maximum volume), test 2: 3971g (compressed)

Average mass of sand, W: 3971g (compressed)

Volume of mould (without collar), $2.3 \times 10^6 mm^3$

Density of sand, (ρ_{max}): $\frac{W}{V} = 1.72 \times 10^{-3} g/mm^3$

5.8.4. Mid-Density (ρ_{mid})

The mid-density required for experimental work was calculated by averaging the minimum and maximum (vibration method) densities.

Mid-density, ρ_{mid}: $\frac{1}{2}(\rho_{min} + \rho_{maxv}) = 1.635 \times 10^{-3} g/mm^3$

5.9. Experimental Procedure

5.9.1. Introduction

To establish that the rig was working satisfactorily and enable the test procedure to be developed a series of preliminary tests were carried out using both unprepared and prepared soil trays and a variety of cleat designs, the results of which are presented in appendix II. The unprepared trays were filled with sand and levelled by hand to save time in the early stages, whereas the prepared trays were constructed with levels of compressed sand using the method described below. The tests using prepared sand were very time consuming since only two or three tests could be carried out on each sand tray, and it took up to two hours to prepare a single tray. If the sand preparation was not satisfactory, for example, the sand surface was not level or the correct density could not be achieved then the tray was made void and the sand preparation repeated. A variety of sand depths were tested and a depth of 114mm was selected, after compression, having obtained the required sand density. This depth was considered to be deep enough to eliminate the effect of the sand sliding against the bottom tray surface. These tests will not be

discussed in detail since they served only to establish the test procedure and select the results and observations to be recorded.

5.9.2. Soil Preparation

The mass of sand was calculated and the depth of sand in the tray, 114mm, was selected to achieve the mid-density value (see soil density requirements). The sand was prepared in approximately 50mm layers so it was necessary to divide the total mass of sand calculated into the required number of layer quantities. The first layer was achieved by pouring the sand into the base and distributing it evenly. A wooden board the same size as the partitioned area was placed over the sand layer and vibrated evenly for a period of time using an electric sander. At first the board was vibrated for three minutes, continually moving the sander over the entire board surface for the duration. It was then found that vibrating the board until the required density (depth) was achieved, like before but without the time constraint, produced more consistent results. The tray was marked with the required depth of each of the sand layers. The next layer was then created like the first and vibrated. The number of layers was dependent upon the depth of sand required. On completion of the sand preparation, the depth of sand was checked to ensure the density was correct. The required density was achieved with an error of less than $\pm$ 5%.

5.9.3. Test Piece Selection

The test piece (shoe last or cleat model) was selected and fitted to the loading pole. The attachment was then secured by tightening the bolts.

5.9.4. Positioning of the Test Piece

Firstly, the soil tray was aligned with the rollers and set in the required position. The soil tray position was then marked and a measuring tape set to record tray movement. The loading pole was then set at the required angle (vertical for all tests) and the horizontal crossbar was then locked to maintain this position. The test piece was then gently lowered onto the sand surface, correctly aligned using

markers on the wall behind the rig and facing the correct direction. The alignment device was then secured to make sure that the loading pole did not rotate during the experiment.

5.9.5. Application of Vertical Load

The required weights were gently placed onto the loading platform so not to disturb the sand unnecessarily. The locking device was then tightened thus securing the weights in position. The initial sinkage due to the application of the vertical load was measured using a metal rule and recorded. Initial sinkage was measured corresponding to the actual sand surface in the tray at that point. Another metal rule was placed on the sand surface from which to accurately measure from.

5.9.6. Application of Horizontal Load

Firstly, the rig was checked to make sure everything was secure and in the correct position. The weight hanger was then connected to the soil tray pulling cord. The cord was checked to make sure it was correctly aligned within the pulley. Weights were then gently added to the weight hanger until the tray began to slide.

During initial tests it was seen that during some tests the rig slipped a small distance prematurely (approximately 10 – 15% of the total slip distance). Premature slip was recognised when slip occurred well before the horizontal load expected to induce slip was applied. When this occurred, all sinkage, slip length and shear zone measurements were taken and observations recorded before continuing with the same test. It was usually found that although the test item had slipped slightly already, the main slip occurred with the same horizontal load as other tests. There is no explanation for this pre-slip phenomenon that occasionally occurs. The test was then continued to induce further slip or made void, and a new test carried out.

5.9.7. Measurements and Observations

When the tray had stopped sliding the applied horizontal load was recorded. Slip distance, i.e. distance of tray movement was also recorded. Sinkage was then

carefully measured at the front, centre and rear of the test item. The sinkage was measured with respect to the displaced sand (denoted by flow), and with respect to the original sand surface (denoted by actual) as shown by figure 5.10. Both measurements were taken at the centre of the front and rear cleats and sinkage with respect to flow only at the centre in between the cleats, as shown below (for illustration purposes, only one of each measurement has been shown). With respect to flow sinkage, a steel rule was used to measure the distance between the sand surface and the top of the test piece, this distance was then subtracted from the total cleat height for the sinkage measurement with respect to sand flow. An accuracy of +/- 1mm was achieved. With respect to actual sinkage, a steel rule was placed on the original sand surface and moved towards the test piece. The distance between the rule and the top of the test piece was then subtracted from the total height for the actual sinkage measurement. The accuracy of which was also +/- 1mm.

The Perspex window of the soil tray was unable to be used during the experimental period due to temporary relocation of the rig. However, it was still possible to make observations from the soil surface when slip was initiated. It could be clearly observed that as the cleat slid along the soil surface it sank, heaving the sand in its path up in front of the cleat. This quantity of sand being heaved up by the cleat movement is the soil shear zone, the wedge of soil that has sheared. Due to the dry sand being cohesionless, the shear zone was produced by granular friction only. The shape of the shear zone in front of the cleat models was seen to be approximately an elliptical plateau, as illustrated by figure 5.11. If an initial premature slip occurred as previously discussed, and the test was continued, more than one shear zone, decreasing in size occurred, illustrated by figure 5.12. The length and height of the shear zone was measured at their respective maximum points using a steel rule. These measurements were taken with respect to the actual sand surface. In the event of multiple shear zones, the maximum length and height of each plateau was recorded.

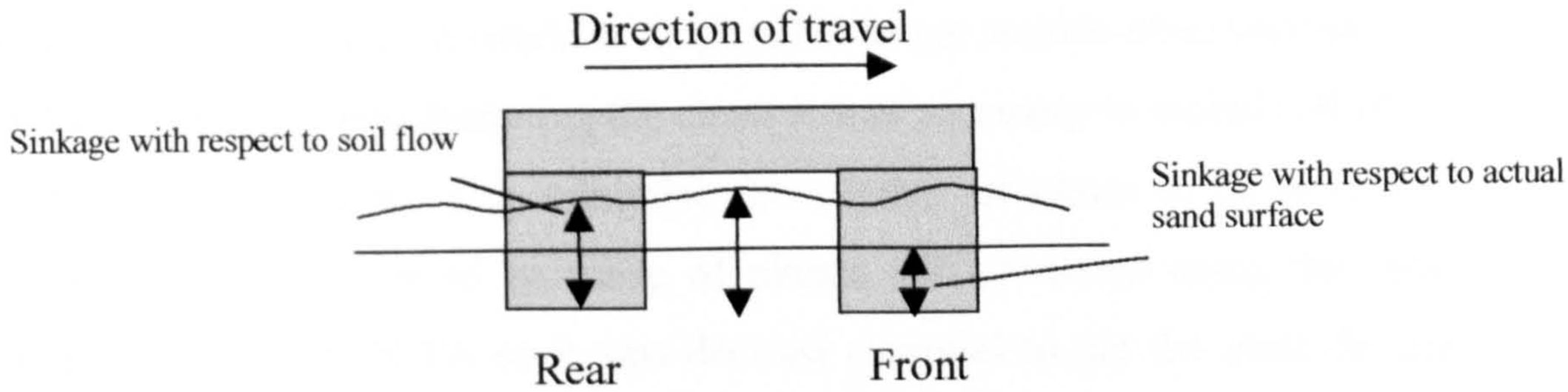

Fig. 5.10: Sinkage measurements.

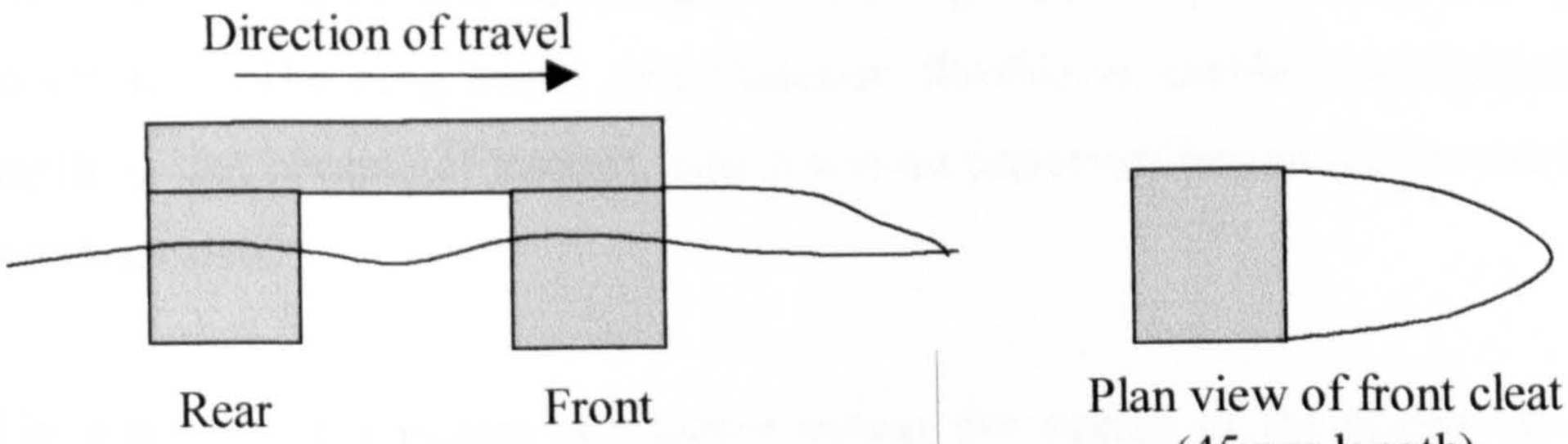

Fig. 5.11: Single soil shear zone.

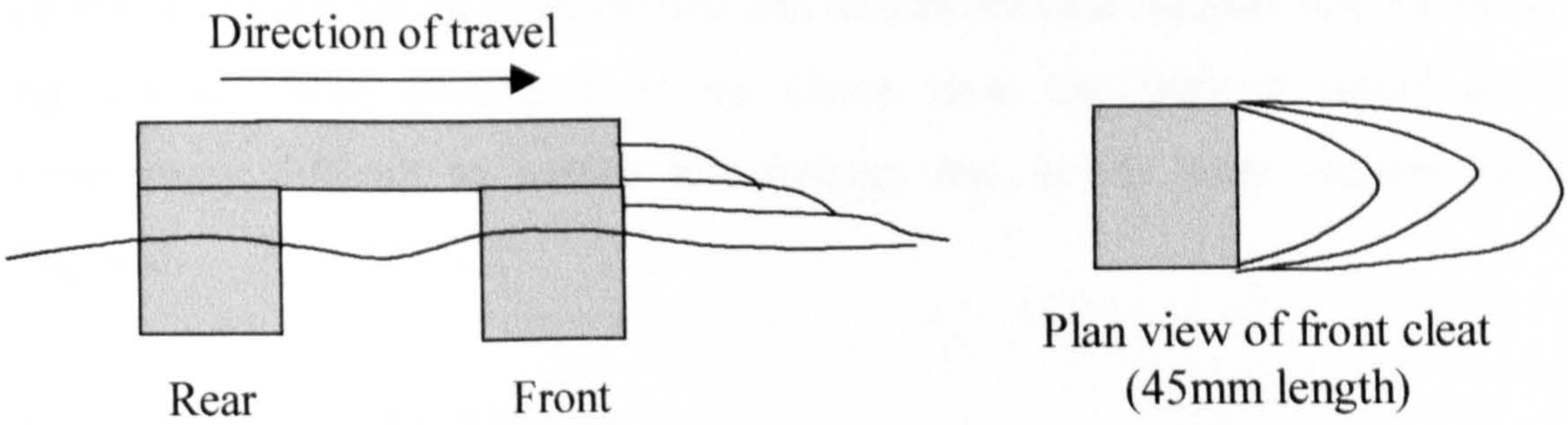

Fig. 5.12: Multiple soil shear zones.

5.10. Scaled up cleats

It would be unlikely that meaningful traction data could be obtained from normal sized cleats. It was therefore decided to use scaled up cleats to validate the mathematical models and to look at the effect of cleat geometry on traction

characteristics. The scaled up cleats would also enable observation of soil behaviour during slip since it would be impossible to get useable observations from normal sized cleats. When designing the cleats it was necessary to include all of the geometric possibilities but also minimise the number of cleats to be produced. Originally the cleats were to be made of plastic and produced using the rapid prototyping facility at DCTA so it was deemed essential to get the cleat designs right. But as the programme of testing continued it was thought to be unnecessary to use plastic cleats since the experiments were purely comparative and the cleat material was not vital at that stage. Also, due to the uncertainty of producing useful results, the experimental programme involved completing the tests one at a time, evaluating the results and repeating or modifying tests if required before moving on to the next. The programme was therefore flexible to enable investigation into anything that became of interest, which was an important reason for the use of the wooden cleats.

The geometric parameters considered during the design of the scaled up cleats included cleat length, l, height, h, width, b, and cleat taper as discussed in section 4.1. The geometric dimensions were a factor of a standard unit of length, d, where d = 45mm, see figure 5.13, for example. This length was considered to be large enough to ensure useful observations and results but of a suitable size for the slip-rig that has been developed. If the cleats were too large it would become increasingly difficult to induce full sinkage due to the large vertical loading required.

For example, $l = 4d$ (180mm)

$h = d$ (45mm)

$b = d$ (45mm)

5.10.1. Comparisons of Cleat Length and 3D End Effects

For investigation of soil flow and three dimensional end effects, a series of cleats were produced with lengths *d/2, d, 2d, 3d, 4d, 5d* and *6d* and two cross sections, normal (b x h) and narrow ($b/2$ x h).

5.10.2. Effects of Cleat Height, Width and Taper

To consider the effects of cleat height, width and taper, all possible geometric combinations of two cleat heights (*h* and *h/2*), two cleat widths (*b* and *b/2*), and with or without taper were produced, all of the same length, $l = 4d$. As the experimental programme progressed it was possible to use the same cleat for different tests, thus saving time.

(All dimensions are given in mm)

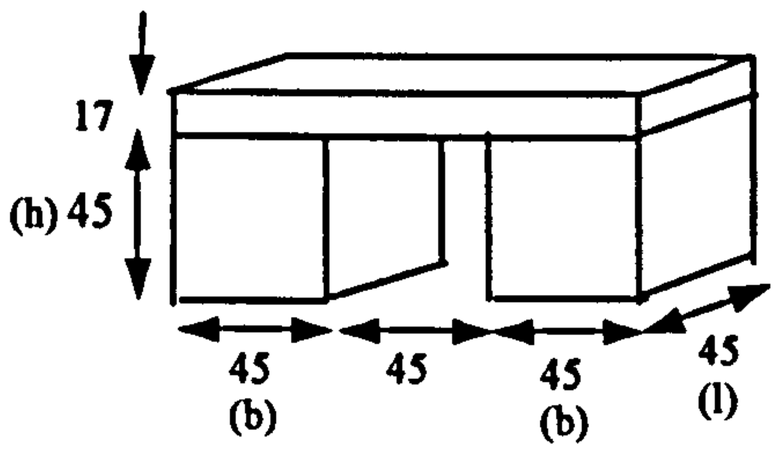

Figure 5.13 (a): No taper, cleat width $b = d$, length $l = d$ and height $h = d$.

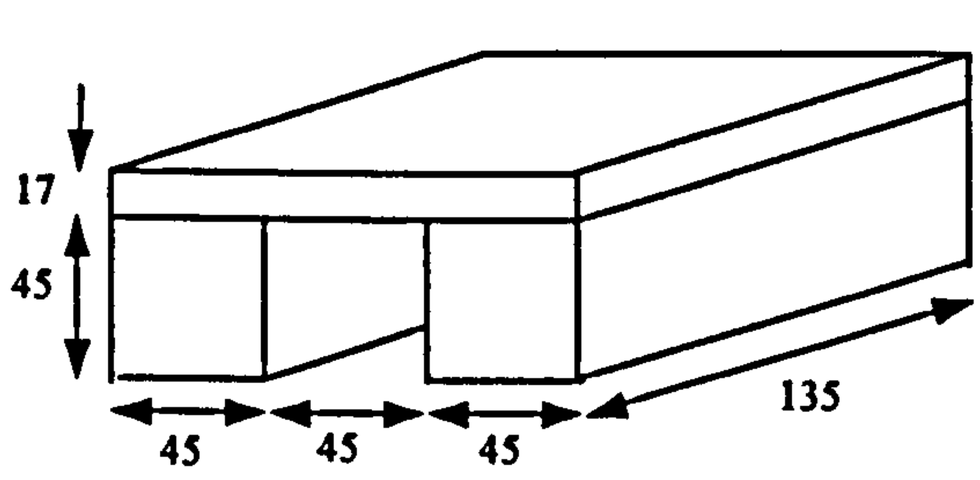

Figure 5.13 (b): No taper, cleat width $b = d$, length $l = 3d$ and height $h = d$.

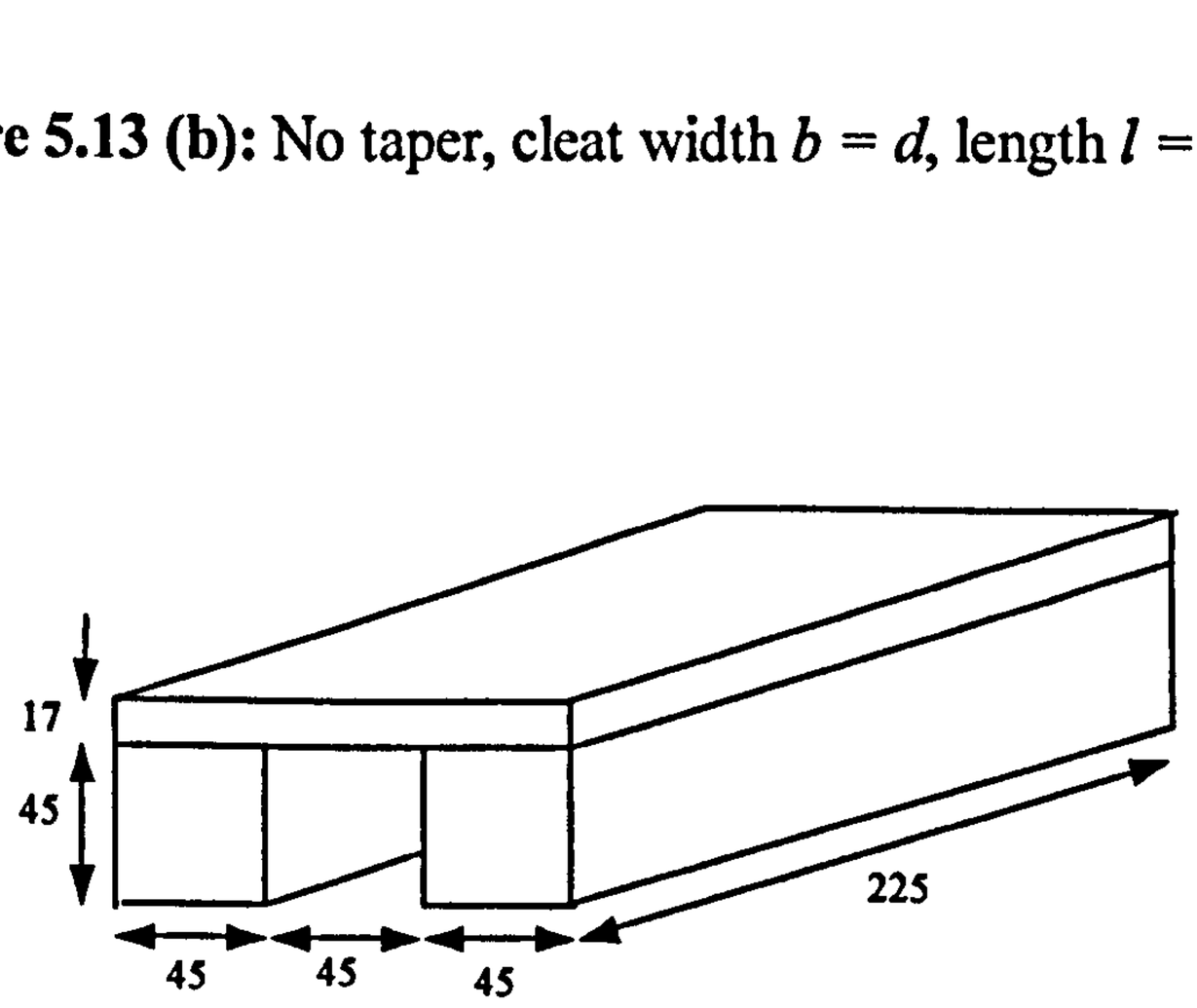

Figure 5.13 (c): No taper, cleat width $b = d$, length $l = 5d$ and height $h = d$.

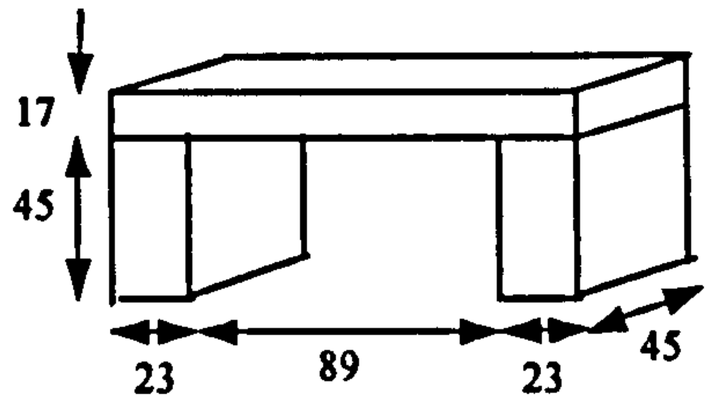

Figure 5.13 (d): No taper, cleat width $b = d/2$, length $l = d$ and height $h = d$.

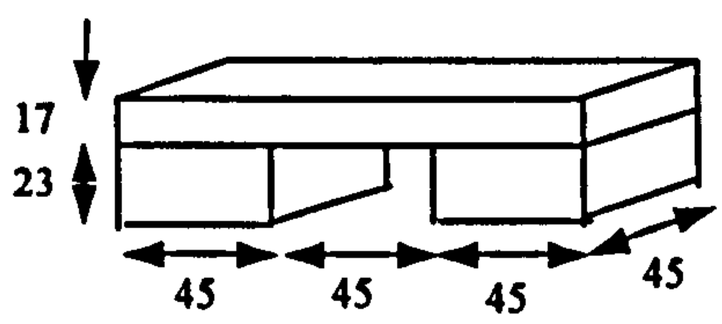

Figure 5.13 (e): No taper, cleat width $b = d$, length $l = d$ and height $h = d/2$.

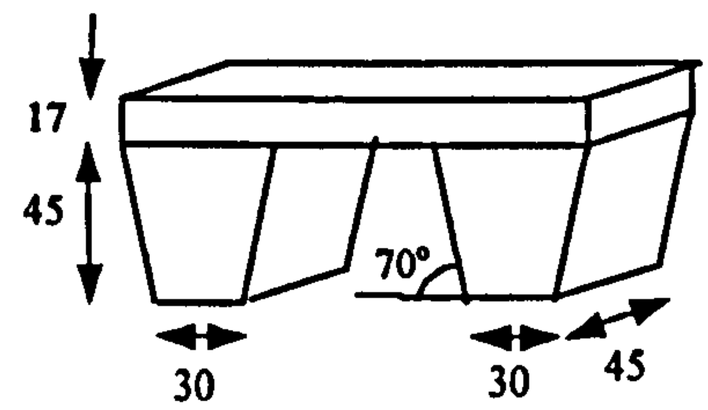

Figure 5.13 (f): Tapered cleats, width b at top, width 2b/3 at taper bottom and length d.

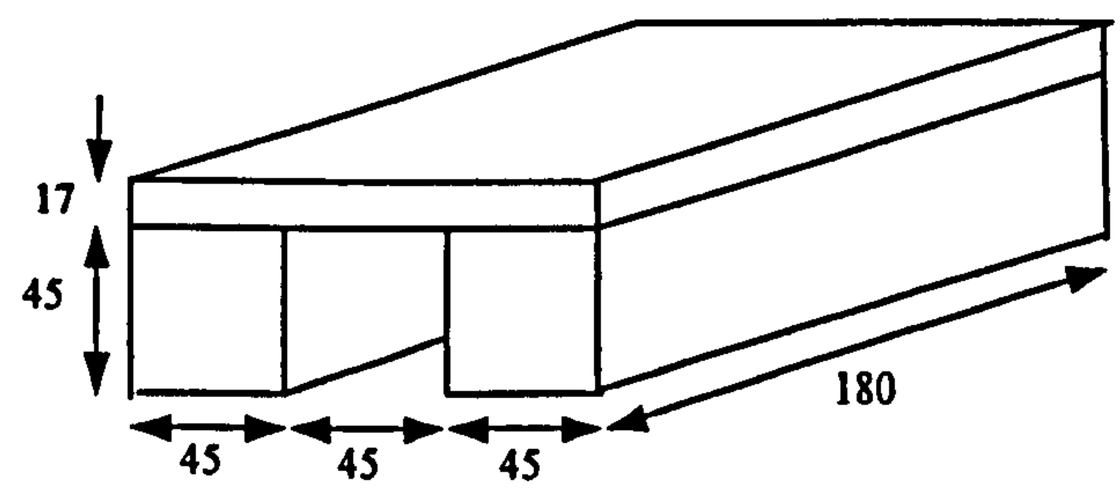

Figure 5.13 (g): No taper, cleat width $b = d$, length $l = 4d$ and height $h = d$.

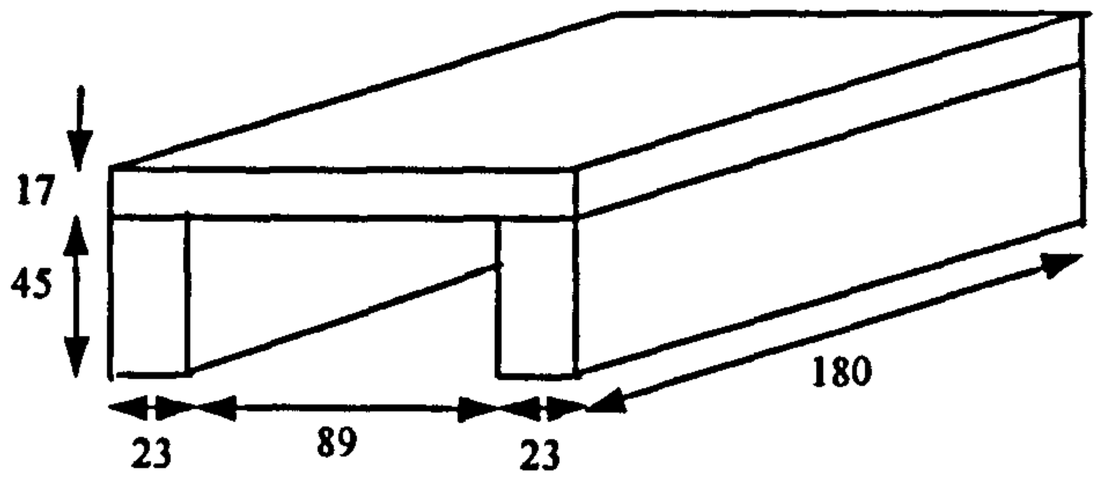

Figure 5.13 (h): No taper, cleat width $b = d/2$, length $l = 4d$ and height $h = d$.

Figure 5.13: Examples of scaled up cleat geometry

6. Experimental Results

6.1. Introduction

The prototype test rig was constructed and initial tests confirmed that the rig was working satisfactorily, enabled a test procedure to be developed, and established what could be achieved with the rig in terms of repeatability and accuracy.

The experimental program was of an exploratory nature so was undefined at the beginning but developed one test at a time throughout the experimental period. The experimental work discussed within this chapter is as follows:

i Initial tests, to develop experimental procedure and establish repeatability.
ii Cleat length and three dimensional soil flow investigation to identify at which cleat length two dimensional effects are dominant.
iii Traction distribution over cleats.
iv Eight, full factorial experiments to investigate the effects of cleat height, width and taper on traction.

Results from the experimental work were also compared with those from the mathematical models, this is discussed in a later chapter.

6.2. Initial Tests to Assess Repeatability

Having established the slip-rig was working satisfactorily further tests were required to establish what could be achieved in terms of accuracy and repeatability. Sinkage tests were required to investigate repeatability of initial sinkage in the same tray of prepared sand. Initial sinkage may be defined as the static sinkage when the vertical load has been applied. It was necessary to establish whether or not the sinkage behaviour was consistent across the entire sand surface and the sand preparation procedure acceptable.

Having established the repeatability of cleat sinkage within a single tray, it was then necessary to establish repeatability in a number of different trays. Three tests were carried out in three trays of prepared sand (nine tests in total). In these tests, slip was initiated to gain as much data as possible from each test, unlike in the previous experiment. Therefore initial sinkage, sinkage after slip and traction results will be discussed as well as soil movement observations.

6.2.1. Experimental Procedure

To establish the repeatability of cleat sinkage within a single tray a tapered cleat (as shown in figure 5.13) of length 45mm was used with an applied vertical load of 20kg. The tapered cleat was selected because of its mid-range sensitivity to external effects, pole vibration for example, which was discovered in the earlier tests. To improve repeatability, tapping the side of the loading pole was considered, but the pole was found to continue sinking without stopping. Weights were applied as gently as possible to prevent the loading pole from vibrating.

The tests were carried out in the numerical order and approximate positions shown in figure 6.1. Two different initial sinkage measurements were taken into consideration since slip was not initiated, actual sinkage of the cleats with respect to the original sand surface on application of the vertical load (actual), and sinkage with respect to the displaced sand (flow). Both measurements were taken at the

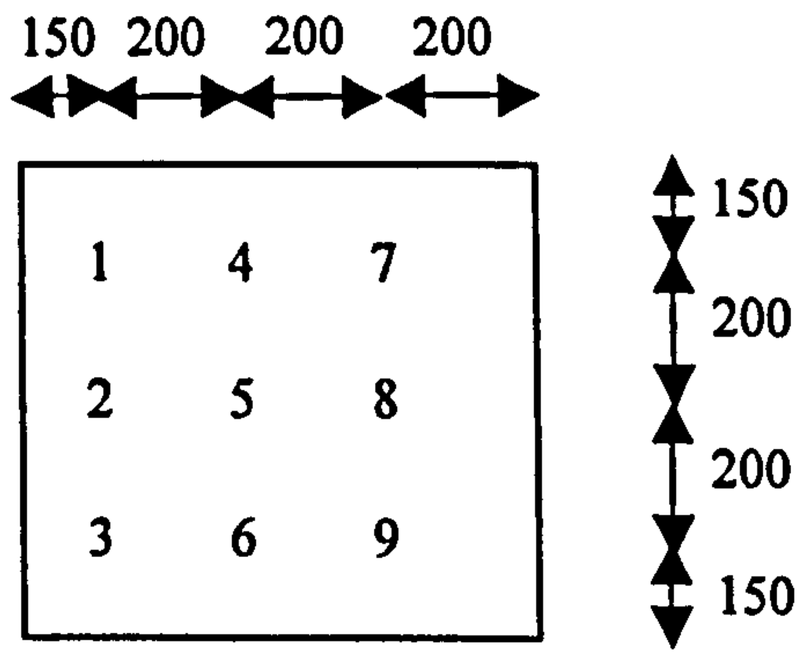

Fig. 6.1: Sinkage test locations (all dimensions in mm).

centre of the front and rear cleats and sinkage with respect to flow only at the centre in between the cleats, as discussed in section 5.9. The results are shown in table 6.1.

To establish tray to tray repeatability, three tests using a tapered cleat of length 135mm, and a 20kg vertical load, were carried out in three different trays of prepared sand (nine tests in total). At that time it was not considered necessary to use the same cleat as before since this was considered a separate experiment, and slip was to be initiated to make the most of the experimental preparation. Although it would have been beneficial to have used the same cleat, the longer cleat was less prone to external disturbances. The required sand density was achieved to within +/- 5%, this was calculated based on the overall depth of the sand since the sand mass and tray internal width and length were known. In previous tests, the tray was prepared in two equal layers, vibrating each layer of sand for two minutes. In these tests the sand was vibrated again in two equal layers as before but the length of time was not restricted. The sand was vibrated until the required sand density was achieved in order to achieve a more level surface. It had been noticed that the time required to reach the specified density varied slightly probably due to the unpredictable nature of sand but it was not considered to be significant.

In the previous sinkage repeatability tests, only initial sinkage was considered since no horizontal slip occurred. In these repeatability tests, sinkage repeatability was also considered after slip had occurred. Therefore an average initial sinkage measurement with respect to the displaced soil surface at the measurement point for the front and rear cleats was recorded as well as the sinkage of the cleats with respect to the nominal soil surface (actual) and displaced soil (flow) after slip had occurred. The horizontal load required to induce the slip was also recorded. Observations of the amount of sand heaved up in front of the cleat after slip were also recorded. The Perspex window of the soil tray was unable to be used during the experimental period due to temporary relocation of the rig. However, it was still possible to make observations from the soil surface. It could be clearly observed from early tests that as the cleat slid along the soil surface it sank further, heaving the sand in its path up in front of the cleat. This soil shear zone is illustrated by figures 5.11 and 5.12. The

depth and length of the shear zone above the sand surface was measured during each test as previously described in section 5.

Tests were carried out in prepared sand of mass 122.66 kg, depth 114 mm and density 1.64×10^{-3} g/mm^3 with a vertical pole position.

Horizontal load required to move empty tray: 1.05kg.
Horizontal load required to move tray and 122.66kg of sand: 1.3kg.

6.2.2. Discussion of Results

6.2.2.1 Sinkage repeatability

The results for initial sinkage repeatability in a single tray are presented in table 6.1. The values of actual sinkage with respect to the nominal sand surface were all within +/- 9% (2mm) of the mean (21.9mm), a variance, σ^2, of 1.83 was calculated. This confirmed that the sand surface was consistent across the entire tray surface and that the sand preparation was sufficient.

Test	Front sinkage (actual)	Rear sinkage (actual)	Front sinkage (flow)	Rear sinkage (flow)	Sinkage between cleats (flow)
1	20	20	28	27	34
2	24	24	31	32	38
3	23	24	32	33	38
4	20	22	30	32	34
5	23	23	31	31	38
6	21	20	27	25	34
7	21	22	30	30	36
8	24	23	31	30	37
9	20	20	29	29	33

All measurements in mm otherwise stated

Table 6.1: Sinkage results in a single tray

The sinkage with respect to sand displacement, flow, was however found to be more variable, -13% (4mm) to +10% (3mm) of the mean (29.8mm). The variance was 3.76, twice that of actual sinkage variance. This was not unexpected due to the unpredictable nature of displaced sand, and the fact that only one measurement was taken at the centre of each cleat. The variability was considered to be acceptable so it was not deemed necessary to take more than one measurement. There were also the time implications to consider.

The depth of sand between the cleats was also observed to assess whether or not the cleats were full after sinkage. This sinkage measurement for each test was greater than the actual cleat sinkage (approximately 1.6 times) because of the occurrence of sand flow around the cleat, and sand retention between the cleats. The degree of sand retention between the cleats was dependent upon the actual cleat sinkage, this is clearly seen in the table of results. The depth of sand measured between the cleats was within +/- 6% (2mm) of the mean (35.8mm).

Having established the repeatability of sinkage within a single tray, it was then necessary to establish the repeatability from tray to tray. The tray to tray repeatability results are presented in table 6.2. The initial sinkage results, were negligible (less than 1mm) for this size cleat (135mm) compared to the cleat size of the previous experiment (45mm) due to the application of the same vertical load and hence the reduced pressure beneath the cleats. The following discussion therefore focuses on the results after horizontal slip has occurred. Variation from the mean of average actual sinkage and sinkage with respect to soil flow over both cleats, in the three trays, is shown in figure 6.2.

The average actual sinkage results over the front and rear cleat after slip had occurred were within +4% (1mm) to -8% (2mm) of the mean 26mm for tray 1, +15% (3.7mm) to -8% (2.3mm) of the mean 24.3mm for tray 2 and +6% (1.3mm) to -3% (0.7mm) of the mean 23.7mm for tray 3. However, the sinkage means for different trays were slightly different. A variation of +13% (3.3mm) to -11% (2.7mm) of the mean (24.7mm) was seen across the three trays for actual sinkage, the variance, σ^2, was 4.2.

Tray	Initial Sink	Rear sink (act)	Front sink (act)	Rear sink (flow)	Front sink (flow)	Sink between cleats	T (kg)	Slip distance	Shear zone length	Shear zone height
1	0.5	27	27	33	32	43	8.5	67	99	26
1	0	24	24	30	32	42	8	63	118	29
1	0.5	27	27	35	37	43	8.5	85	102	32
2	0	23	23	32	32	42	8.5	84	95	34
2	0.5	22	22	30	32	41	7.5	75	127	31
2	0.5	28	28	33	36	42	8	76	98	33
3	0	25	24	32	34	41	7.5	74	100	30
3	0	23	25	27*	29	37	8	48	107	21
3	0	23	22	33	32	44	8.5	75	89	34

All measurements in mm unless otherwise stated.

Table 6.2: Tray to tray repeatability results (* denotes rogue result discounted from analysis).

The average sinkage results with respect to soil flow over the front and rear cleat after slip had occurred were within +8% (2.8mm) to -6% (2.2mm) of the mean 33.2mm for tray 1, +6% (2mm) to -5% (1.5mm) of the mean 32.5mm for tray 2 and

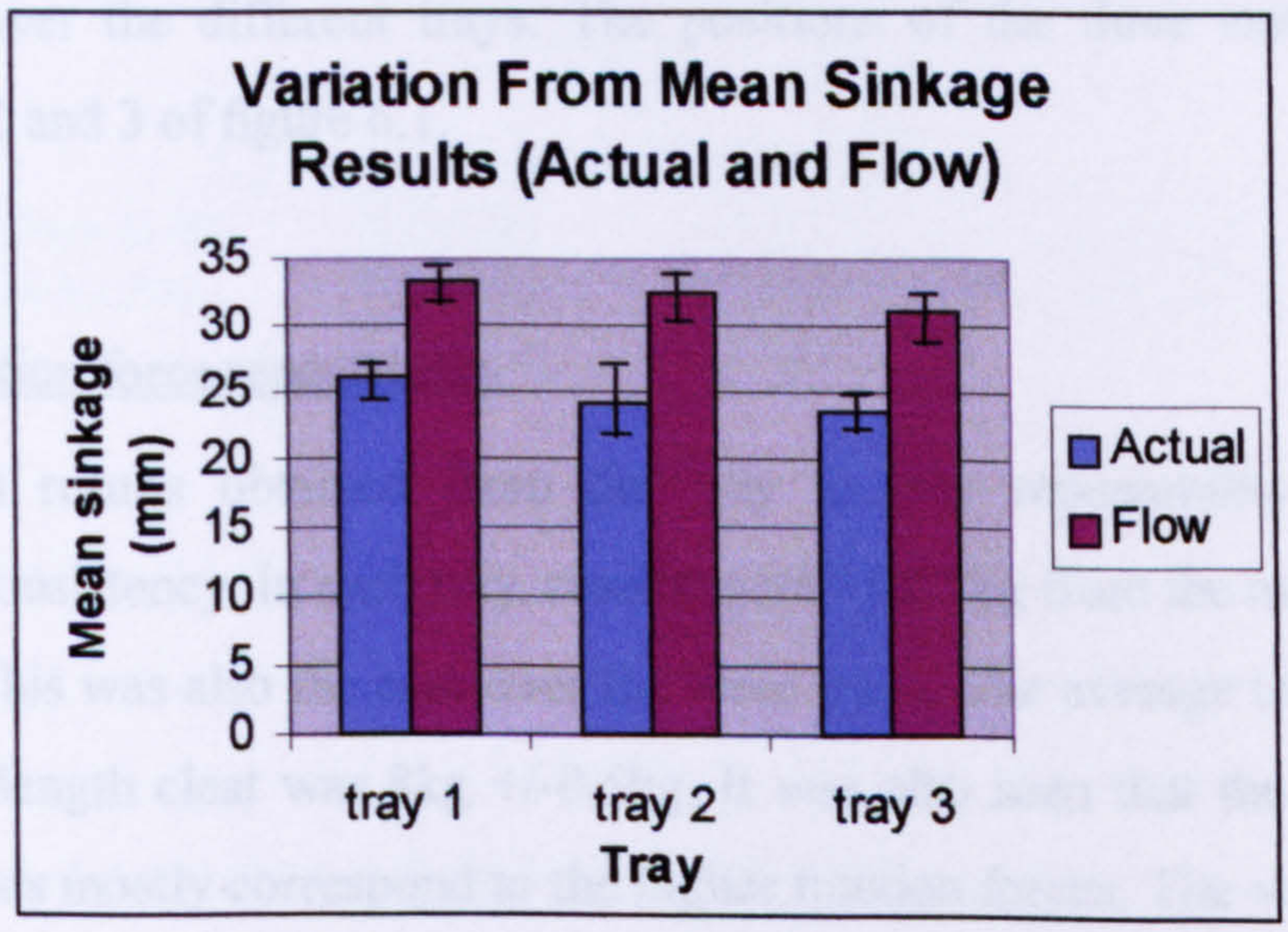

Figure 6.2: Graph showing variation from the mean for sinkage repeatability tests in three different trays

+6% (1.8mm) to -10% (3.2mm) of the mean 31.2mm for tray 3. A variation of +2% (0.7mm) to -13% (4.3mm) of the mean (32.3mm) was seen across the three trays for sinkage with respect to flow, the variance, σ^2, was 4.6.

A greater variation of the sinkage results with respect to soil flow was expected due to the nature of dry sand. The difference in initial sinkage (sinkage after vertical load was applied but before horizontal load was applied) was negligible for the 135mm length of cleat, due to the reduced pressure beneath the cleats under vertical loading with the larger surface area. It was also less sensitive to external effects than the 45mm cleat used in the previous experiments, such as vibration whilst applying the vertical load.

In summary, the tray to tray sinkage repeatability was established as a necessary prerequisite for differentiation between different cleats in different trays. It was also seen, in the initial sinkage tests in the one tray, that the sand density was not consistent over the whole tray surface by comparing the test locations, even though as much care as possible had been taken in the tray preparation. The problem of the soil surface not being level was overcome by vibrating the sand for as long as necessary, up to four minutes, after which the tray was made void. It was also important to note that the position of each of the three test runs in each tray remained unchanged over the different trays. The positions of the three tests were as per locations 1, 2 and 3 of figure 6.1.

6.2.2.2. Traction force repeatability

The traction results obtained from the tray to tray repeatability tests showed reasonable consistency. In each tray, results were +/-0.5kg from the mean, a variation of +/-6 %. This was also the case over the three trays. The average traction force for the 135mm length cleat was 8kg +/-0.5kg. It was also seen that the slightly higher sinkage values mostly correspond to the higher traction forces. The variability within the traction results was expected to be reduced if smaller increments of horizontal load (traction force) were applied.

The shear zones in the preliminary tests were all of a similar length and height, regardless of cleat model. For the 135mm length tapered cleat, the shear zone length range was +23mm to -15mm from the mean 104mm. The shear zone height range was +4mm to -9mm from the mean 30mm.

Soil flow occurred as the cleat slipped causing the shear zone at the front of the cleats to fail at the edges and flow round the sides, this is illustrated by figure 6.3. Also the soil within the cleats flowed out to the sides as the cleat moved forward. The amount of soil flow was seen to be dependent upon the length of the cleats and the height of the cleats from the preliminary tests. The shorter the cleats the more the soil was able to flow, creating soil movement in all directions, forwards and upwards, backwards and also out to the sides. If the cleats were long, the soil that flows around the sides was very small in comparison to what was collected at the front. This observation initiated further investigation into three dimensional soil flow for different cleats which is discussed in more detail in the next section.

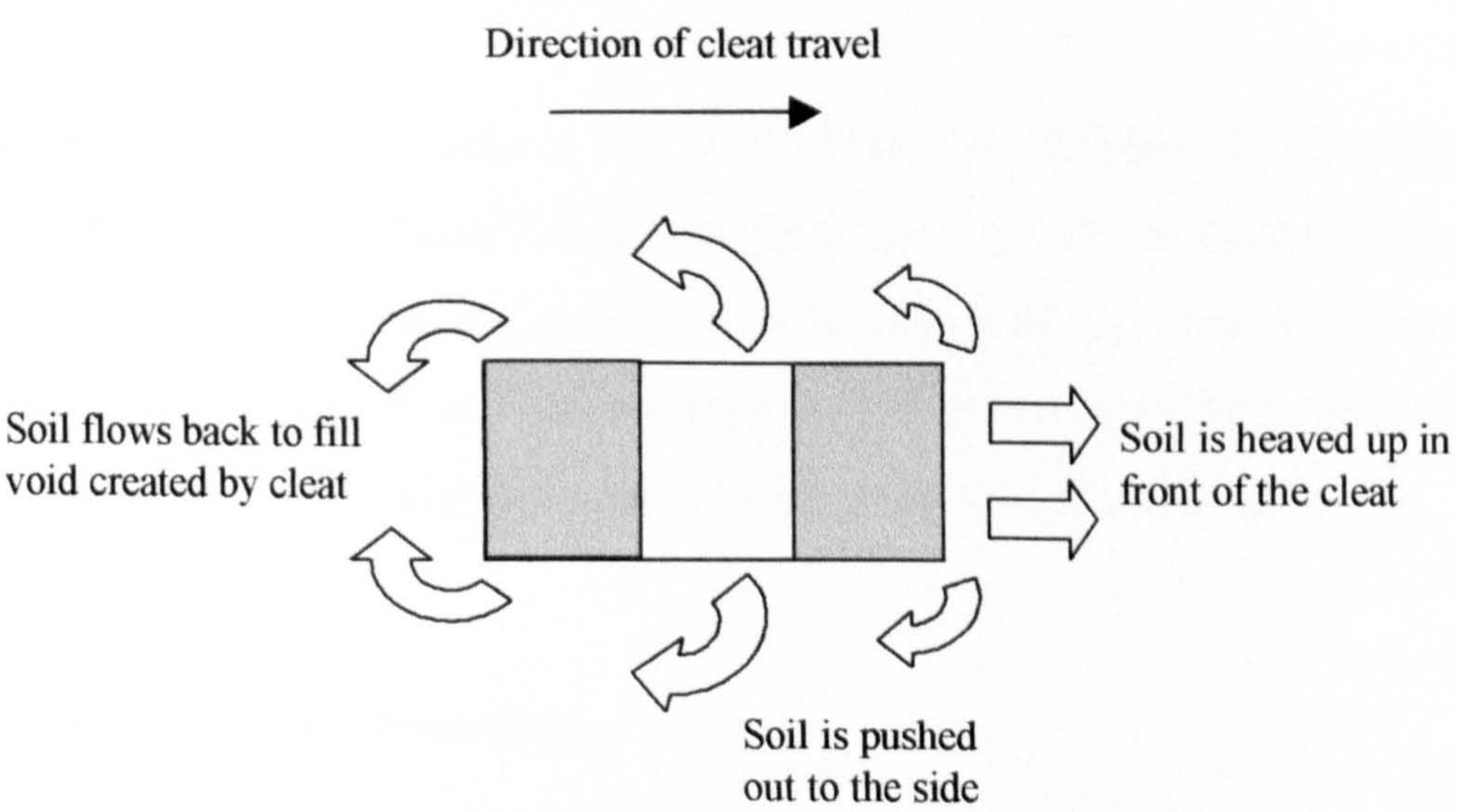

Fig. 6.3: Plan view of cleat and sand flow during slip.

6.3. Comparisons of Cleat Length and Three Dimensional End Effects

6.3.1. Introduction

Since the mathematical models were two dimensional, it was important that the experimental results to be compared also represented two dimensional behaviour. Observations from previous tests have demonstrated that the extent of soil flow was dependent upon the cleat length. As the cleat length increased, the soil flow around the sides of the cleats decreased in significance. It was deemed necessary to investigate this phenomenon to find at what lengths the soil behaviour constituted a three dimensional problem with lateral soil flow as opposed to a two dimensional problem where the effect of lateral soil flow was negligible.

During the preliminary tests (results in appendix II) the cleats used were of:

lengths $l = d$, $3d$ and $5d$

width $b = d$

height $h = d$

where the cleat dimensions were all multiples of d = 45mm, and the same vertical load of 20kg was applied irrespective of cleat length.

However, in order to achieve a true comparison of different length cleats and to investigate the effects of soil flow around the cleats, i.e. three dimensional effects, it was necessary to increase the vertical load in proportion to cleat length so that the nominal pressure beneath each of the cleats was then the same. Therefore differences in traction performance would be due to three dimensional end effects only.

6.3.2. Experimental Procedure

The tests were carried out using the experimental procedure in section 5.9. Vertical loads of 10kg, 30kg and 50kg were applied to non tapered cleats of height $h = d$, width $b = d$ and lengths $l = d$ (45mm), $3d$ (135mm) and $5d$ (225mm) respectively for the first tests. In this way, the nominal pressure beneath the cleats was the same for all of the cleats. It became apparent that more results were required for a comprehensive investigation and accurate horizontal load (traction force) against

cleat length curves, therefore further tests were carried out. The same cleat shape was used with additional lengths of $l = d/2$ (23mm), $2d$ (90mm), $4d$ (180mm) and $6d$ (270mm) with vertical loads of 5kg, 20kg, 40kg and 60kg respectively. The tests were then all repeated with a different cleat shape. A narrower cleat width of $b = d/2$ (23mm) was selected with the same lengths $l = d/2$ (23mm), d (45mm), $2d$ (90mm), $3d$ (135mm), $4d$ (180mm), $5d$ (225mm) and $6d$ (270mm) and corresponding vertical loads as before. The horizontal load (traction force) per unit of cleat length (load per d) and sinkage were plotted against cleat length.

6.3.3. Sinkage Results

The results of the first tests using cleats of width $b = d$ and height $h = d$ are shown in table 6.3 and are illustrated by figure 6.4. Initial sinkage was on average 2mm for the cleat length $l = d/2$ (23mm) and 3mm for the cleat length $l = d$ (45mm). Initial sinkage was negligible for all the other lengths.

Actual sinkage and sinkage with respect to soil flow for the front and rear cleat are shown for the different cleat lengths in figure 6.4. It may be seen that actual sinkage at both the front and rear cleat is approximately consistent over all cleat lengths with the exception of length $l = d$. This demonstrates that actual sinkage is, as expected, determined by the nominal pressure beneath the cleats, which was the same for all lengths. Sinkage with respect to soil flow, however, was affected more by three dimensional effects. Flow sinkage at the front cleat was greater than that of the rear cleat due to sand flowing from the front around the sides, and sand moving around the rear cleat filling in behind. It may be seen that the flow sinkage decreases with increased cleat length (except for length $l = d/2$), due to the three dimensional effects becoming less significant. For cleat length $l = d/2$, the reduced sinkage with respect to soil flow was thought to be due to the minimal amount of sand heaved up at the front and flow and therefore lower around the sides.

cleat len	Rr sin (act)	Rr sink (flo)	Fr sink (act)	Fr sink (flo)	sink bet cleats	Init sink	slip dist	T (kg)	sh zone len	sh zone hei	vert load	load/d
d/2	36	44	35	46	44	2	44	3	62	17	5	6
d/2	40	44	41	48	45	3	35	3.2	66	18	5	6.4
d/2	27	28	27	30	29	3	17	3.2	46	13	5	6.4
d/2	26	34	26	37	38	1	31	2.5	44	15	5	5
d/2	43	29	43	29	32	3	23	2.5	44	10	5	5
d/2	28	32	28	37	30	2	39	3.5	46	19	5	7
d/2	24	30	24	32	29	2	18	3	51	9	5	6
d/2	27	32	27	35	35	2	25	3	57	9	5	6
d/2	27	32	27	34	33	2	12	3.3	56	10	5	6.6
	mean=30.9	mean=31.7	mean=30.9	mean=36.4				mn=3.0				mn=6.0
d	31	36	31	38	43	4	45	4	65	18	10	4
d	39	43	40	51	45	2	103	5.5	86	27	10	5.5
d	32	38	33	42	44	4	66	4.5	89	25	10	4.5
d	36	44	36	48	45	3	90	5	84	29	10	5
d	34	41	35	46	45	3	83	4..8	86	28	10	4.8
	mean=34.4	mean=40.4	mean=35.0	mean=45.0				mn=4.8				mn=4.8
2d	30	37	30	38	45	1	60	7	102	34	20	3.5
2d	29	31	30	37	45	0.5	52	6	116	29	20	3
2d	28	37	29	37	45	1	60	6.5	109	32	20	3.3
2d	31	42	32	49	45	1	105	8.5	121	42	20	4.3
2d	31	42	32	44	45	0.5	92	9	108	46	20	4.5
2d	3	37	32	39	45	1	71	7.5	111	33	20	3.8
	mean=30.0	mean=37.7	mean=30.5	mean=40.7				mn=7.4				mn=3.7
3d	28	33	30	41	45	0.5	79	11.5	142	34	30	3.8
3d	28	37	27	41	45	0.5	96	12.5	106	40	30	4.2
3d	28	38	28	42	45	0.5	89	11.5	123	40	30	3.8
3d	32	48	32	51	45	0.5	119	13	141	47	30	4.3
3d	27	35	26	37	45	0.5	75	11.4	116	35	30	3.8
	mean=28.6	mean=38.2	mean=28.6	mean=42.4				mn=12				mn=4.0
4d	32	27	34	26	45	1	74	11.5	128	27	40	2.9
4d	32	34	31	28	45	1	77	12.5	165	60	40	3.1
4d	29	35	30	36	45	1	62	9.5	125	25	40	2.4
4d	32	38	33	38	45	0.5	70	12.5	147	50	40	3.1
4d	30	39	30	40	45	0.5	78	12.5	134	33	40	3.1
	mean=30.7	mean=34.7	mean=31.5	mean=34.3				mn=11.7				mn=2.9
5d	24	33	26	39	42	1	54	12	141	26	50	2.4
5d	28	34	32	41	43	0.5	85	13	154	33	50	2.6
5d	37	44	29	44	44	0.5	89	12	145	37	50	2.4
5d	25	32	3	29	45	0.5	68	14.3	132	27	50	2.9
5d	27	32	32	35	45	1	63	13.2	135	29	50	2.6
	mean=28.2	mean=35.0	mean=29.8	mean=37.6				mn=12.9				mn=2.6
6d	31	37	31	35	45	1	66	16.5	142	28	60	2.8
6d	29	35	29	37	45	1	62	16.5	135	26	60	2.8
6d	28	32	26	29	45	1	48	17	158	28	60	2.8
6d	32	33	28	28	45	0.5	66	17	150	29	60	2.8
	mean=30.0	mean=35.0	mean=285	mean=32.3				mn=16.8				mn=2.8

Table 6.3: Cleat width $b = d$ (45mm) and height $h = d$ (45mm). Measurements in mm unless stated.

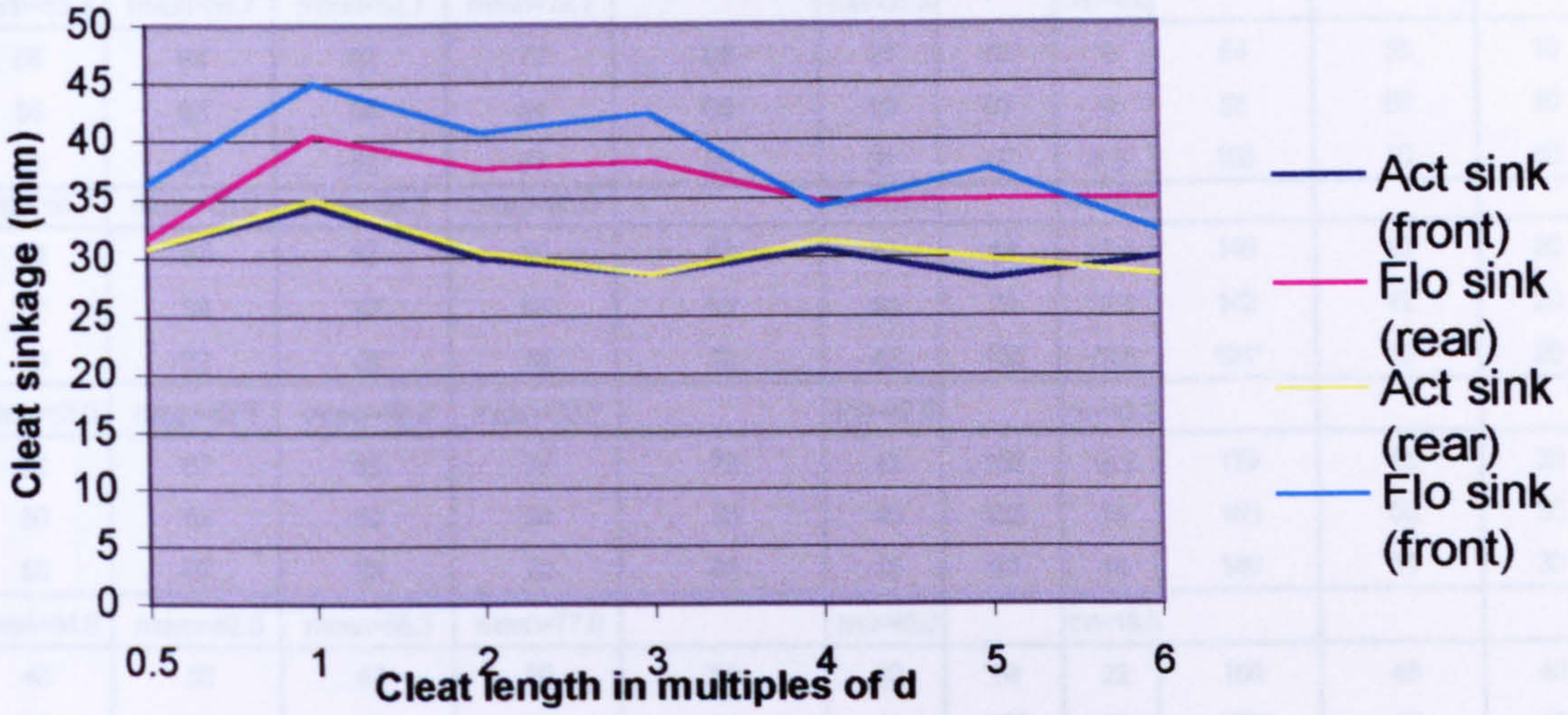

Figure 6.4: Actual and flow sinkage against cleat length for cleat $b = h = d$

The tests were then repeated using cleats of width $b = d/2$ (23mm) and height $h = d$ (45mm). The results shown are shown in table 6.4 and figure 6.5. On initial loading the cleats of width 23mm produced virtually full sinkage.

Actual sinkage and sinkage with respect to soil flow for the front and rear cleat are again shown for the different cleat lengths in figure 6.5. Overall, sinkage was seen to be approximately proportional to nominal pressure, the cleat width $b = d/2$ was approximately double that of $b = d$. Actual sinkage at both the front and rear cleat is approximately constant over all cleat lengths with the exception of length $l = 5d$. This again demonstrates that actual sinkage is determined by the nominal pressure beneath the cleats, which was the same for all cleat lengths. Sinkage with respect to soil flow, however, showed greater three dimensional effects. During virtually all the tests the sand flowed over the top of the front cleat as slip occurred. The sinkage measurement included the total height of the cleat (62mm) and the depth of sand on top of the cleat.

cleat len	Rr sin (act)	Rr sink (flo)	Fr sink (act)	Fr sink (flo)	sink bet cleats	init sink	slip dist	T (kg)	sh zone len	sh zone hei	vert load	load/d
d/2	52	59	51	72	62	32	71	7	51*	30	5	14
d/2	52	57	51	74	61	31	75	7	40*	30	5	14
d/2	56	60	56	72	64	28	75	6.5	81	25	5	13
	mean=53.3	mean=58.7	mean=52.7	mean=72.7		mn=31.3		mn=6.8				mn=13.7
d	56	64	52	73	69	21	83	9	64	35	10	9
d	56	63	56	64	66	19	67	9	58	60	10	9
d	55	63	55	67	66	31	62	8.5	106	30	10	8.5
	mean=55.7	mean=63.3	mean=54.3	mean=68.0		mn=23.7		mn=8.8				mn=8.8
2d	55	67	57	69	69	43	88	13.5	145	43	20	6.8
2d	12*	59	10*	67	63	40	70	12.5	142	42	20	6.3
2d	49	62	49	76	70	43	100	13.5	124*	35	20	6.8
	mean=52.0	mean=62.7	mean=53.0	mean=70.7		mn=42.0		mn=13.2				mn=6.6
3d	62	67	63	77	72	45	153	18.5	179	58	30	6.2
3d	50	67	50	84	70	45	136	19	165	50	30	6.3
3d	50	52	53	70	65	45	80	18	149	51	30	6
	mean=54.0	mean=62.0	mean=55.3	mean=77.0		mn=45.0		mn=18.5				mn=6.2
4d	48	56	47	66	60	42	84	22	156	45	40	5.5
4d	47	55	47	69	61	41	105	23	130*	47	40	5.8
4d	51	60	51	79	64	44	135	23	192	49	40	5.8
	mean=48.7	mean=57.0	mean=48.3	mean=71.0		mn=42.3		mn=22.7				mn=5.7
5d		52		87	69	40	180	27.5	198	70	50	5.5
5d	52	54	75	73	64	42	118	27	179	55	50	5.4
5d	51	58	51	80	67	45	160	28.5	192	59	50	5.7
	mean=51.5	mean=54.7	mean=68	mean=80.0		mn=42.3		mn=27.7				mn=5.7
6d	41	50	42	74	64	45	80	29.5	172	49	60	4.9
6d	45	57	45	77	63	45	122	30	175	48	60	5
6d	45	57	45	73	58	45	115	30.5	169	53	60	5.1
	mean=43.6	mean=54.7	mean=44	mean=74.7		mn=45.0		mn=30.0				mn=5.0

*Rouge results not included within mean. All measurements in mm unless otherwise stated.

Table 6.4: Cleat width $b = d/2$ (23mm) x height $h = d$ (45mm).

Flow sinkage at the front cleat was greater than that of the rear due to sand flowing from the front around the sides, and sand moving around the rear cleat filling in behind. It may be seen that the flow sinkage at the front increased slightly with increased cleat length, whereas flow sinkage at the rear decreased slightly with increased cleat length. The amount of flow sinkage at the rear cleat approached that of actual sinkage. It was thought that sand flow from in between the cleats was made easier because of the smaller cleat width and therefore greater gap. There was also much greater sinkage overall for the narrower cleat, increasing the amount of sand heaved up at the front, and flowing around the sides.

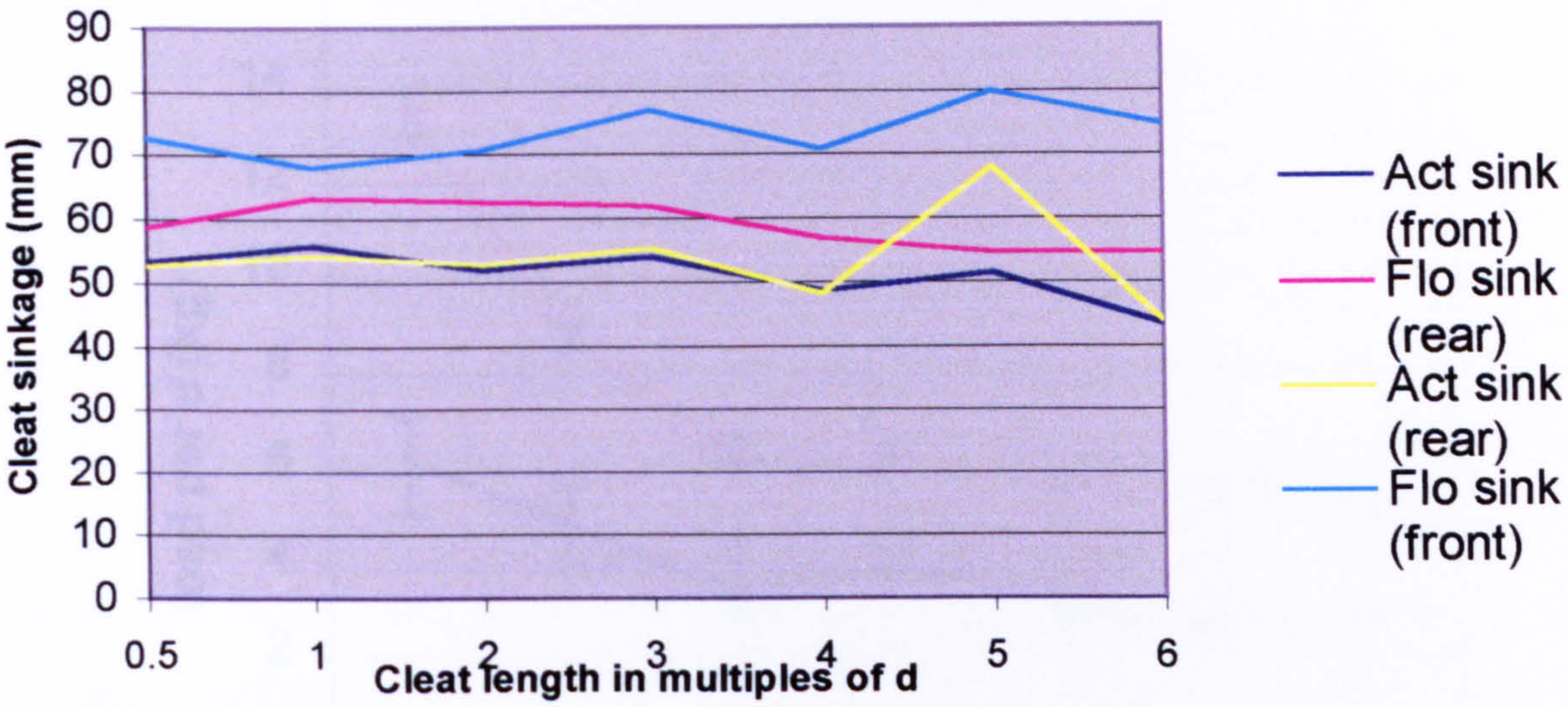

Figure 6.5: Actual and flow sinkage against cleat length for cleat $b = d/2$, $h = d$

6.3.4. Traction Force Results

Overall, the horizontal loading required to induce slip followed a consistent pattern. Figure 6.6 shows traction force (horizontal load) per unit length *d* (load per *d*) against cleat length for both the 23mm and 45mm cleat widths. From the graph it can be seen, for the smaller cleat lengths, up to 90mm *(2d)*, the load per length *d* required to induce slip is significantly greater, but reduces with increased length. This effect is due to the three dimensional flow of sand apparent with the smaller cleat lengths. As the cleat length increases, it can be seen that the three dimensional effects become less significant. The three dimensional end effects are shared between each unit of cleat length *d* and as the length increases, the effects become a smaller part of the traction per unit length (*d*). Hence the curve becomes horizontal as each unit of cleat length (*d*) contributes approximately the same constant traction force.

Having carried out the first experiments using the 45mm width cleat the experiments were repeated with another cleat width, 23mm, to check that the curves became

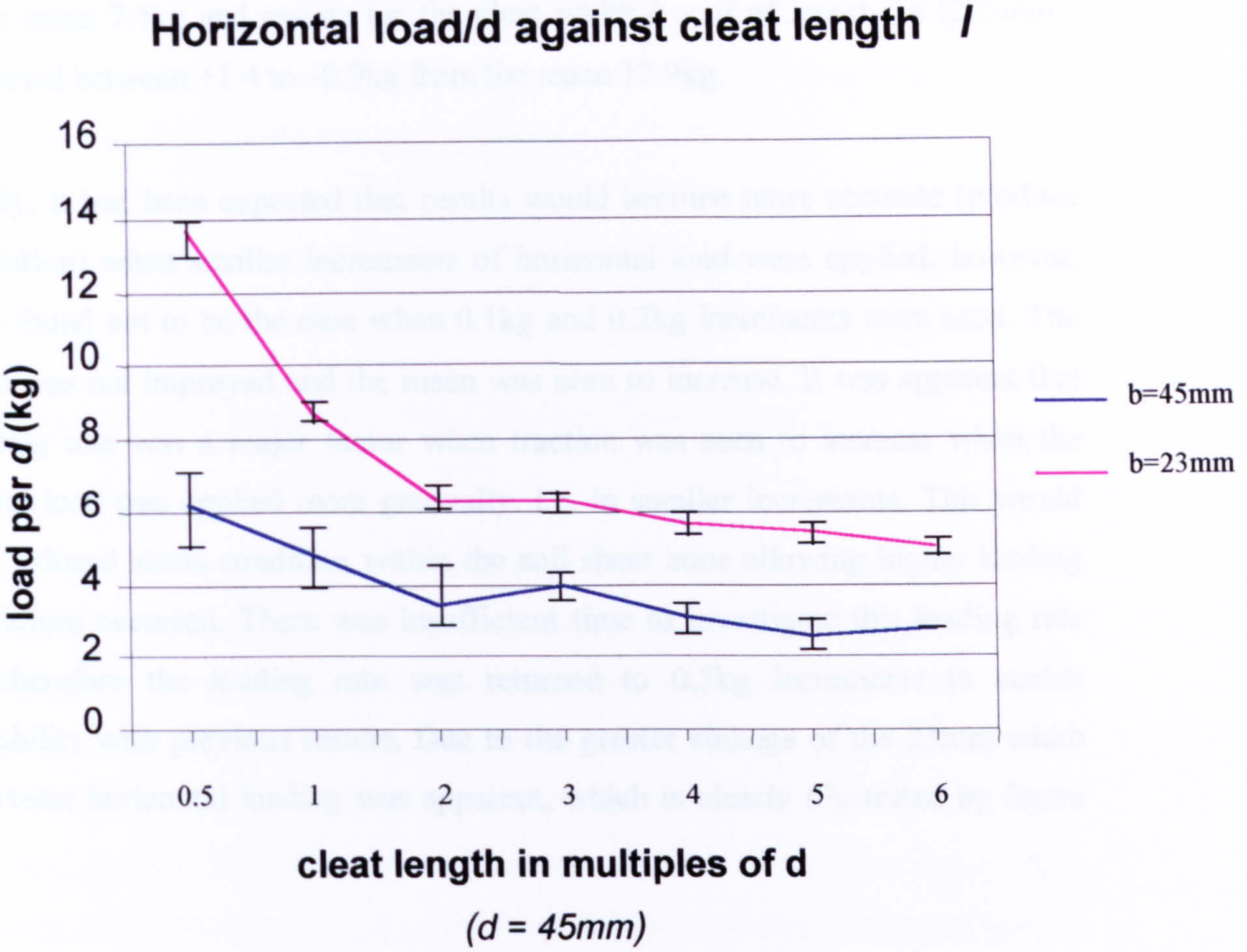

Fig. 6.6: Load/d against cleat length

horizontal in a similar way and this could then be assumed for all cleat shapes. The reason for the anomaly at cleat length *3d* is unknown.

The 23mm width cleats produced nearly twice as much sinkage as the 45mm cleats which has contributed to the greater resistance to slip, and hence greater horizontal load per unit cleat length (*d*). The variation of horizontal loading for each of the cleats was also much less for the 23mm width cleats. It can be seen from the graph that the variation has almost halved. This suggests that greater initial sinkage probably helps repeatability.

The results for each of the cleats were all within +/- 1kg with the exception of results for the cleat width $b = d$ of length *2d* (90mm), which varied between +1.6 to –1.4kg

from the mean 7.4kg and results for the cleat width $b = d$ of length $5d$ (225mm), which varied between +1.4 to –0.9kg from the mean 12.9kg.

Originally, it had been expected that results would become more accurate (produce less variation) when smaller increments of horizontal load were applied, however, this was found not to be the case when 0.1kg and 0.2kg increments were used. The variation was not improved and the mean was seen to increase. It was apparent that the loading rate was a major factor when traction was seen to increase when the horizontal load was applied more gradually, i.e. in smaller increments. This would imply a reduced stress condition within the soil shear zone allowing higher loading before failure occurred. There was insufficient time to investigate this loading rate effect, therefore the loading rate was returned to 0.5kg increments to enable comparability with previous results. Due to the greater sinkage of the 23mm width cleat, greater horizontal loading was apparent, which is clearly illustrated by figure 6.6.

6.3.5. Conclusions

It was expected that as cleat length increased, the three dimensional effects of soil flowing around the sides of the cleats would become less significant. Therefore a number of tests were carried out using two cleat widths, 23mm and 45mm, and seven cleat lengths 23mm, 45mm, 90mm, 135mm, 180mm, 224mm and 270mm. The vertical load that was applied during these tests was in proportion to cleat length, 10kg per 45mm *(d)*, so that the nominal pressure beneath all cleats was the same.

Referring to figures 6.4 and 6.5, as expected, sinkage is approximately constant because it is determined by the nominal pressure beneath the cleats. Sinkage was much greater for the 23mm width cleats than for the 45mm cleats. In fact, it can be seen that the sinkage approximately doubled which implies that sinkage is proportional to nominal pressure.

From figure 6.6, the three dimensional end effects were seen to become less significant as cleat length increased. The curves are seen to approach the horizontal

at *4d*, for both cleat widths, and at that cleat length, approximately two dimensional behaviour is assumed. To reduce the experimental time, the cleat length *4d* was selected to represent a two dimensional problem.

It can be seen that the amount of sinkage significantly affected traction force.

6.4. Proportion of Traction from Different Cleat Areas

6.4.1. Introduction

In previous tests the net traction force that was measured included compressive and friction forces between sand and cleats at the front, rear, sides and base. However, it was not possible to differentiate between the contributions of these different forces. From previous tests it could be seen that the amount of cleat sinkage and therefore amount of sand heaved up at the front of the cleat during slip corresponded with traction performance. The effect of sand heaving up at the front of the cleats during slip was originally thought to be the major contribution to overall traction although it was apparent that the friction forces were also important contributory factors. To enable traction performance to be properly considered in cleat design it was necessary to determine the contribution to traction of the various cleat parts. It was also necessary to measure the shear resistance of the sand in front, in between and to the rear of the cleat as well as surface friction distribution over the cleat to enable comparisons with the results from the mathematical models, which can be used to calculate these separate components.

.

6.4.2. Experimental Procedure

To enable comparisons to be made between the experimental results and mathematical modelling results the experiments had to be conducted in such a way as to create approximately two dimensional soil behaviour. Therefore a cleat length of 180mm (*4d*) was selected based on the previous investigation of three dimensional end effects. However, as a comparison to this test a cleat length of 45mm (*d*) was also used with the same height and width but with restrictions on soil flow so to also

represent a two dimensional problem. The traction distributions obtained using the two techniques were then compared.

For the 45mm length cleats, to produce two dimensional shear of the sand between the cleats, in front of the front cleat and rear of the rear cleat, it was necessary to stop sand flow around the cleat sides. In addition, it was considered necessary to achieve full sinkage in all cases to enable proper comparisons to be made. It was therefore decided to use the 23mm width cleat with 3mm Perspex sides, as illustrated by figure 6.7, because it required less vertical load to initiate full sinkage. By removing sand and using Perspex sides to prevent sand from flowing out from in between the cleats a representative two dimensional problem was created. The cleat was loaded with 10kg and the loading pole gently tapped on its side with a steel rule to achieve full initial sinkage (45mm) of the cleats. The sand surrounding the cleat was then removed by hand at either the sides, in front of the front cleat or to the rear of the rear cleat depending on the experiment. The sand was removed carefully so not to collapse the sand sides. The horizontal load was applied in 100g increments using the same experimental procedure as before (section 5.9) because of the reduced sinkage resistance having removed surrounding sand. This technique was found to be more repeatable.

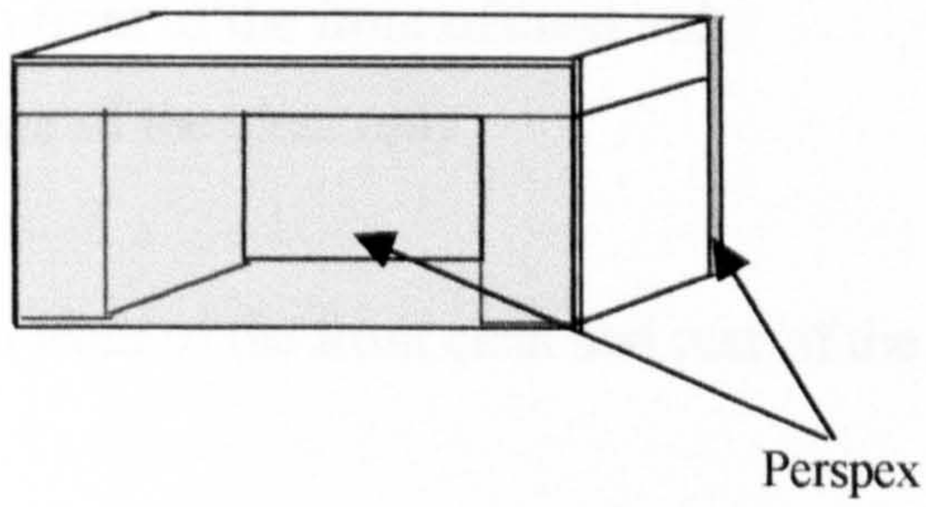

Figure 6.7: Cleat of width 23mm with Perspex sides

The tests using the 45mm cleat were repeated for:

1. Removal of sand from in front of the front cleat, rear of the rear cleat and from the Perspex sides.
2. Removal of sand from in front of the front cleat only
3. Removal of sand from rear of the rear cleat only
4. No removal of sand
5. Removal of sand from in front of the front cleat and rear of the rear cleat.

The experiments were repeated six times for each case.

For the 180mm, *(4d)* cleats, the length had already been identified as producing a two-dimensional effect, therefore Perspex sides were not required. Sand was not removed from the sides of the cleats because lateral soil flow had a minimal effect and also to restrain the sand in between the cleats from flowing out. The same cleat height of 45mm and width 23mm was used as before. A 40kg vertical load was applied and the horizontal load was applied in 500g increments due to the larger shear resistance. The nominal pressure beneath both the 45mm cleats and the 180mm cleats was then consistent. Full initial sinkage of 45mm was again achieved by gently tapping on the side of the loading pole before horizontal loading.

The tests using the 180mm cleat were repeated for:

6. Removal of sand from in front of the front of cleat only
7. Removal of sand from rear of the cleat only
8. No removal of sand
9. Removal of sand from in front of the front cleat and rear of the rear cleat only.

The experiments were repeated five times for each case.

In experiment 1 the sand was removed from in front of the front cleat, from behind the rear cleat and from the outside of the Perspex sides of the 45mm length cleats, so that only the shear of the sand in between the cleats was considered. However, adhesive and friction forces beneath the cleats would also be included within this

result. Passive and active earth pressures, adhesion at the front and rear and friction and adhesion at the sides have been eliminated.

In experiment 2 sand was removed from in front of the front cleat only, so that the shear resistance of the sand in between the cleats, friction and adhesion at the sides, rear and beneath, and active earth pressure at the rear of the cleat contributing to slip (a negative effect on traction) was considered.

In experiment 3 sand was removed from the rear of the rear cleat only, so that the shear resistance of the sand between the cleats, friction and adhesion at the sides, front and beneath, and the passive earth pressure at the front of the cleat was considered. As the sand is heaved up at the front it acts like a brake. Removal of sand at the rear, increases overall traction since the active earth pressure at the rear is removed.

In experiment 4 when no sand was removed, shear resistance, friction and adhesion on all surfaces was considered as well as passive and active earth forces. The experiment also acts as a control throughout the series of tests enabling the investigation into the effect of active and passive pressure as well as traction distribution over the whole cleat.

In experiment 5 sand was removed from in front of the front cleat and from behind the rear of the 45mm length cleats, so that only the shear of the sand in between the cleats and friction and adhesion at the sides was considered. However, adhesive and friction forces beneath the cleats would also be included within this result. Passive and active earth pressures and adhesion at the front and rear have been eliminated.

In experiment 6 removal sand was removed from in front of the front cleat only for the 180mm cleat, so that the shear resistance of the sand between the cleats, friction and adhesion at the sides and beneath, and active earth force at the rear was considered.

In experiment 7 sand was removed from the rear of the rear cleat only so that the shear resistance of the sand between the cleats, friction and adhesion at the sides and beneath, and the passive earth pressure at the front of the cleat was considered, as in experiment 3.

In experiment 8 when no sand was removed around the 180mm cleat, shear resistance, friction at the sides and beneath the cleats, and adhesion on all surfaces was considered as well as passive and active earth forces.

In experiment 9 sand was removed from in front of the front cleat and from behind the rear of the 180mm length cleats, so that only the shear resistance of the sand in between the cleats and friction and adhesion at the sides and beneath was considered. Passive and active earth pressures and adhesion at the front and rear have been eliminated as in experiment 5.

6.4.3. Results Using Cleat Length 45mm (*d*).

The mean and variation have been calculated for each of the five experiments. Since 100g increments were used when loading horizontally the results were all within +/- 5% of the mean with the exception of experiment 4, which was +15/-20%. Variation of results was also minimised due to the consistency of the sinkage condition, which was full in all cases. The cleats were also positioned in the same part of the tray for each experiment and a stopper was used to stop the tray from sliding off the end of the rollers. Maximum slip distance was achieved for the second and fifth experiment, tables 6.6 and 6.9 respectively. It can be seen that the net horizontal force, traction, has been minimised with the removal of sand from in front of the front cleat, i.e. removing the passive earth resistance.

Traction was seen to increase when sand was removed from the rear, since active earth pressure was removed. However, unexpectedly, the greatest traction force was seen when no sand was removed, when all forces were applied to the cleats and sand.

Initial sinkage (mm)	Slip distance (mm)	Horizontal load (kg)
45 (full)	128	6.2
45 (full)	199	6.5
45 (full)	215	6.2
45 (full)	252	6.5
45 (full)	370	6.6
45 (full)	315	6.5

Mean 6.42 +0.18/-0.22kg

Table 6.5: Exp.1 Removal of sand from front, rear and sides of cleat (length *d*).

Initial sinkage (mm)	Slip distance (mm)	Horizontal load (kg)
45 (full)	378	6.1
45 (full)	387	5.9
45 (full)	378	5.7
45 (full)	378	6.3
45 (full)	374	6.0
45 (full)	373	5.9

Mean 5.98 +0.32/-0.28kg

Table 6.6: Exp. 2 Removal of sand from front of cleat only (length *d*).

Initial sinkage (mm)	Slip distance (mm)	Horizontal load (kg)
45 (full)	127	8.5
45 (full)	105	8.5
45 (full)	235	8.5
45 (full)	144	8.5
45 (full)	221	9.0
45 (full)	110	8.5

Mean 8.58 +0.42/-0.08kg

Table 6.7: Exp. 3 Removal of sand from rear of cleat only (length *d*).

Initial sinkage (mm)	Slip distance (mm)	Horizontal load (kg)
45 (full)	117	9.0
45 (full)	105	9.0
45 (full)	220	8.5
45 (full)	331	8.5
45 (full)	115	8.5
45 (full)	68 (premature slip) 336 (full slip)	7.0 8.0

Mean 8.75 +1.25/-1.75kg

Table 6.8: Exp. 4 No removal of sand (length *d*).

Initial sinkage (mm)	Slip distance (mm)	Horizontal load (kg)
45 (full)	380	6.8
45 (full)	377	6.6
45 (full)	372	6.9
45 (full)	379	6.7
45 (full)	380	6.8
45 (full)	375	6.8

Mean 6.77 +0.13/-0.17kg

Table 6.9: Exp. 5 Removal of sand from front and rear of cleat only (length *d*).

This was thought to be due to the resistance to sand displacement, for example, when sand has been removed from the rear of the cleat the remaining sand at the front and sides can flow into that space, but when no sand has been removed there is no space in which to flow, which means the flow of sand is made more difficult. Therefore flow was increased when sand was removed from the sides, front or rear of the cleats.

	Load (kg)	% Total traction
Total traction (exp. 4)	8.75	100
Traction from between* cleats only (exp. 1)	6.42	73.4
Traction from between* cleats and side adhesion (exp. 5)	6.77	77.4
Traction from front, between* and sides (exp. 3)	8.58	94.3
Traction from behind, between* and sides (exp. 2)	5.98	68.3
Traction from behind cleat (from exp. 5 & 2)	-0.79	-9.0
Traction from behind cleat (from exp. 4 & 3)	0.17	1.9
Traction in front of cleat (from exp. 5 & 3)	1.81	20.7
Traction in front of cleat (from exp. 4 & 2)	2.77	31.7
Adhesion on cleat sides incl. Perspex (from exp. 1& 5)	0.35	4.0

* Note that "between cleats" is shorthand for "in between and beneath cleats"

Table 6.10: Traction distribution

The percentage traction contributions have been calculated from the means for each experiment, table 6.10. The control experiment where no sand has been removed has been taken as total traction, i.e. 100%. The individual traction contributions of the different cleat areas include in between and beneath the cleats, cleat sides, in front of the front cleat and behind the rear cleat.

There were two different ways of calculating the traction contributions from behind and in front of the cleats depending on the experiments used. Both methods have been used and the results included in the table below. The percentage of traction from behind the rear cleat may be calculated from either experiments 5 and 2, or from 4 and 3 with a difference of 5.5%. The percentage of traction from in front of the front cleat may be calculated from either experiments 5 and 3, or from 4 and 2 with a difference of 11%. The average traction distribution result was taken from both calculation methods for both the front and rear, 26.2% and –5.45% respectively, as shown in the traction distribution summary of figure 6.8.

The error produced when totalling the individual load contributions, 8.58kg, (including average front and rear calculations, adhesion and shear resistance between

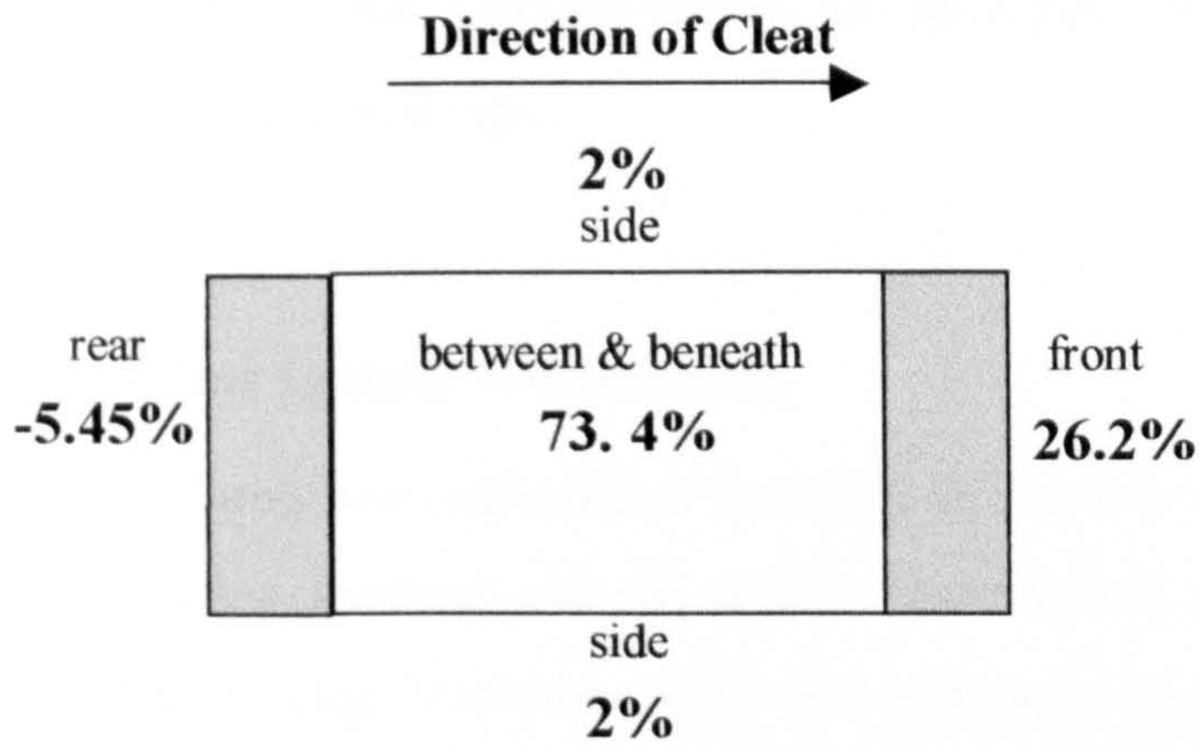

Figure 6.8: Traction distribution

cleats) is 1.9% of the total horizontal load 8.75kg. However, it must be noted that the errors incurred if the calculations for front and rear traction contributions had not been averaged were of -10% or +10% depending on which calculations were used. This experimental error has therefore been averaged out. It is also thought that the resistance due to soil flow increases traction, which is reduced when areas of sand are removed. For example, removing sand in one area of the cleat, affects the earth forces in a different area, i.e. removing sand at the rear reduces passive earth force at the front. This is shown in the control experiment, total traction, when no sand has been removed where the greatest traction force has been produced. However, this has not been investigated at this stage of the research.

The sand at the rear of the cleat aids slip and is therefore regarded as a negative contribution to traction, it includes both adhesion and active earth pressure. The sand at the front of the cleat resists slip and is therefore regarded as a positive contribution to traction, it includes both adhesion and passive earth pressure. The passive earth pressure was found to be significantly larger than the active earth pressure, this was to be expected from the mathematical modelling work that has been carried out.

Originally, the sand that was heaved up in front of the cleat during slip was thought to be the major contributor to slip resistance, but this was discovered not to be the case. The shear resistance between and beneath the cleats in fact provided most of

the traction. This is apparent for wooden cleats on sand and will obviously vary according to cleat material and soil type.

6.4.4. Results Using Cleat Length 180mm (*4d*).

The mean and variation have been calculated for each of the four experiments. 500g increments were used when loading and the results were again accurate with only small variation, less than +/-1kg. Variation of results was again minimised due to the consistency of the sinkage condition, which was full in all cases. The cleats were also positioned in the same part of the tray for each experiment. The minimum traction was produced with the removal of sand from both in front of the front cleat and behind the rear cleat. Traction increased when sand was removed from the rear compared to the control experiment when no sand was removed, since active earth pressure was removed.

The percentage traction contributions have been calculated based upon the means from each experiment, table 6.15. The control experiment where no sand has been removed has been taken as total traction, i.e. 100%, and the individual traction contributions were calculated as before.

Both methods of calculating the traction behind and in front of the cleats depending on the experiments used are included within the results table below. The percentage of traction from behind the rear cleat may be calculated from either experiments 6 and 9, or from 8 and 7 with a percentage difference of 1.3%. The percentage of traction from in front of the front cleat may be calculated from either experiments 7 and 9, or from 8 and 6 with a similar difference in percentage of 2.2%. The average traction distribution result was taken from both calculation methods for both the front and rear, 23.4% and –1.1% respectively, as shown in the traction distribution summary figure of 6.9.

Initial sinkage (mm)	Slip distance (mm)	Horizontal load (kg)
45 (full)	144	17.5
45 (full)	112	17.5
45 (full)	164	18
45 (full)	152	18.5
45 (full)	132	17.5

Mean 17.8 +0.7/-0.2kg

Table 6.11: Exp. 6 Removal of sand from front of cleat only (length *4d*).

Initial sinkage (mm)	Slip distance (mm)	Horizontal load (kg)
45 (full)	111	24
45 (full)	97	23
45 (full)	88	22
45 (full)	62	23
45 (full)	103	23

Mean 23 +/- 1kg

Table 6.12: Exp. 7 Removal of sand from rear of cleat only (length *4d*).

Initial sinkage (mm)	Slip distance (mm)	Horizontal load (kg)
45 (full)	123	23
45 (full)	84	22
45 (full)	105	23
45 (full)	97	23
45 (full)	109	23.5

Mean 22.9 +0.6/-0.9kg

Table 6.13: Exp. 8 No removal of sand (length *4d*).

Initial sinkage (mm)	Slip distance (mm)	Horizontal load (kg)
45 (full)	112	17
45 (full)	93	17.5
45 (full)	85	17.5
45 (full)	137	18
45 (full)	67	17

Mean 17.4 +0.6/-0.4kg

Table 6.14: Exp. 9 Removal of sand from front and rear of cleat only (length *4d*).

	Load (kg)	% Total traction
Total traction (exp. 8)	22.9	100
Traction from between* cleats and sides only (exp. 9)	17.4	75.98
Traction from front, between* and sides (exp. 7)	23	100.44
Traction from behind, between* and sides (exp. 6)	17.8	77.73
Traction from behind cleat (from exp. 6 & 9)	-0.4	-1.75
Traction from behind cleat (from exp. 8 & 7)	-0.1	-0.4
Traction from in front of cleat (from exp. 7 & 9)	5.6	24.45
Traction from in front of cleat (from exp. 8 & 6)	5.1	22.3

* Note that "between cleats" is shorthand for "in between and beneath cleats"

Table 6.15: Traction distribution

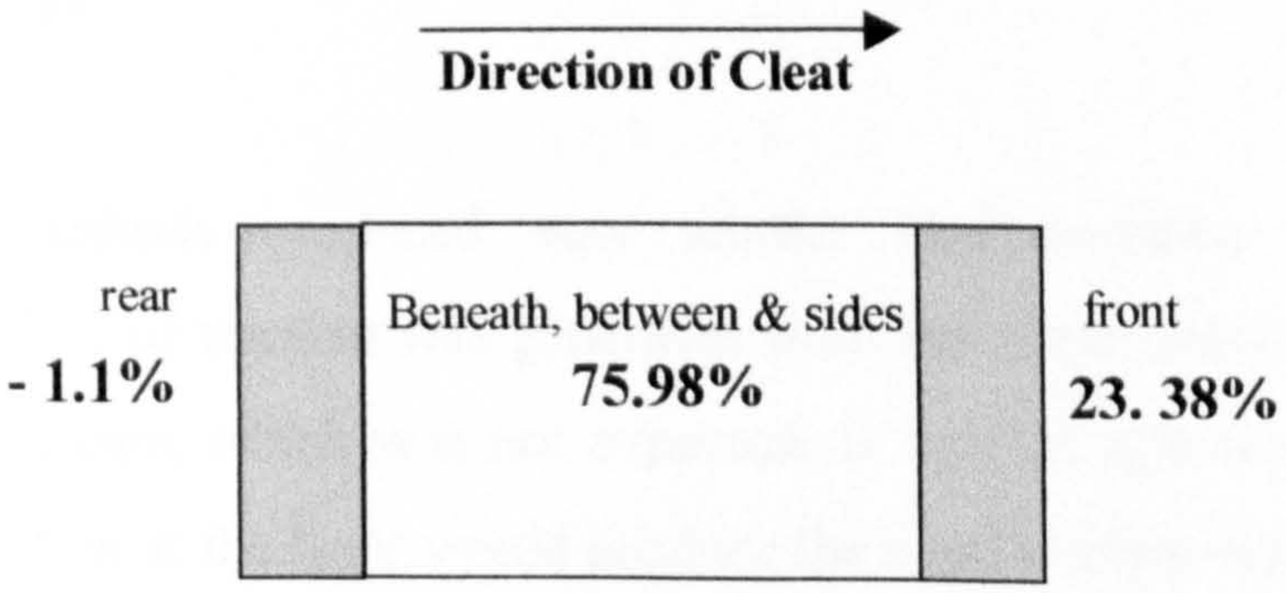

Figure 6.9: Traction distribution

The error produced when totalling the individual load distributions, 22.5kg, (including average front and rear calculations, adhesion and between cleats) is 1.7% of the total horizontal load 22.9kg. The experimental errors were of similar magnitudes irrespective of averaging or which calculation was used for the front or rear traction contribution.

These four experiments have enabled the calculation of traction distribution for a two dimensional problem, without the use of Perspex sides.

6.4.5. Conclusions

Traction distribution has been investigated using two methods to approximate a two dimensional problem. One method used Perspex sides to prevent three dimensional soil flow and the other used a cleat long enough to reduce the significance of three dimensional soil flow as concluded from previous analysis. The two sets of results are in good agreement.

The use of Perspex sides and a small cleat length has produced an error, 1.9% compared to 2.8% for the cleat length *4d*. However, had the traction contributions from the front and rear not been averaged for the 45mm cleat length, the error would have been significantly larger, +/-10%. A reduction in active earth force (including adhesion forces) is apparent between the two cleat lengths, with the 45mm length having P_a (including adhesion forces) of –5.45% compared to –1.1% for the 180mm length. Passive earth force is also greater for the shorter cleat length, 26.2% compared to 23.38%.

Overall, both methods produced very similar characteristics. The majority, approximately 75%, of traction was generated from the shear resistance in between and beneath the cleats, which was not expected. It was thought that the resistance from sand heaved up at the front would produce the most traction but instead was on average 25% of the total traction force. The negative contribution to traction, from the rear was small, in comparison, on average 3%. The adhesion between the cleat

sides was 4% of the total traction with Perspex sides from the 45mm cleat experiments but was not calculated separately for the 180mm cleat.

6.5. Effects of Cleat Height, Width and Taper.

6.5.1. Introduction

A two level, full factorial, investigation was conducted to consider all possible combinations of two cleat heights ($h = d$ and $d/2$), two cleat widths ($b = d$ and $d/2$), with and without a cleat taper, where the base unit d, is 45mm. The full factorial investigation, considering all possible geometric combinations, created eight (2^3) experiments:

1. $h = d$, $b = d$ (no taper)
2. $h = d$, $b = d$ (taper)
3. $h = d$, $b = d/2$ (no taper)
4. $h = d$, $b = d/2$ (taper)
5. $h = d/2$, $b = d$ (no taper)
6. $h = d/2$, $b = d$ (taper)
7. $h = d/2$, $b = d/2$ (no taper)
8. $h = d/2$, $b = d/2$ (taper)

All experiments were carried out using a cleat length $l = 4d$ (180mm) since this length was considered to have negligible three-dimensional effects as discussed previously, and a vertical load of 40kg. Each test was repeated five or six times.

For two of the experiments (5 and 7) using a 23mm cleat height ($h = d/2$), a shallower sand depth of half that used previously, but with the same sand density, was tried to see if tray preparation time could be reduced. Traction forces were compared for both sand depths but no significant differences were seen. The shallower depth could only be used for the shorter cleat height $h = d/2$. In order to

compare these experiments with the others it was necessary to account for the reduction in tray weight, 0.125kg was therefore added to the horizontal loads of experiments 5 and 7. This weight addition was calculated based upon the horizontal load required to pull an empty tray, a tray full of the normal mass of sand in previous tests without the application of a loaded cleat, and therefore the difference in horizontal load required to pull a tray with half the normal mass of sand.

6.5.2. Results

The results for each of the eight experiments are summarised in table 6.16, and the cleats are ranked according to their tractive performance. Brief comments on each experiment are given below. A detailed statistical analysis of these results is reported in chapter 7.

Exp	Cleat height h (mm)	Cleat width b (mm)	Taper	Av. initial sink. (mm)	Av. Sink. after slip (mm)	Av. Horizontal load T (kg)	Av. Load/d	Rank
1	d (45)	d (45)	90°	0.6	31.1	11.7	2.9	7th
2	d (45)	d (45)	70°	28.2	33.4	17.7	4.4	6th
3	d (45)	d/2 (23)	90°	42.3	48.5 (full)	22.7	5.7	2nd
4	d (45)	d/2 (23)	70°	41.8	47.9 (full)	23.6	5.9	1st
5	d/2 (23)	d (45)	90°	0.5	20.4	11.33 (11.2 + 0.125)	2.9	8th
6	d/2 (23)	d (45)	70°	23 (full)	28.5 (full)	19.1	4.7	4th
7	d/2 (23)	d/2 (23)	90°	23 (full)	23 (full)	18.73 (18.6 + 0.125)	4.7	5th
8	d/2 (23)	d/2 (23)	70°	23 (full)	23.9 (full)	21.3	5.3	3rd

Table 6.16: Cleat geometry combinations (d = 45mm)

6.5.2.1. Experiment 1

The average horizontal load was 11.67kg with a range of 9.5-12.5kg. The cleats themselves were not considered to be fully sunk during slip in most cases (see table 6.16), but the soil flow out of the sides was restricted during slip due to the length of the cleats, which were observed to be full towards the centre of the cleat length.

6.5.2.2. Experiment 2

For the first tapered experiment, the horizontal load was 17.67kg with a range of 17-18.5kg. For most of the tests the cleats became full. It must also be noted that on applying the vertical load, without any horizontal load, the initial sinkage was small. However, when approximately 5kg of horizontal load was applied, a large amount of sinkage was produced with minimal slip. The tests were therefore continued until slip occurred.

6.5.2.3. Experiment 3

The average horizontal load was 22.67kg with a range of 22-23kg. The cleat became full after slip for all of these tests.

6.5.2.4. Experiment 4

For the second tapered experiment, the average horizontal load was 23.6kg with a range of 23-24kg. Virtually full sinkage was produced after initial vertical loading.

6.5.2.5. Experiment 5

The average horizontal load was 11.33kg with a range of 9.625-12.125kg. The cleats themselves were not considered to be fully sunk during slip in most cases (see table 6.16), but as with experiment 1, soil flow out of the sides was restricted during slip and therefore the cleats became full towards the centre of the cleat length.

6.5.2.6. Experiment 6

For the third tapered experiment, the average horizontal load was initially 10.3kg with a range of 9-11.5kg. Very small initial sinkage was achieved on initial loading but the cleats became full after slip. The slip distance was also very small. The tests were therefore repeated since the first series of tests only considered the small amount of slip associated with initial horizontal loading as in experiment 2. After full slip was initiated the average horizontal load was increased to 19.1kg with a range of 18-20kg.

6.5.2.7. Experiment 7

The average horizontal load was 18.73kg with a range of 17.625-19.625kg. The cleats became full for four out of the six tests. The other two tests were carried out using a force meter due to the non-availability of weights within the laboratory. The horizontal load was therefore removed as slip occurred, not creating as much soil flow.

6.5.2.8. Experiment 8

For the fourth tapered experiment, the average horizontal load was 21.3kg with a range of 20.5-22.5kg. For three of the tests, very small sinkage occurred after initial vertical loading, however, during initial horizontal loading the cleats fully sank with minimal slip as in previous experiments. The remaining tests became full on initial vertical loading. Similar results were obtained for all tests regardless of initial sinkage conditions.

6.5.3. Preliminary Observations

The effects of cleat height, width and taper on traction are analysed using ANOVA in chapter 7, however, sinkage and its effect on traction will be discussed here. The cleats have been ranked from first to eighth, with the first having the most traction and the eighth having the least.

Comparing experiments 1 and 5, both of cleat width $b = d$, both did not sink after vertical loading. On slip, the cleats were still not fully sunk. The small amount of sinkage resulted in a reduced traction force, only 11.33kg and 11.7kg for cleat height $h = d/2$ and $h = d$ respectively.

With the exception of the cleat of width $b = d$ (experiment 5) all cleats, with and without taper, of height $h = d/2$ fully sank after initial loading, resulting in high traction forces.

The cleats of height $h = d$ did not sink fully on initial vertical loading. The two narrow cleats produced the greatest sinkage. As mentioned previously, the cleat width $b = d$ did not sink at all under initial vertical loading.

All cleats that sank fully after slip produced greater traction forces than those that were not full regardless of cleat height.

In all cases, comparing tapered to non-tapered cleats, i.e. experiments 1 and 2, 3 and 4, 5 and 6, and 7 and 8, the taper produced greater traction although not necessarily greater sinkage. For wider cleats, the taper increased sinkage during slip and for the narrower cleats, the taper produced a reduction in sinkage. Comparing narrow to wide cleats, i.e. experiments 3 and 1, 5 and 7, 2 and 4, and 6 and 8, the narrow cleats all produced significantly more traction and sinkage than the wider cleats.

The full sinkage of the height $h = d/2$ cleats (experiment 6) when compared to the partial sinkage of the cleat of height $h = d$ (experiment 2) was more significant in providing traction than the increase in cleat height. In previous experiments it has become clear that wide, non-tapered cleats (experiment 1) do not sink and provide little traction as seen again in these experiments. The taper improved sinkage and traction considerably for both cleat heights $h = d$ and $h = d/2$. Although this is apparent for wooden cleats on sand, it is not to say that the same would occur in different terrain conditions and with different cleat materials, although it is expected that similar results would be found.

Regarding the accuracy of these tests, some results were very close together. For example, experiments 1 and 5 ranked seventh and eighth respectively, and experiments 6 and 7 ranked fourth and fifth respectively. With such small differences in horizontal load the rank order should not be considered significant. However, the other tests results indicate a clear rank order.

7. Analysis of Experimental Results Using Taguchi Methods

7.1. Introduction

A two level, full factorial, investigation was conducted to consider all possible combinations of two cleat heights, two cleat widths, and with or without a taper, as discussed in section 6.5. The sinkage results have been previously discussed, however, the effects of cleat height, h, cleat width, b, and taper, T, are now analysed using the statistical analysis tools of Taguchi.

Taguchi's method utilises conventional statistics in the design and quality improvement of products and processes. Taguchi's strategy aims to reduce variation and improve quality at lower cost simply by following strict guidelines for experimental layout and analysis of results. The statistical tools used provide a highly effective technique for design optimisation.

Taguchi uses orthogonal arrays to minimise the number of experiments needed for the consideration of main effects and some interaction effects. The analysis of variance (ANOVA) is used to interpret the experimental data and make decisions regarding which parameters affect the average performance and to what degree. It provides methods for estimating percentage contribution, the mean, confidence intervals and experimental error.

7.2. Experimental Design

7.2.1. The Variables

Eight experiments, 2^3 full factorial, were used to investigate the effects of three factors; cleat height (h), cleat width (b), and taper (T). The experiments were two level, using the values shown in table 7.1, which results in the following eight experiments:

1. $h = d$, $b = d$ and no taper

Factors	Level 1	Level 2
h (height)	$h_1 = d$	$h_2 = d/2$
b (width)	$b_1 = d$	$b_2 = d/2$
T (taper)	T_1 (no taper)	$T_2 = 70°$(taper)

Table 7.1: Three factors, two levels.

2. $h = d$, $b = d$ and taper
3. $h = d$, $b = d/2$ and no taper
4. $h = d$, $b = d/2$ and taper
5. $h = d/2$, $b = d$ and no taper
6. $h = d/2$, $b = d$ and taper
7. $h = d/2$, $b = d/2$ and no taper
8. $h = d/2$, $b = d/2$ and taper

7.2.2. Interaction

Interaction describes a condition where the influence of one factor upon the result is dependent on another factor. Interaction is expressed by inserting '×' between the interacting factors. For example, if the factors h and T were said to interact, this effect would be written as $h \times T$. Changing the level of h would alter the influence of T on the result and visa versa.

It was considered necessary to consider all of the interactions between factors in these experiments, $(h \times b)$, $(h \times T)$ and $(T \times b)$, as well as the main effects h, b and T (but not the three way interaction).

7.2.3. The L_8 Experimental Design

To investigate the three main effects and three interaction effects mentioned above an appropriate orthogonal array is required. This enables the separate effects to be

readily identified. The orthogonal array shown in table 7.2 [86] enables a 2^3 full factorial set of experiments to be analysed.

The factor level combinations for the eight experiments are defined by the L_8 orthogonal array. The three factors are assigned to columns *1*, *2* and *4*. The other columns are assigned to the various interactions. For any one factor (or interaction), at one level, all other factors (and interactions) are set an equal number of times at level *1* and at level *2*. For example, consider the first four experiments (trials), cleat height is set at level 1 and all other factors (and interactions) are set an equal number of times at level *1* and at level *2*. This means that, when the four results for cleat height (*h*) at level *1* are averaged, the effects of the other factors and interactions occur equally at all levels. Hence, the mean result for *h* at level *1* takes account of all other factors and interactions at all levels.

The seventh column of the L_8 array, interaction *(h × b × T),* was not used because the three way interaction was neglected. The eight experiments were all repeated six times. The average results for the eight experiments are shown in table 7.3, and the six repetition results from each experiment are shown in table 7.4. The computation for ANOVA is now carried out.

Columns: / Trial	h	b	h × b	T	h × T	T × b	h × b × T	Average
	1	2	3	4	5	6	7	Results
1	1	1	1	1	1	1	1	11.7
2	1	1	1	2	2	2	2	17.7
3	1	2	2	1	1	2	2	22.7
4	1	2	2	2	2	1	1	23.6
5	2	1	2	1	2	1	2	11.3
6	2	1	2	2	1	2	1	19.1
7	2	2	1	1	2	2	1	18.7
8	2	2	1	2	1	1	2	21.3
								Total = 146.2

Table 7.2: L_8 orthogonal array

Trial	h (mm)	b (mm)	T	Av. initial sink. (mm)	Av. Sink. after slip (mm)	Av. Horizontal load (kg)	Rank
1	d (45)	d (45)	90°	0.6	31.1	11.7	7th
2	d (45)	d (45)	70°	28.2	33.4	17.7	6th
3	d (45)	d/2 (23)	90°	42.3	48.5 (full)	22.7	2nd
4	d (45)	d/2 (23)	70°	41.8	47.9 (full)	23.6	1st
5	d/2 (23)	d (45)	90°	0.5	20.4	11.3	8th
6	d/2 (23)	d (45)	70°	23 (full)	28.5 (full)	19.1	4th
7	d/2 (23)	d/2 (23)	90°	23 (full)	23 (full)	18.7	5th
8	d/2 (23)	d/2 (23)	70°	23 (full)	23.9 (full)	21.3	3rd

Table 7.3: Experimental results

Trial	R_1	R_2	R_3	R_4	R_5	R_6	Average
1	12.5	11.5	12.5	12.5	11.5	9.5	11.7
2	17.5	17	17.5	18	17.5	18.5	17.7
3	22	23	23	23	22	23	22.7
4	23.5	23.5	23	24	24	24	23.6
5	11.5	9.5	11.5	12	11.5	13	11.3
6	18.5	18	18.5	20	19.5	20	19.1
7	18.1	18.6	18	18.5	19.5	19.5	18.7
8	21	22	20.5	22.5	20.5	21	21.3

Table 7.4: Results with six repetitions

7.3. Analysis of Variance (ANOVA)

The Analysis of Variance (ANOVA) is a statistical technique used to analyse and provide a measure of confidence in the experimental results. ANOVA determines the variability of the data being measured and hence the confidence that can be attributed to the results of the analysis.

In the analysis of variance a number of quantities such as degrees of freedom, sums of squares, mean squares, pure sums of squares, etc., are computed and arranged in a standard tabular format. These ANOVA quantities are estimates of population parameters dependent upon the size of sample investigated. The estimates improve as the number of samples increases.

The purpose of this section is to record the ANOVA calculations undertaken and not to fully explain the principles of ANOVA which are well explained in Roy [86]. The calculations recorded were undertaken using the procedures described in Roy [86].

7.3.1. Degrees of Freedom (DOF)

The degrees of freedom concept may be considered to allow one degree of freedom for each independent comparison that can be made in the data. Each of the three factors (*h*, *b* and *T*) has a DOF of 1 (number of levels – 1). The DOF for the interactions are computed by multiplying the DOF of each of the interacting factors. The total DOF for each of the three factors and three interactions is in this case 6. The appropriate Taguchi array cannot have a DOF less than the total DOF of the experiment. Since the L_8 array has a DOF of 7, it is suitable.

In these experiments there are *n* trials ($n = 8$) and *r* trial repetitions ($r = 6$) and therefore $n \times r$ trial runs (see table 7.4), therefore the total DOF becomes:

$$f_t = n\,r - 1$$

$$f_t = 47$$

The error DOF can then be calculated by subtracting the DOF for factors and interactions from the total DOF.

$$f_e = f_t - f_H - f_b - f_{H\times b} - f_T - f_{H\times T} - f_{b\times T}$$

$$f_e = 41$$

7.3.2. Level Totals and Their Averages

The level totals are obtained by adding the results of all trial conditions at the level considered. Their average is obtained by dividing the totals by the number of data points added. For example, the total for cleat height at level 1 (h_1) is obtained by adding all the results for trials 1 to 4 (six repeats of each) from table 7.4.

$$\sum h_1 = 12.5 + 11.5 + 12.5 + 12.5 + 11.5 + 9.5 + 17.5 + 17 + 17.5 + 18 + 17.5 + 18.5 + 22 + 23 + 23 + 23 + 22 + 23 + 23.5 + 23.5 + 23 + 24 + 24 + 24$$

$$= 454$$

$$\overline{h_1} = 454 / 24$$

$$= 18.92$$

$\sum h_2 = 423.2$ $\quad \overline{h_2} = 17.63$

$\sum b_1 = 359.5$ $\quad \overline{b_1} = 14.98$

$\sum b_2 = 517.7$ $\quad \overline{b_2} = 21.57$

$\sum (h\times b)_1 = 415.7$ $\quad \overline{(h\times b)_1} = 17.32$

$\sum (h\times b)_2 = 461.5$ $\quad \overline{(h\times b)_2} = 19.23$

$\sum T_1 = 387.2$ $\quad \overline{T_1} = 16.13$

$\sum T_2 = 490$ $\quad \overline{T_2} = 20.42$

$\sum (h\times T)_1 = 448$ $\quad \overline{(h\times T)_1} = 18.67$

$\sum (h\times T)_2 = 429.2$ $\quad \overline{(h\times T)_2} = 17.88$

$\sum (T\times b)_1 = 408.5$ $\quad \overline{(T\times b)_1} = 17.02$

$\sum (T\times b)_2 = 468.7$ $\quad \overline{(T\times b)_2} = 19.53$

Column	Factors	Level 1	Level 2	(L2 - L1)
1	h	18.92	17.63	- 1.29
2	b	14.98	21.57	6.59
3	(h × b)	17.32	19.23	1.91
4	T	16.13	20.42	4.29
5	(h × T)	17.88	18.67	0.79
6	(T × b)	19.53	17.02	- 2.51

Table 7.5: Average effects

The results for each factor and level are presented in Table 7.5. The difference between the average for each factor at levels 1 and 2 indicates the influence of the factor. The larger the difference, the stronger the influence.

Looking at the main effects, since 'bigger is better', improvements at level 2 are seen for factors *b* and *T* while level 2 for factor *h* causes a decrease in performance. Hence the optimum factor levels are h_1 b_2 and T_2 which is experiment number four with the highest traction force.

In table 7.5, the mean influence of individual factors (main effects) is separated from the influence of interaction between factors. However, interactions can be revealed by the graphical method, figure 7.1. For example, figure 7.1 shows the main effects *h* and *b*, at levels 1 and 2, with and without taper, (T_1 and T_2). If the lines are parallel then there is no or slight interaction, if the lines are not parallel the factors *h* and *b* interact. Since factors *b* and *h* without taper, (T_1), will cross interaction between the two factors (*h* and *b*) is present. Since *b* and *h* with taper, (T_2), also cross interaction is also present. The relative significance of these interaction effects and the main effects is obtained by ANOVA.

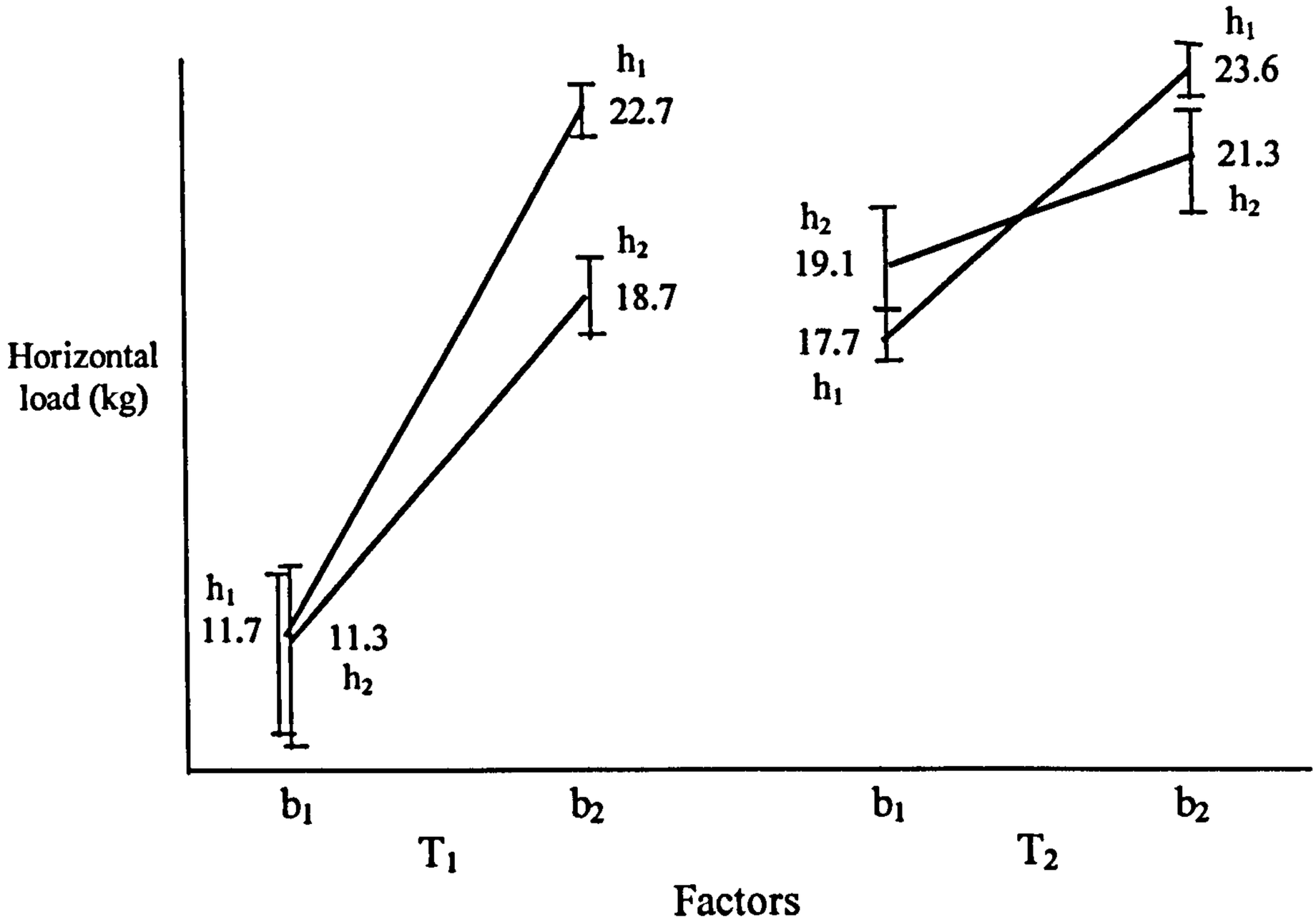

Figure 7.1: Interaction of main effects (*h*×*b*)

7.3.3. Sum of Squares

The sum of squares is a measure of the total deviation from the mean of the experimental data. The total deviation is obtained by summing each squared deviation.

Total sum of squares:

$$S_t = \sum_{i=1}^{n} \left(Y_i - \overline{Y}\right)^2$$

where $\overline{Y}$ is the average of Y_i and Y_i is the traction value of each of the 48 trial runs.

Or,

$$S_t = \sum y_i^2 - (t^2/n) = 16944.82 - 16030.83 = 913.99$$

Where,

Total of all results, $t = 877.2$

Total number of experiments, $n = 48$

Factor sum of squares:

$$S_h = \frac{\left(\sum h_1 - \sum h_2\right)^2}{\left(N_{h_1} + N_{h_2}\right)} = \frac{\left(423.2 - 454\right)^2}{\left(24 + 24\right)} = 19.76$$

where, N_{h1} = total number of experiments in which factor h_1 is present.

N_{h2} = total number of experiments in which factor h_2 is present.

$S_b = 521.40$

$S_{(h\times b)} = 43.70$

$S_T = 220.16$

$S_{(h\times T)} = 7.36$

$S_{(T\times b)} = 75.50$

$$S_e = S_t - (S_h + S_b + S_{(h\times b)} + S_T + S_{(h\times T)} + S_{(T\times b)})$$

$$= 913.99 - 887.88$$

$$= 26.11$$

7.3.4. Mean Square (Variance)

Variance measures the distribution about the mean of the data.

$$\text{Variance} = \frac{\text{Sum of Squares}}{\text{Degrees of Freedom}} = S_t / f$$

$V_h = S_h / f_h = 19.76/1 = 19.76$

$V_b = S_b / f_b = 521.40/1 = 521.40$

$V_{(h\times b)} = S_{(h\times b)} / f_{(h\times b)} = 43.70/1 = 43.70$

$V_T = S_T / f_T = 220.16/1 = 220.16$

$V_{(h\times T)} = S_{(h\times T)} / f_{(h\times T)} = 7.36/1 = 7.36$

$V_{(T\times b)} = S_{(T\times b)} / f_{(T\times b)} = 75.51/1 = 75.51$

$V_e = S_e / f_e = 26.11/(47\text{-}6) = 0.637$

7.3.5. Variance Ratio

The variance ratio, F, is the ratio of variance due to the effect of a factor and variance due to the error term. F is used to measure the significance of the factor under consideration with respect to all the factors included in the error term. The F value is calculated and then compared with a value of F obtained from standard tables for a given level of statistical significance. The F-tables used in this analysis are given in Appendix IV. When the computed F value is less than the value of F determined from the tables for a particular level of significance, the factor is deemed insignificant.

To calculate F:

$F_h = V_h/V_e = 19.76/0.637 = 31.02$

$F_b = V_b/V_e = 521.40/0.637 = 818.52$

$F_{(h\times b)} = V_{(h\times b)}/V_e = 43.70/0.637 = 68.60$

$F_T = V_T/V_e = 220.16/0.637 = 345.62$

$F_{(h\times T)} = V_{(h\times T)}/V_e = 7.36/0.637 = 11.55$

$F_{(T\times b)} = V_{(T\times b)}/V_e = 75.51/0.637 = 118.54$

$F_e = V_e/V_e = 1$

To use the F-tables, the DOF of the numerator determines the column and the DOF of the denominator determines the row. The intersection is the F value. A higher confidence value may be chosen to reduce the risk of an error, but then a larger variance ratio (F value) will be required to conclude that the factor is significant at that level of confidence.

7.3.6. Pure Sums of Squares

The variation in the traction results can be attributed to significant factors, or interactions, by calculating their percentage contribution. This is a function of the sums of squares for each significant item and indicates the relative power of the factor to influence variation in the results. In these calculations the pure sums of squares are used, which are obtained by subtracting an error term as follows [85].

$$S'_h = S_h - f_h V_e = 19.76 - 1 \times 0.637 = 19.12$$

$$S'_b = S_b - f_b V_e = 521.40 - 1 \times 0.637 = 520.76$$

$$S'_{(h\times b)} = S_{(h\times b)} - f_{(h\times b)} V_e = 43.70 - 1 \times 0.637 = 43.06$$

$$S'_T = S_T - f_T V_e = 220.16 - 1 \times 0.637 = 219.52$$

$$S'_{(h\times T)} = S_{(h\times T)} - f_{(h\times T)} V_e = 7.36 - 1 \times 0.637 = 6.72$$

$$S'_{(T\times b)} = S_{(T\times b)} - f_{(T\times b)} V_e = 75.51 - 1 \times 0.637 = 74.86$$

$$S'_e = S_e + V_e (f_h + f_b + f_{(h\times b)} + f_T + f_{(h\times T)} + f_{(T\times b)}) = 26.27 + 0.637(6) = 30.12$$

7.3.7. Percentage Contribution

The percentage contribution of a factor is obtained by dividing the pure sum of squares for that factor by the total sum of squares, S_t, and multiplying the result by 100.

$$P_h = S'_h \times 100/S_t = 2.09$$

$$P_b = S'_b \times 100/S_t = 56.98$$

$$P_{(h\times b)} = S'_{(h\times b)} \times 100/S_t = 4.71$$

$$P_T = S'_T \times 100/S_t = 24.02$$

$$P_{(h\times T)} = S'_{(h\times T)} \times 100/S_t = 0.74$$

$$P_{(T\times b)} = S'_{(T\times b)} \times 100/S_t = 8.19$$

$$P_e = S'_e \times 100/S_t = 3.3$$

The results of the analysis of variance are summarised in table 7.6.

7.3.8. Pooling

The effect of factor *(h × T)* is very small, only 0.74%. This factor can be pooled to obtain a new estimate of S_e and f_e, as follows.

Sum of Squares of error:

$$S_e = S_t - (S_h + S_b + S_{(h\times b)} + S_T + S_{(T\times b)}) = 913.99 - 880.53 = 33.46$$

DOF of error term:

$$f_e = f_t - f_h - f_b - f_{h\times b} - f_T - f_{b\times T} = 47 - 5 = 42$$

Variance of error term:

$$V_e = S_e / f_e = 33.46/42 = 0.797$$

F Ratios:

$$F_h = V_h/V_e = 19.76/0.797 = 24.79$$
$$F_b = V_b/V_e = 521.40/0.797 = 654.2$$
$$F_{(h\times b)} = V_{(h\times b)}/V_e = 43.70/0.797 = 54.83$$
$$F_T = V_T/V_e = 220.16/0.797 = 276.24$$
$$F_{(T\times b)} = V_{(T\times b)}/V_e = 75.51/0.797 = 94.74$$
$$F_e = V_e/V_e = 1$$

Pure Sums of Squares:

$$S'_h = S_h - f_h V_e = 19.76 - 1 \times 0.797 = 18.96$$
$$S'_b = S_b - f_b V_e = 521.40 - 1 \times 0.797 = 520.60$$
$$S'_{(h\times b)} = S_{(h\times b)} - f_{(h\times b)} V_e = 43.70 - 1 \times 0.797 = 42.90$$
$$S'_T = S_T - f_T V_e = 220.16 - 1 \times 0.797 = 219.36$$
$$S'_{(T\times b)} = S_{(T\times b)} - f_{(T\times b)} V_e = 75.51 - 1 \times 0.797 = 74.71$$

$$S'_e = S_e + V_e\,(f_h + f_b + f_{(h\times b)} + f_T + f_{(T\times b)}) = 33.46 + 0.797(5) = 37.45$$

Percentage contributions:

$$P_h = S'_h \times 100/S_t = 2.07$$

$$P_b = S'_b \times 100/S_t = 56.96$$

$$P_{(h\times b)} = S'_{(h\times b)} \times 100/S_t = 4.69$$

$$P_T = S'_T \times 100/S_t = 24.0$$

$$P_{(T\times b)} = S'_{(T\times b} \times 100/S_t = 8.17$$

$$P_e = S'_e \times 100/S_t = 4.1$$

The results of the pooled analysis of variance are summarised in table 7.7.

Pooling increases the DOF of the error term, which increases the confidence level of the other factors. Since trials have been repeated, a naturally large error DOF results, therefore pooling is not always necessary. By increasing the number of trial repeats, the error DOF increases, and therefore the level of confidence will increase. However, since repeating trial runs may be expensive or time consuming, the number of repeats

Factor	DOF f	Sum of Squares	Variance V	Variance Ratio F	Pure Sum of Squares S'	Percentage Contribution P
h	1	19.76	19.76	31.02	19.12	2.09
b	1	521.40	521.40	818.52	520.76	56.98
$(h \times b)$	1	43.70	43.70	68.60	43.06	4.71
T	1	220.16	220.16	345.62	219.52	24.02
$(h \times T)$	1	7.36	7.36	11.55	6.72	0.74
$(b \times T)$	1	75.51	75.51	118.54	74.86	8.19
Error/ other	41	26.27	0.637	1	30.12	3.3
Total	47	887.89				100

Table 7.6: Analysis of Variance (ANOVA) Table

Factor	DOF f	Sum of Squares	Variance V	Variance Ratio F	Pure Sum of Squares S'	Percentage Contribution P
h	1	19.76	19.76	24.79	18.96	2.07
b	1	521.40	521.40	654.20	520.60	56.96
$(h \times b)$	1	43.70	43.70	54.83	42.90	4.69
T	1	220.16	220.16	276.24	219.36	24.0
$(h \times T)$	(1)	(7.36)	*Pooled*			
$(b \times T)$	1	75.51	75.51	94.74	74.71	8.17
Error/ other	42	33.46	0.797	1	37.45	4.1
Total	47	887.89				100

Table 7.7: Pooled Analysis of Variance (ANOVA) Table

must be weighed against the accuracy of the estimate. Sometimes pooling is required until the pooled DOF equals approximately half of the total DOF but not in this case.

To determine whether a factor should definitely be pooled a test of significance should be performed. A level of confidence between 90% and 99% is usually used. From the F table at a confidence level of 90%, $F_{0.1}(1,42)$:

$F = 2.8354$

From the F table at a confidence level of 99%, $F_{0.01}(1,42)$:

$F = 7.3141$

At 99% confidence, i.e. 1% risk, in this case all of the factors and interactions are significant since the F ratios are all greater than the F table value. This is true whether or not we pool the $(h \times T)$ interaction term. Since the percentage contribution due to error is low, 15% or less [85], then it is assumed that no important factors were omitted from the experiment. Note that, although we can

say that, with 99% confidence, all factors and interactions are significant, their relative importance is determined by their percentage contribution.

7.3.9. Confidence Interval of Factor Effect

The confidence interval is a minimum and maximum value between which the true average should fall at some particular confidence level. A high confidence level may reduce risk but it results in a wider confidence interval, lowering the chance of the true average being outside the stated limits.

$$\text{C.I.} = \sqrt{\frac{F(1,n_2)V_e}{n}}$$

Where

$F(1,n_2)$ = F value from F table at required confidence level at DOF 1 and error DOF n_2

V_e = Variance of error term

n = Number of trials

At a confidence level of 99%,

n_2 = 41, or 42 (pooled), and F = 7.3141

V_e = 0.637, or 0.797 (pooled)

n = 8

C.I. = +/- 0.763kg at the 99% confidence level (before pooling)

C.I. = +/- 0.854kg at the 99% confidence level (after pooling)

And, at a confidence level of 90%,

F = 2.8354

C.I. = +/- 0.475kg at the 90% confidence level (before pooling)

C.I. = +/- 0.531kg at the 90% confidence level (after pooling)

The C.I. applies to all main and interaction effects.

It can be seen that pooling produced larger confidence intervals. Therefore the pooling strategy was not necessary and deeming factor ($h \times T$) to be insignificant was not useful as it increased the confidence interval.

7.4. Discussion of Results

Taguchi's method has been used to analyse the results of eight experiments (a full factorial set). It has not been used to minimise the number of experiments. The analysis of variance (ANOVA) has determined the significance of main effects *h, b* and *T* and interaction effects *(h × b), (h × T)* and *(T × b)* of cleat geometry on traction.

Considering the percentage contributions in the ANOVA table, table 7.6, main factors *b* and *T* are seen to have a very strong influence on cleat traction performance with only a slight influence by factor *h*. The percentage contributions of *b* and *T* are 56.98% and 24.02% respectively, *h* is 2.09%. Interactions between factors are also confirmed present. Interactions *(h × b)* and *(b × T)* are 4.71% and 8.19% respectively. The interaction effect ($h \times b$) is greater than the main effect *h*. Therefore, due to the interaction ($h \times b$), see figure 7.1, the cleat height should be set to $h = d$ (h_1) to maximise the influence of *b*. There is a strong interaction between factors *b* and *T*, and *b* and *h* with only a slight interaction between *h* and *T*. Such interaction activity has confirmed the decision to use full factorial experiments. If the number of experiments had been minimised, the interaction effects would have been neglected. Initially, the interaction *(h × T)* was pooled because its contribution was so small, 0.74%. However, pooling of this factor was found to increase confidence intervals. All main factor effects and interaction effects were found to be significant at a confidence level of 99%.

The optimum factor levels are h_1 b_2 and T_2, trial number 4 with the highest traction result (horizontal load of 23.6kg). This means that traction performance is increased with a decrease in cleat width, an increase in cleat height and a taper. Since factors b and T have a great effect on traction performance these should be the focus of further study of cleat geometry on traction performance. More than two levels should be investigated.

At a 99% confidence level, the experimental error was 4.1%. Since it is low it is assumed that no important factors were omitted from the experiment.

A confidence interval of +/- 0.531 kg (pooled) compared to +/- 0.475 kg (before pooling) was calculated at the 90% confidence level. Pooling was therefore not necessary and in fact reduced confidence. As confidence increases, the confidence interval decreases. This interval could be slightly improved with further trial repetitions, but the time consumption deems this unpractical. Current confidence intervals are considered satisfactory.

8. Comparisons of Mathematical and Experimental Results

8.1. Introduction

In this chapter, the mathematical models developed in chapter 4 are validated by comparing theoretical results with the experimental results reported in chapters 6 and 7.

A number of experiments have been carried out using the soft ground slip-rig. Initially the tests were to evaluate the performance and repeatability of the rig, and to establish a test procedure. The testing then investigated cleat length and three dimensional soil flow (end effects) to identify at which cleat length two dimensional effects were dominant. A series of traction distribution experiments using two different cleats were then carried out and compared. Finally eight, full factorial experiments were also conducted to investigate the effects of cleat height, width and taper on traction, which were then analysed using Taguchi's techniques.

The experimental work was conducted in parallel with the mathematical modelling development. To validate the mathematical models, some of the experiments were simulated. Sinkage results were input into the models, with the corresponding vertical load, cleat geometry and cleat and soil friction properties thus enabling experimental and theoretical results to be compared.

The experiments to investigate the effects of cleat height, width and taper were simulated in MATLAB using the total traction model, developed from triangular and quadrilateral shear zone models. The total traction model (section 4.5) assumes passive and active triangular shear zones at the front of the front cleat and rear of the rear cleat, respectively, and the interaction of passive and active quadrilateral shear zones in between the cleats as illustrated by figure 8.1. The amount of initial sinkage was input into the model so that the full and partially full sinkage conditions could be modelled.

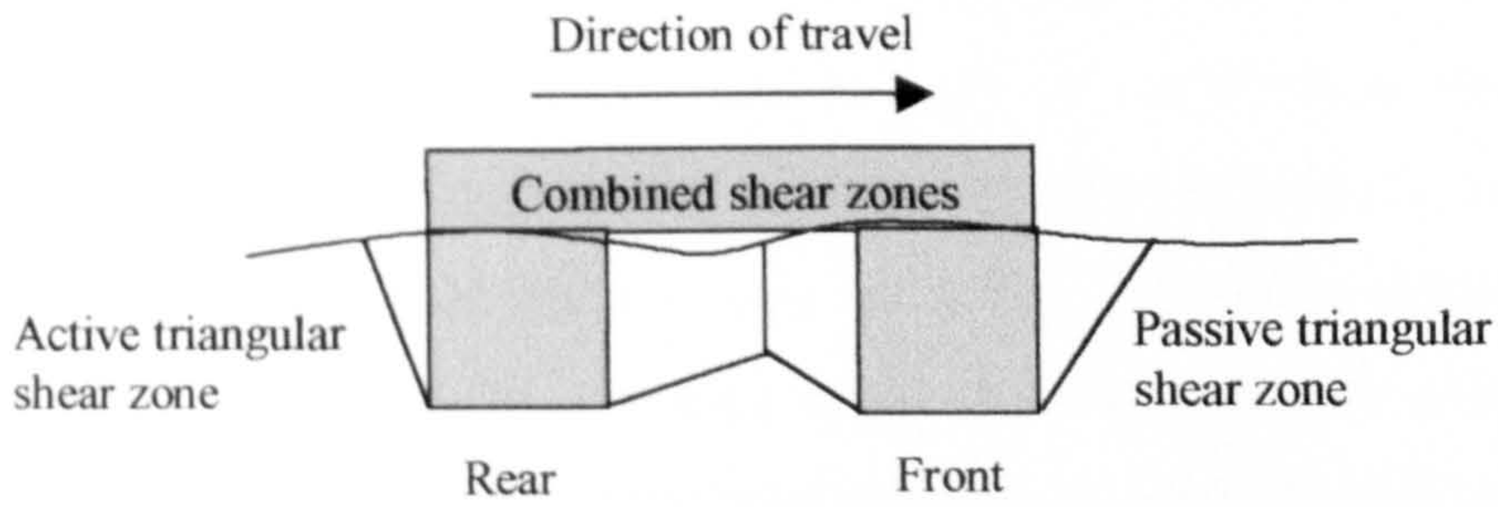

Figure 8.1: Simulation of total traction

The traction distribution experiments were also simulated using the total traction model. Since full sinkage was induced, the applied vertical load was applied uniformly to the sand between and beneath the cleats. The various contributions to the total traction force were obtained from the computer models and compared to experimental results.

8.2. Effects of Cleat Width, Height and Taper on Traction

The experimental work, reported in section 6.5, has been simulated using the mathematical models to enable comparisons to be made. Eight experiments were used to investigate the effects of cleat height, width and taper and have been analysed using Taguchi's techniques in the previous section. A cleat length of $l = 4d$ (180mm) was used since this length was shown to have negligible three dimensional effects as discussed in section 6.3. The two dimensional modelling results could therefore be compared to the experimental results.

The unit weight, γ, of the dry sand used in the mathematical models was calculated based on the density of sand used during the experiments, $\gamma = 0.016 \times 10^{-3} N/mm^3$. The soil shear angle ($\phi$) for dry sand of the required density was estimated to be 27° [11]. The friction angle (δ) for dry sand on the wood used for the cleat pieces was unknown, therefore $\delta = 10°$ was selected based on the mathematical modelling results. For $\delta = 10°$, the magnitudes of total traction were smaller than that of the experimental results but minimum variation from the experimental results was

achieved. The sand was also assumed to behave as a purely granular soil, therefore cohesion, c_s, and adhesion, c_c, were equal to zero. A direct shear test would, however, have provided more accurate values. The cleat geometry and initial sinkage results for an applied vertical load of 40kg, (F_b) were input into the computer models for total traction. For the first set of results using the total traction model (table 8.1) all of the cleats were considered to be partially full so that the vertical load was not applied to the soil between the cleats. Although sinkage increased with slip, the initial sinkage results were input into the model to achieve the lower limit. The vertical load was assumed to act approximately equally across each cleat, $F_b/2$ was therefore transferred to the soil beneath each cleat. For the second set of results using the total traction model (table 8.2), the cleats were considered to be full. The cleats were considered to be completely full of soil to achieve the upper limit, even though during the experiments the cleats were not entirely full. It was expected that the experimental results would fall between the upper and lower limits. The vertical load applied to the cleats was applied to the soil in between and beneath the cleats. The transfer of load to the soil via the cleats or the soil in between was assumed to be at the same pressure, which was

Exp	Cleat height H (mm)	Cleat width b (mm)	Taper	Init. sinkage (mm)	Min total traction T (N)	Quad shear zone bet'n cleats		Triang'r passive zone		Triang'r active zone	
						α_{aq}°	α_{pq}°	Ppt (N)	α_{pt}°	Pat (N)	α_{at}°
1	45	45	90°	1	69.232	25	25	0.005	24.5	0.0	55.5
2	45	45	70°	28	77.337	0.5	0.5	6.146	18.5	0.353	51.5
3	45	23	90°	43	83.885	1.5	1.5	9.583	24.5	1.0	55.5
4	45	23	70°	42	88.346	1.5	2.5	13.828	18.5	0.795	51.5
5	23	45	90°	1	69.232	25	25	0.005	24.5	0.0	55.5
6	23	45	70°	23	74.110	0.5	3.5	4.147	18.5	0.238	51.5
7	23	23	90°	23	74.255	35.5	21.5	2.742	24.5	0.244	55.5
8	23	23	70°	23	75.646	0.5	5.5	4.147	18.5	0.238	51.5

Table 8.1: Total traction results including passive and active earth forces in front of the front cleat and behind the rear cleat respectively, and all shear angles, for partially full cleats ($c_s = c_c = 0$). Refer to figure 4.13.

calculated using the vertical force over the total width of cleats, and gap between the cleats ($2b_1 + b_2$). A vertical load of 40kg was used as in the experiments for 180mm length cleats. This mass simulates the applied vertical force on the ground due to the bodyweight of a soldier.

8.2.1. Partially Full Condition

The experimental results were simulated using the MATLAB computer model for total traction and assuming all cleats were partially full. The rank order of the cleats, in terms of total traction force and based on the theoretical results, matched the experimental results with two exceptions. Experiment 2, the tapered cleat of height, *d*, and width, *d*, which resulted in the sixth highest traction performance in the experimental results was third in the modelling results. Experiment 6, the tapered cleat of height, *d/2*, and width, *d*, which resulted in the fourth highest traction performance in the experimental results was sixth in the modelling results. However, the rank order of the other cleats was the same for the experimental results and modelling results.

It can be seen in table 8.1 that for partially full cleats and a cohesionless granular soil, the passive earth resistance at the front of the front cleat contributes most to traction, an average of 9% for tapered cleats and 4% for non tapered cleats.

The active thrust behind the rear cleat, which has a negative affect on traction performance, was an average of 0.6% of the total traction for both tapered and non tapered cleats.

The contribution of active and passive earth forces increases with increased sinkage, as does the total traction. Referring to figure 4.13 the remaining contribution to traction is produced from the horizontal components of R_c, R_p and R_a since cohesive and adhesive forces are zero in this case.

The cleats of full height, 45mm, and narrow width, 23mm, (experiments 3 and 4) were seen to produce significantly higher passive resistance than the others cleats

as shown in table 8.1. The tapered cleat (experiment 4) produced the greatest passive earth force whereas the non-tapered (experiment 3) produced the greatest active force. Experiments 1 and 5, however, produced the least passive and active earth force, similar to the actual experiments, due to their lower sinkage. It may be concluded that a greater passive earth resistance is achieved with greater sinkage. When comparing tapered to non tapered cleats of the same geometry, the tapered were seen to produce the greater passive earth force due to the greater sinkage achieved. So it can be seen that the passive and active earth forces increase significantly with sinkage, especially when full sinkage occurs.

Comparing tapered to non tapered cleats for the same cleat height and width, the taper significantly increases the passive earth force but this is not so apparent for the active earth force. For example, considering cleats of height d and width $d/2$ (experiments 3 and 4), which also have the same amount of sinkage, P_{at} is reduced from 0.921N to 0.717N with taper, and P_{pt} is increased from 9.583N to 13.828N with taper. However, for cleats with minimal sinkage (experiments 1 and 5), these trends do not apply since the passive and active earth forces are negligible.

The minimum passive earth force for the triangular shear zone at the front was achieved at the same shear angle for tapered cleats, $\alpha_{pt} = 18.5°$, and the same shear angle for non tapered cleats, $\alpha_{pt} = 24.5°$ (angle was required to be greater than zero, minimum angle 0.5°). The maximum active earth force for the triangular shear zone at the rear was also always achieved at the same shear angle for tapered cleats, $\alpha_{at} = 51.5°$, and the same shear angle for non tapered cleats, $\alpha_{at} = 55.5°$ (angle was required to be greater than zero, minimum angle 0.5°). The shear angles for triangular shear zones were therefore independent of sinkage for the triangular shear zones.

For the interacting passive and active quadrilateral shear zones between the cleats, non tapered cleats are seen to produce equal passive and active zone shear angles with the exception of experiment 7. The shear angles for the interacting passive and active quadrilateral shear zones between the cleats are quite varied due to the various sinkage levels that have been attained, from 0.5° for experiments 2, 6 and 8

to 35.5° for experiment 7 (passive shear zone). Unlike the triangular shear zones, the shear angles for the interacting quadrilateral shear zones were dependent on sinkage, although it is not possible to determine a pattern from the results.

The theoretical magnitudes of the total traction force, for partially full cleats, are significantly lower than the experimental values (range of approximately 69N-88N compared to a range of 80N-230N for the experiments). The magnitude of the theoretical results, however, increases with increased friction angle, δ, due to the horizontal component of R_c but $\delta = 10°$ for the wooden cleat material was selected. The low traction force results from the mathematical model are probably due to the build up of sand in front of the cleat test piece that occurs during slip (see figures 5.10-5.12). Since sinkage also increases during slip, the amount of soil that forms in front of the cleats also increases with slip, and the model does not take this into consideration, thus the passive earth force in front of the front cleat is underestimated.

8.2.2. Full Condition

Despite the fact that not all cleats achieved full sinkage all of the cleats were then modelled as being full to obtain upper limits. When the cleats were considered to be full of sand the magnitude of all the forces became significantly larger, as shown by the results in table 8.2, since the vertical load was also applied to the sand in between the cleats, as well as that under the cleats. It is not possible to compare the rank order of experimental and theoretical results in terms of total traction force due to the fact that most of the cleats in the experimental work did not actually achieve full sinkage.

It can be seen in table 8.2 that for full cleats and a cohesionless granular soil, the passive earth resistance at the front of the front cleat contributes an average of 4% for non tapered cleats and 6% for tapered cleats.

The active thrust behind the rear cleat, which has a negative effect on traction performance, was an average of 0.36% of total traction for both tapered cleats and

Exp	Cleat height H (mm)	Cleat width b (mm)	Taper	Full sinkage (mm)	Min total traction T (N)	Quad shear zone bet'n cleats		Triang'r passive zone		Triang'r active zone	
						α_{aq}°	α_{pq}°	Ppt (N)	α_{pt}°	Pat (N)	α_{at}°
1	45	45	90°	45	133.887	0.5	0.5	10.495	24.5	1.084	55.5
2	45	45	70°	45	139.343	0.5	0.5	15.874	18.5	0.823	51.5
3	45	23	90°	45	185.763	0.5	0.5	10.495	24.5	1.084	55.5
4	45	23	70°	45	189.471	0.0	2.5	15.874	18.5	0.823	51.5
5	23	45	90°	23	125.829	0.5	0.0	2.742	24.5	0.263	55.5
6	23	45	70°	23	149.748	0.5	2.5	4.147	18.5	0.215	51.5
7	23	23	90°	23	175.103	0.5	0.5	2.742	24.5	0.263	55.5
8	23	23	70°	23	181.930	0.5	5.5	4.147	18.5	0.215	51.5

Table 8.2: Total traction results including passive and active earth forces in front of the front cleat and behind the rear cleat respectively, and all shear angles, for full cleats ($c_s = c_c = 0$). Refer to figure 4.13.

non tapered cleats.

The magnitude of the total traction force has significantly increased for all experiments when modelled as full compared to partially full, the vertical force due to body weight being applied to the soil between and beneath the cleats. For the theoretical models, $\delta = 10°$ and the corresponding horizontal component of R_c, R_p and R_a are significant contributors to total traction. However, the magnitude of the total traction force for full cleats remains low, with the exception of experiments 1 and 5, when compared to the experimental results. As discussed previously, this is probably due to the low passive earth force achieved from the theoretical model, which does not consider the build up of sand at the front during slip. Full sinkage maximises this error since the passive and active earth forces, at the front and rear of the test piece, increases with sinkage and build up due to the increased weight of the triangular soil shear zones.

The shear angles for both triangular shear zones (passive and active) remained unchanged from the partially full condition, for all cases. However, the shear

angles for the interacting passive and active quadrilateral shear zones were different for the full condition. The active quadrilateral zone shear angle, α_{aq}, was equal to 0.5° for all experiments and the passive quadrilateral zone shear angle, α_{pq}, was equal to 0.5° for all non tapered cleats and between 0.5° and 3.5° for tapered cleats. Thus approximately horizontal shear occurred in all cases.

Although the shear angles for both the passive and active triangular shear zones remained unchanged from the partially full condition, the magnitudes of the passive and active earth forces have increased with sinkage. Obviously, for those experiments that achieved full sinkage (experiments 6, 7 and 8) but were modelled as partially full without the applied vertical load to the soil between the cleats, these earth forces remain the same for both partially full and full conditions.

When cleats of the same geometry but different heights (*d* and *d/2*) are compared, i.e. experiments 1 and 5, 2 and 6, 3 and 7, 4 and 8, the total traction forces for the cleats of height $h = d/2$ are approximately 6% below those of height $h = d$ with the exception of experiment 6. This demonstrates the factor of height, *h*, has little effect on increasing traction. This was to be expected since the majority of traction is obtained from the soil in between the cleats, which remained the same. When tapered and non tapered cleats of the same geometry are compared, traction is increased (up to 16%) as seen in the experimental results. Comparing the two cleat widths, *d* and *d/2*, for cleats of the same remaining geometry, i.e. experiments 1 and 3, 2 and 4, 5 and 7, 6 and 8, the total traction force for the narrower cleat width, *d/2*, and therefore greater gap between the cleats, is 28% greater than cleats of width, *d*. This again demonstrates the importance of the factor of width, *b*, to increasing traction since the majority of traction was produced from the soil in between and beneath the cleats.

8.2.3. Comparison of Modelling and Experimental Results

The experimental results are compared to the total traction model results (for both partially full and full) in table 8.3. When the modelling results for both the partially

Exp	Cleat height H (mm)	Cleat width b (mm)	Taper	Init. sinkage (mm)	Full sinkage (mm)	Part full cleats total traction T (N)	Full cleats total traction T (N)	Exper. Results Total traction T (N)
1	45	45	90°	1	45	69.232 [=7]	133.887 [7]	114.78 [7]
2	45	45	70°	28	45	77.337 [3]	139.343 [6]	173.64 [6]
3	45	23	90°	43	45	83.885 [2]	185.763 [2]	222.69 [2]
4	45	23	70°	42	45	88.346 [1]	189.471 [1]	231.52 [1]
5	23	45	90°	1	23	69.232 [=7]	125.829 [8]	111.15 [8]
6	23	45	70°	23	23	74.110 [6]	149.748 [5]	187.37 [4]
7	23	23	90°	23	23	74.255 [5]	175.103 [4]	182.76 [5]
8	23	23	70°	23	23	75.646 [4]	181.930 [3]	208.95 [3]

[n] Rank order in terms of total traction force for full and partial full model and experimental results

Table 8.3: Total traction model results for partially full and full cleats and total traction experimental results ($c_s = c_c = 0$).

full and full conditions are compared to the experimental results, the magnitude of the theoretical total traction force results are small. The partially full model was based on initial sinkage data, even though the cleats were seen to sink further during slip. Conversely, the full model assumes the weight is evenly distributed over the soil beneath and in between the cleats hence the two models were considered to represent two extremes for sinkage conditions. The modelling of full cleats assumes the cleats to be completely full, whereas in the experiments full sinkage could only be achieved in the centre of the gap between the cleats. Therefore, it would be expected ideally for the experimental results to fall somewhere in between the two sets of theoretical results.

The rank order in terms of horizontal traction force is now compared for the theoretical models and experimental results (bearing in mind not all cleats became fully sunk). The rank order of the partially full cleats is the same as the experimental rank order with the exception of experiment 2. Experiment 2

($h = d$, $b = d$ and tapered), ranked third for the partially full model but sixth in the experimental results. The rank order of the full cleats is the same as the experimental rank order with the exception of experiments 6 and 7. Experiments 6 ($h = d/2$, $b = d$ and tapered) and 7 ($h = d/2$, $b = d/2$ and non tapered), ranked fifth and fourth respectively for the partially full model but fourth and fifth in the experimental results. Although the magnitudes of total traction produced by the models differ from the experimental work, the same traction versus cleat geometry trends are demonstrated. Experiment 4 ($h = d$, $b = d/2$ and taper) produces the greatest traction force and experiment 5 ($h = d/2$, $b = d$ and no taper) produces the least traction force in all three cases for both theoretical and experimental results as shown in tables 8.3.

In the experimental work, greater sinkage was shown to increase traction performance, this was also demonstrated by the models. All components of the total traction force were seen to increase with greater sinkage. Full sinkage was seen to be the major factor in maximising traction in both the experimental and modelling results. The geometric factors of taper, smaller cleat width and greater cleat height were all seen to increase sinkage as well as increase traction independently of sinkage in both the experimental work and in the modelling work. The full model showed the cleat height to increase traction by 6%, cleat taper by up to 16% and cleat width was shown to increase traction by 28%.

8.3. Traction Distribution

Some further experimental work has been simulated using the mathematical models. Tests were carried out to investigate the distribution of traction over various parts of the cleats such as the sand between the cleats, in front of the cleats (passive earth force), behind the cleats (active earth force) and under the bottom of the cleat test pieces. In the experimental work, two dimensional soil flow was produced by firstly, adding Perspex sides to the cleats, and secondly, using 180mm ($4d$) length cleats which were shown to produce negligible three dimensional effects. The experimental work using the cleat length of $4d$ was simulated using the theoretical model. In the model, cohesion and adhesion were equal to zero due to

using dry sand and the friction angle δ was selected to equal to 10° based on the modelling results. The experimental work has been discussed in full within section 6.4, including the proportion of traction from different cleat areas.

The passive traction force produced at the front of the cleat was simulated using a triangular shear zone as illustrated by figure 8.1. The active traction force at the rear of the cleat, acting in a negative direction, and therefore opposing traction, was simulated using a triangular shear zone. The sand in between the cleats was simulated using the combined passive and active quadrilateral shear zones model. The traction produced from beneath the cleats, the horizontal component of R_c, was also included. The geometric factors of the non tapered cleat used to investigate traction distribution ($h = d$, $b = d/2$ and $l = 4d$) were input into the MATLAB model to enable a two dimensional simulation and comparison of results.

The full sinkage condition was achieved for the traction distribution experiments so that the sinkage variable was removed. Therefore only the full sinkage model for total traction was used. For this condition, the pressure beneath the cleats and on the soil in between the cleats was the same.

8.3.1 Comparison of Modelling and Experimental Results

The shear angles for the passive and active triangular shear zones, α_{pt} and α_{at}, were 24.5° and 55.5° respectively for the non tapered cleat. The passive shear zone is seen to be larger than the active shear zone as reported in soil mechanics texts

	Traction (N)	% Total Traction
Traction Total	189.471	100
Traction in front of cleat, P_p	15.874	8.4
Traction rear of cleat, P_a	-0.823	-0.4
Traction between cleats	174.420	92.1

Table 8.4: Traction distribution for mathematical model, full condition.

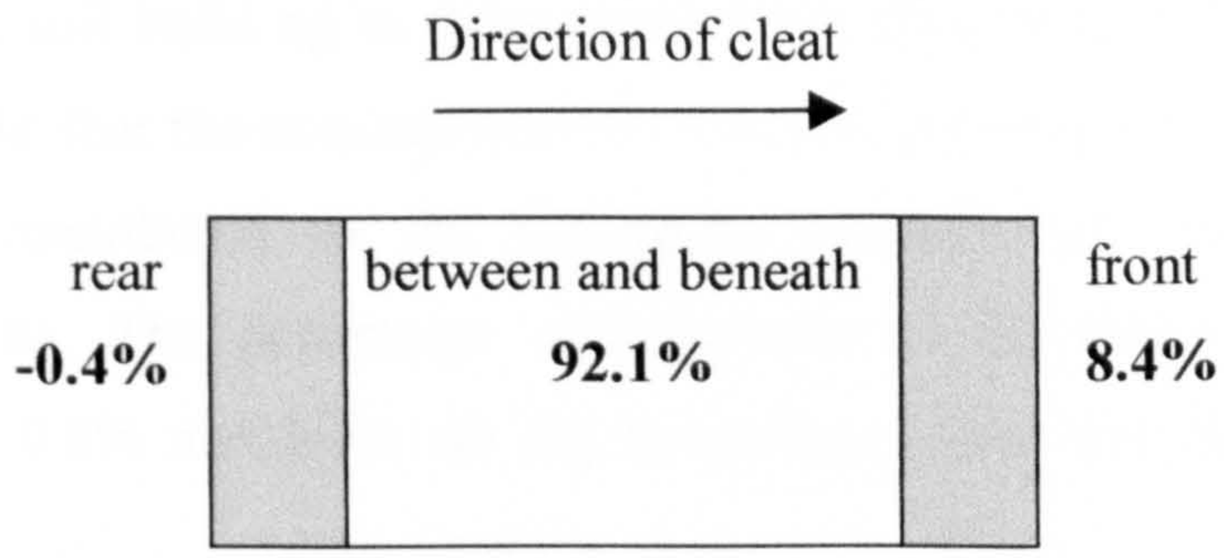

Figure 8.2: Traction distribution obtained from mathematical model

[8,11]. The combined passive and active quadrilateral shear zones model was used to calculate the shear angles in between the cleats, α_{pq} and α_{aq}, which were nearly all 0.5° (angle was required to be greater than zero, minimum angle 0.5°). The traction distribution results (table 8.4) are illustrated by figure 8.2. The traction distribution obtained from the mathematical model may be compared to the distribution obtained from the experimental work, figure 8.3.

The total traction from the mathematical model, 189.471N may be compared to 224.65N obtained from the experiments for the same cleat and full sinkage. The distribution figure produced from the theoretical model for full cleats illustrates how the passive earth force at the front of the front cleat is under estimated. 8.4% was achieved by the model compared to 23.4% for the experiment, due to what is

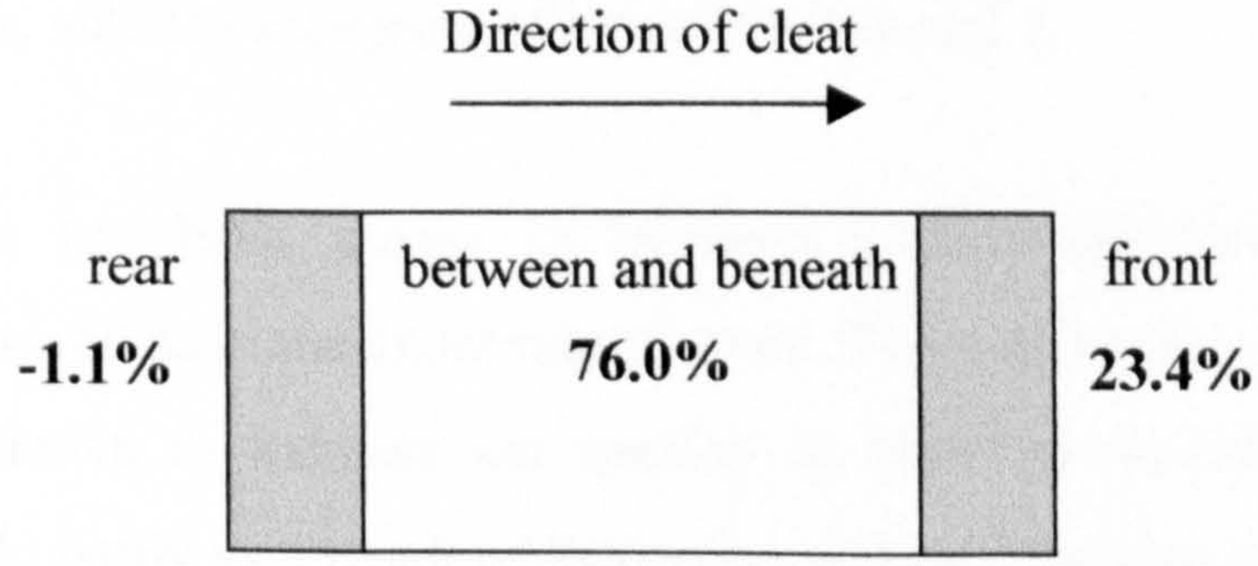

Figure 8.3: Traction distribution obtained from practical experiment using *4d* length cleat (also see figure 6.9).

expected to be the soil build up in front of the front cleat being neglected in the model. It is thought that the assumptions of Coulomb, presented in section 3.4.1, may have also contributed to the difference between the theoretical and experimental results. The percentage contributions of the active earth force, opposing traction, 0.8% and 1.1% for the theoretical model and the experiment work respectively.

8.4 Conclusions

8.4.1. Total Traction Model

A two dimensional total traction model has been developed and coded in MATLAB consisting of passive and active triangular soil shear zones, developed from standard soil mechanics retaining wall theory, and a newly developed model for interacting passive and active quadrilateral shear zones between the cleats. Cleat geometry, cleat and soil material properties and sinkage have been input into the model to simulate the experimental work for comparison purposes.

8.4.2. Effects of Cleat Height, Width and Taper

The eight experiments to investigate the effects of cleat height, width and taper have been simulated using the total traction model. The net traction force rank order obtained from the model for partially full cleats was the same as that of the experimental work, with the exception of experiment 2. The net traction force rank order obtained from the model for full cleats was also similar to that of the experimental work, with the exception of experiments 6 and 7.

Increased sinkage has been shown to increase traction significantly in the modelling work as well as in the experimental work. Taper and reduced cleat width have also been shown to increase net traction in both the modelling and the experimental work, partly as a result of increasing sinkage, but also independently of sinkage.

When compared to the experimental results, the magnitudes of net traction obtained from the total traction models are smaller for both the partially full cleats (by up to approximately three fold) and full cleat simulations (by up to approximately 20%) when compared to the experimental results. This is thought to be due, primarily, to the omission of soil build up in front of the test piece from the model and possibly due to the assumptions made by Coulomb.

8.4.3. Traction Distribution

The distribution of net traction for the cleat length *4d*, at the front of the front cleat, rear of the rear cleat, and in between and beneath the cleats was obtained from the total traction model.

The percentage distribution of traction over different parts of the cleat produced from the model was seen to be representative of that obtained from the experimental work. However, the magnitude of passive earth force at the front of the front cleat, 8.4%, obtained from the model was small when compared to the experimental result, 23.4%. This therefore affected the magnitude of total traction force and the traction produced from in between and beneath the cleats, 92.1% from the model compared to 76.0% from the experiment. The active earth force was -0.4% from the model compared to -1.1% from the experiment.

8.4.4. Performance of the Mathematical Model

The two dimensional mathematical model that has been developed to simulate the net traction of the front and rear cleat assembly has replicated the trends produced in the experimental cleat geometry investigation and traction distribution work. However, the magnitudes of the modelling results are low when compared to experimental results.

Cleat surface friction angle, δ, was selected to equal to 10° for the modelling work. For δ = 10°, the magnitudes of total traction were smaller than that of the experimental results but minimum variation from the experimental results was

achieved. The sand was also assumed to behave as a purely granular soil, therefore cohesion, c_s, and adhesion, c_c, were equal to zero.

The experimental work was designed to represent a two dimensional problem, which could be reproduced in the mathematical models to investigate the effects of cleat geometry on traction and traction distribution, as previously reported.

For the eight full factorial experiments to investigate cleat geometry, the accuracy of the modelling results was affected by the underestimation of passive earth force at the front of the test piece and the omission of build up sand during slip in the model. The experimental results did not fall between the upper and lower limits obtained from the theoretical results, which would have been ideal. However, the traction versus cleat geometry trends are both successfully replicated in both the partially full and full theoretical models.

9. Conclusions and Further Discussion

9.1 Conclusions

- Soil mechanics has been successfully applied to the theoretical modelling of footwear on soft ground. A two dimensional total traction model has been created.

- A soft ground slip-rig has been designed and commissioned. The rig produced repeatable results using scaled up cleats.

- The effects of soil flow, cleat geometry and traction distribution have been investigated. Long cleats ($l \geq 4d$) with respect to small cleat width ($b = d$) were found to closely represent two dimensional soil flow.

- Experimental results have been analysed using Taguchi's statistical tool Analysis of Variance (ANOVA).

- The theoretical models have been validated using the slip-rig. Although the theoretical model underestimated total traction, the traction versus cleat geometry trends were in good agreement.

- It was found that traction is optimised with taper, increased cleat height and narrower cleat width.

The above conclusions are discussed in more detail in the remainder of this chapter.

9.2 Mathematical Modelling

Soil mechanics theory has been applied in the mathematical modelling of footwear and soft ground interaction. The mathematical models coded in MATLAB have been developed from standard retaining wall theory and include complex shear

zone interactions and total traction models for different sinkage conditions. The results from these models have been compared with the experimental results.

The two dimensional mathematical models that have been developed enable investigation into the effects of cleat geometry, material properties and soil conditions on traction performance. The models are based on simple tread geometry that was readily reproduced in both the experimental work and the mathematical modelling work. The models enable the variation of cleat height, width and taper as well as material properties. The models are applicable to different soils, cohesive or granular, and different sinkage conditions, which include no sinkage, partial sinkage and full sinkage.

Referring to figure 4.13, the total traction model considers the passive earth force at the front of the front cleat, the active earth force behind the rear cleat, the interacting passive and active quadrilateral shear zones in between the cleats and the friction beneath the cleats for different sinkage conditions, with an applied vertical load.

The traction models require the amount of sinkage to be input and therefore a separate sinkage model was considered necessary. Bearing capacity theory, using shape factors, would determine when the cleats would sink but would not be able to predict the amount of sinkage. It was therefore decided to develop an empirical model based on experimental data. Sinkage data from the eight, full factorial experiments was used to investigate the relationship between sinkage, vertical load and cleat geometry. However, due to the large amount of scatter it was not possible to determine any relationships from this data.

For comparison purposes, the mathematical models were used to simulate the eight, full factorial experiments to investigate the effects of cleat height, width and taper on traction. Both partially full and full conditions were modelled. The traction distribution experiment, using the non tapered cleat of length *4d*, was also simulated. The modelling results used for comparison were obtained by assuming the following properties for the scaled up wooden cleat pieces and the dry sand:

Friction angle for wood on sand, δ, delta = 10°

Friction angle for sand, ϕ, = 27°

Unit weight of sand, γ, = 0.000016 N/mm^3

Cohesion, C_s, = 0 N

Adhesion, C_c, = 0 N

9.3 Experimental Work

A soft ground slip-rig has been developed since it was not considered feasible to use or modify existing rigs. The slip-rig uses simple mechanical mechanisms and weights to provide applied vertical and horizontal forces, and has shown good repeatability. Although a simple design, it is easy to use and calibration of the equipment is not required. When the preparation of a soil tray is taken into consideration, the addition of a control system or measuring devices would not make the experiments easier or quicker to perform or the results more repeatable. The experimental results have shown the effects of cleat geometry on total cleat traction for sand, and in particular the geometric characteristics that promote traction and reduce traction. Scaled up cleats were used to ensure that meaningful results could be obtained and so that observations could be made of actual soil movement during sinkage and slip.

In the experimental work, initial tests were carried out to evaluate the repeatability and accuracy of the rig and to establish an experimental procedure. Further tests were carried out to investigate three dimensional end effects and to identify at which cleat length soil flow became representative of a two dimensional problem. Eight full factorial experiments were then conducted to investigate the effect of cleat geometry on traction. The results were analysed using Taguchi's statistical tools. Traction distribution was also investigated to understand the contribution to traction of different parts of the cleats.

From the investigation into three dimensional end effects, a minimum cleat length of *4d* (180mm) was shown to represent a two dimensional problem. This length was therefore applied to both the experimental and mathematical modelling work.

The eight full factorial experiments identified traction and sinkage trends with changing geometry for tests with sand. A different soil, clay for example, would be expected to produce different trends. Traction was seen to increase with taper, greater cleat height and narrower cleat width as represented by experiment 4. Sinkage was shown to significantly affect traction force, greater sinkage resulted in increased traction. Full sinkage was shown to produce a further significant increase in traction and this coincided with reduced soil movement during slip, from in front of the cleats and around the sides. Greater slip resistance was achieved due to the vertical load being applied to the soil in between, as well as beneath the cleats. When results from both cleat widths were compared during the investigation into three dimensional end effects, sinkage was shown to be proportional to nominal pressure beneath the cleats. Cleats that did not sink on initial vertical loading, due to a large base surface area (experiments 1 and 5) produced little traction. Sinkage, however, increased during slip, this was clearly observed and confirmed when initial sinkage on loading results were compared to sinkage after slip.

During the traction distribution investigation a Perspex sided cleat and a cleat length of *4d* were both used to simulate two dimensional soil behaviour. Results for both were very similar. Approximately 76% of the total traction was obtained from in between and beneath and the cleats, and the cleat sides, 25% from the front of the front cleat (passive earth force) and 3% opposing traction behind the rear cleats (active earth force). A 2% error was produced in totalling individual load contributions. It was initially expected that the majority of traction would be produced from soil heaved up in front of the front cleat but this was shown clearly not to be the case.

Taguchi's statistical analysis tools have been applied to the results of the eight full factorial experiments. The analysis of variance (ANOVA) has been used to determine the variability of the experimental data and hence the confidence that can be attributed to the results. ANOVA has determined the significance of the main effects, cleat height, h, width, b, and taper, T, and of the interaction effects $(h \times b)$, $(h \times T)$ and $(T \times b)$ on traction. The significance of the effects of b, T and h, on traction, in terms of percentage contributions, are 56.98%, 24.02% and 2.09%

respectively. Cleat width was found to be the most important factor for maximising traction, whereas cleat height has only a small effect. The influence of one factor upon another factor, in other words interaction between factors, was confirmed present. Interactions *(h × b)*, *(T × b)* and *(h × T)* are 4.71%, 8.19% and 0.74% respectively. The strong interaction between b and T shows that the effect of cleat width can be optimised when taper is present. Since the interaction ($h \times b$) is greater than the effect of h itself, cleat height should be set to level h_1 to maximise the effect of cleat width b. The optimum factor levels, were cleat height at level h_1 ($h = d$), cleat width at level b_2 ($b = d/2$) and cleat taper at level T_2 (tapered), which corresponds to experiment 4 with the highest traction result.

9.4 Comparison of Experimental and Modelling Results

The experiments to investigate the effects of cleat height, width and taper were simulated in MATLAB using the total traction model, developed from triangular and quadrilateral shear zone models. The initial sinkage, vertical load, cleat geometry and cleat and soil friction properties were input into the model so that the full and partially full sinkage conditions could be modelled and the experimental and theoretical results compared. The traction distribution experiments were also simulated using the total traction model. Since full sinkage was induced, the applied vertical load was applied to the sand between and beneath the cleats. The various contributions to the total traction force were obtained from the computer models and compared to experimental results.

When the eight full factorial experiments were modelled as partially full, the rank order in terms of traction performance was seen to be the same as that of the experimental results with the exception of experiments 2 and 6. The passive earth resistance at the front produced 9% and 4% of total traction for tapered and non tapered cleats respectively, with the active earth force at the rear, opposing traction, being 0.6% for both tapered and non tapered cleats. Generally, total traction, including passive and active earth forces, was seen to increase with sinkage. Experiment 4 ($h = d$, $b = d/2$ and tapered) produced significantly more traction than the other cleats in line with the experimental results.

The shear angles for the triangular passive and active shear zones were independent of sinkage, whereas the shear angles for the interacting passive and active quadrilateral shear zones were dependent on sinkage, although it was not possible to determine any trends.

The magnitudes of the theoretical total traction force results, for partially full cleats, were lower than the experimental values (69N to 88N compared to 80N-231N). This was thought to be due to the underestimation of the passive earth force in front of the front cleat due to the build up soil at the front of the test piece during slip, which was not considered in the model.

The eight full factorial experiments were then modelled as full. The rank orders, in terms of net traction force, for experimental and theoretical results were the same with the exception of experiment 6. The traction produced by the passive earth resistance at the front was an average of 4% of total traction for non tapered cleats and 6% for tapered cleats. The active earth force at the rear opposing traction was an average of 0.36% for both tapered cleats and non tapered cleats.

Total traction was seen to significantly increase for the full sinkage condition due to the loading of the soil in between the cleats. Although most cleats did not actually achieve full sinkage experimentally, with the exception of experiments 6, 7 and 8, the magnitude of the total traction force for full cleats remains low when compared to experimental results (125N to 189N compared to 111N to 231N) due to the model neglecting soil build up during slip and hence underestimating the passive earth force at the front. It was also thought that the assumptions made by Coulomb, including the assumption of plane failure (triangular and quadrilateral shear zones), could contribute to the error. Although the practical experiments produced repeatable results, the effects of experimental error on the comparison of results must also be considered.

The shear angles for both passive and active triangular shear zones remained unchanged from the partially full condition, for all cases. For the interacting quadrilateral zones approximately horizontal shear occurred.

Generally, in both the experimental and theoretical results, greater sinkage was shown to increase traction performance. All components of the total traction force were seen to increase with greater sinkage. Full sinkage was seen to be the major factor in maximising traction in both the experimental and modelling results. The geometric factors of taper, smaller cleat width and greater cleat height were all seen to increase sinkage and hence traction, but also increased traction independently of sinkage in both the experimental and modelling work. The full model showed increases in traction attributed to factors cleat height, cleat taper and cleat width by 6%, up to 16% and 28% respectively. This supports the order of importance indicated by applying ANOVA to the experimental results.

The traction distribution was also compared for both experimental and modelling results. The non tapered cleat of height $h = d$, width $b = d/2$ and length $l = 4d$ was used, thus representing a two dimensional problem. The contribution to traction from beneath and in between the cleats was 92.1% for the mathematical model compared to 76.0% for the experiment. The contribution to traction from the passive earth force in front of the front cleat was 8.4% for the mathematical model and 23.4% for the experiment. The active force opposed to traction from behind the rear cleat was 0.4% for the mathematical model and 1.1% for the experiment. This again demonstrates that the model underestimates the passive earth force, reducing the magnitude of the total traction force and altering the percentage contributions.

Although an empirical sinkage model based on cleat geometry, load and sinkage could not be established due to the scatter of the eight full factorial experimental data, during the experiments to determine three dimensional effects using non tapered cleats of length $l = 4d$, height $h = d$, and width $b = d/2$ and $b = d$, sinkage was seen to be proportional to nominal pressure beneath the cleats.

9.5 Future Work

This research has provided useful background information for DCTA on foot-ground interaction, and a platform from which to build since little work has previously been carried out in this area. Modelling tools have been presented and a

soft ground slip-rig developed. However, there are interesting and important possibilities for future work.

9.5.1 Slip-Rig Improvements

Having used the slip-rig, a number of improvements may be suggested. Currently, the contact angle between the cleat assembly (or boot) and the ground is determined by the rotation of the cross bar, which leads to an undesirable bending moment being applied to the loading pole, especially with a large vertical load applied. It is therefore recommended that the angle adjustment be provided at the cleat or boot mounting at the end of the loading pole, so that the loading pole remains vertical at all times.

9.5.2 Mathematical Modelling

It is recommended that the mathematical modelling be further developed using finite element techniques. In reality, failure probably occurs along curved shear surfaces and not flat planes as assumed by Coulomb, and therefore the shear zones may not be triangular or quadrilateral. By using a finite element approach the true nature of soil shear could be established.

Although the difficulty of modelling sinkage has been demonstrated, a sinkage model is necessary to enable a full understanding of the interaction between footwear and soft ground. The input of actual experimental data would then not be required and increasing sinkage during slip could be modelled.

The mathematical modelling presented in this thesis has been two dimensional, however, three dimensional effects including flow of soil around the sides of cleats and the build up of soil during slip must now be considered. Cleat design could then utilise the three dimensional effects of soil flow to obtain optimal traction, which should aim to maximise the soldier performance, whilst minimising the risk of injury.

The research project that has followed on from this work is based upon finite element analysis, further developing the soil mechanics theory that has been reported.

9.5.3 Future Experimental Investigations

The experimental work to date has been based on wooden cleats on sand. Experimenting with clay and mud would be useful to validate the theoretical models for use with cohesive soils, however, routine measurement of soil parameters would be required because of their variability with any soil other than dry sand. Further testing procedures would need to be developed.

The use of scaled up plastic cleats would enable the investigation of adhesion, cleat flexibility and mud shedding.

Having investigated cleat geometry and traction distribution, it would seem logical to develop this further by investigating the effects of cleat configurations (tread patterns) on traction for different soils.

Appendix I

1. Soft Ground Slip-Rig Main Frame and Soil Tray Dimensions

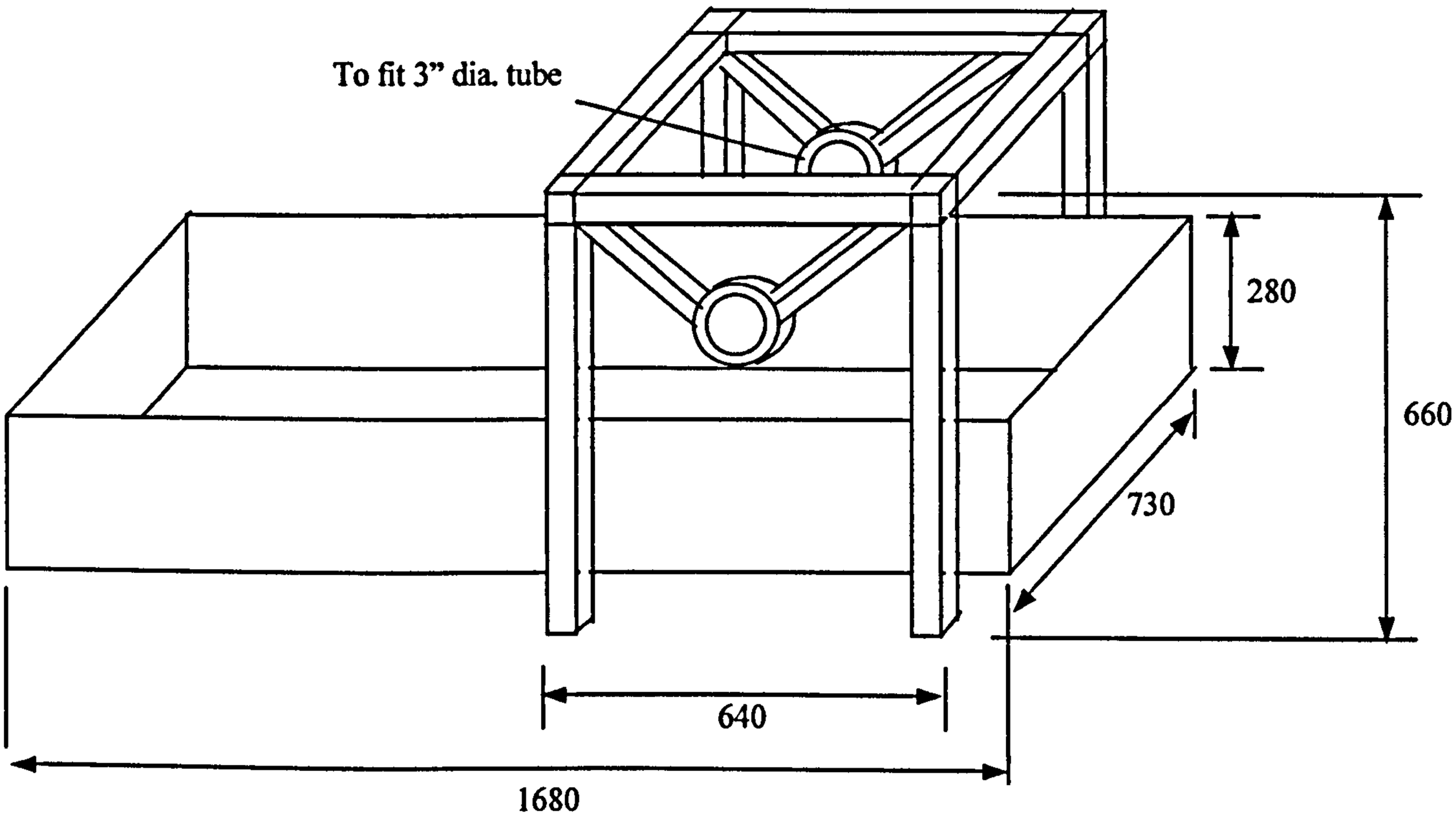

All dimensions in mm.
Drawing approximately to scale

2. Bearing Shaft / Shoe Last Attachment

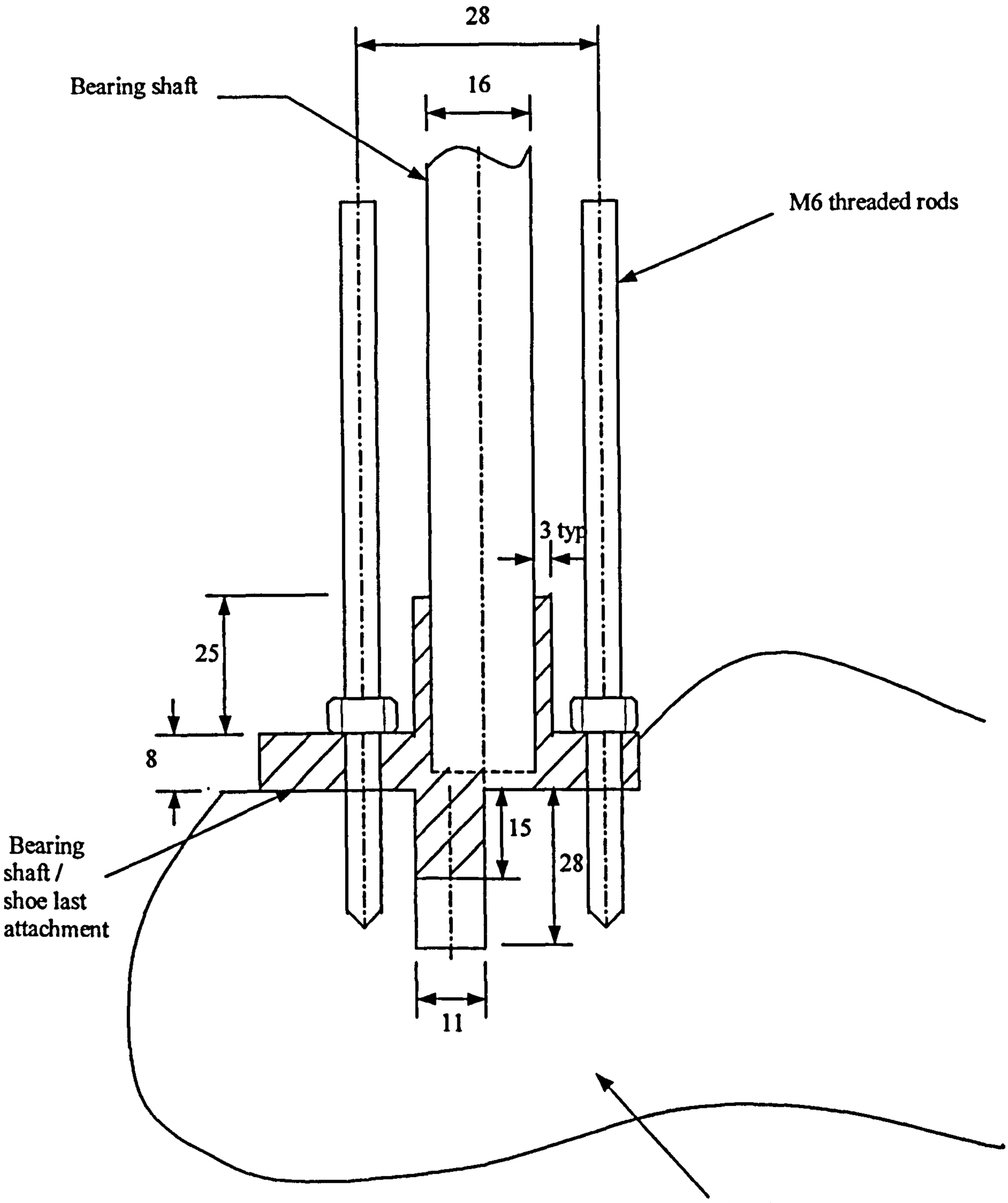

All dimensions in mm.
Drawing approximately to scale

3. Shoe Last Attachment

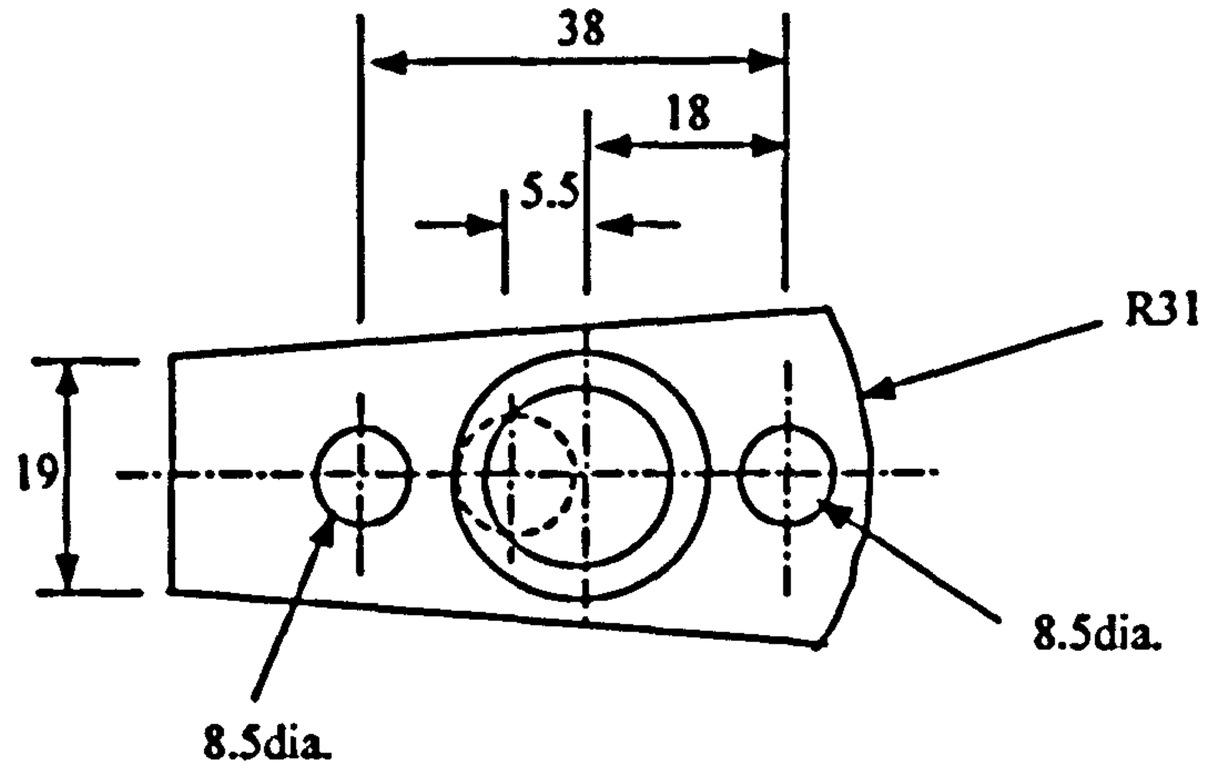

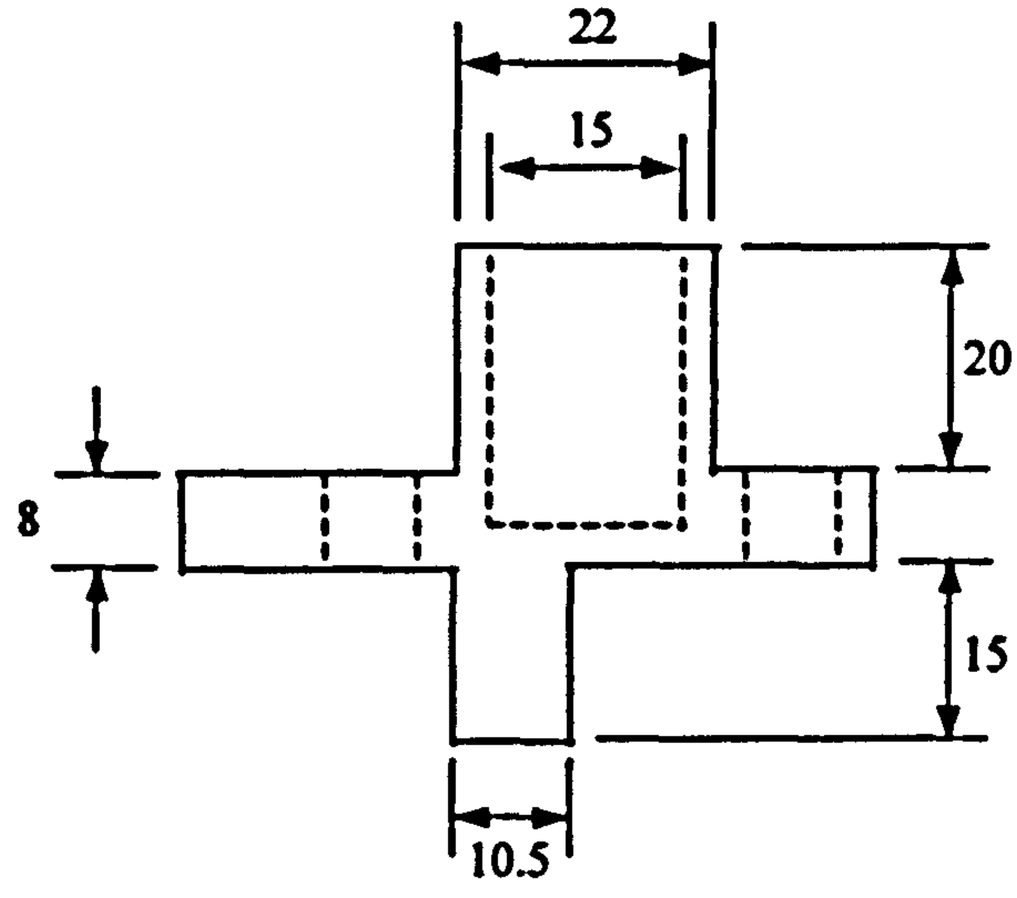

All dimensions in mm.
Drawing approximately to scale

4. Linear Bearing Assembly

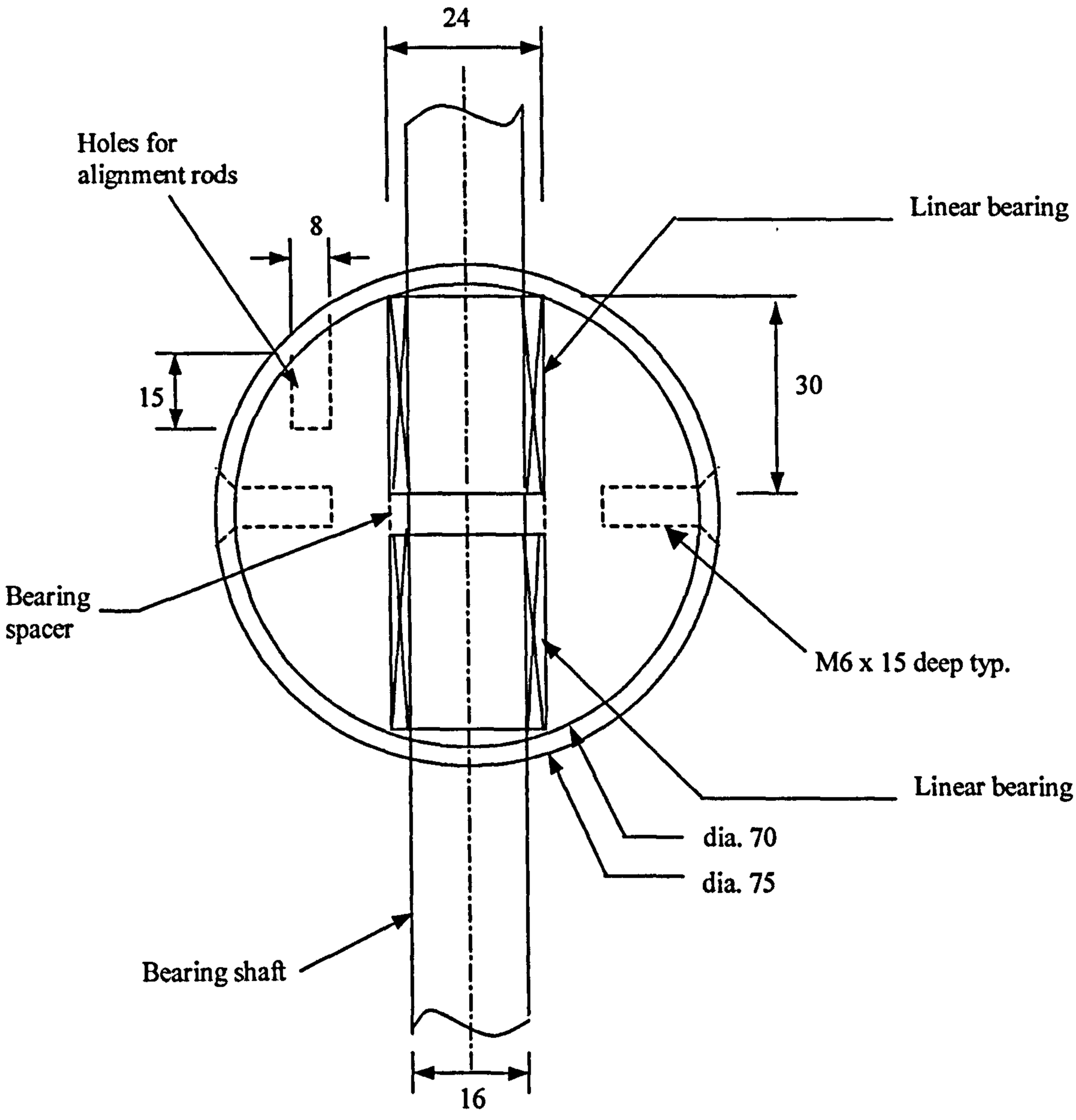

All dimensions in mm.
Drawing approximately to scale

5. Bearing Assembly and Vertical Alignment Rod Holes

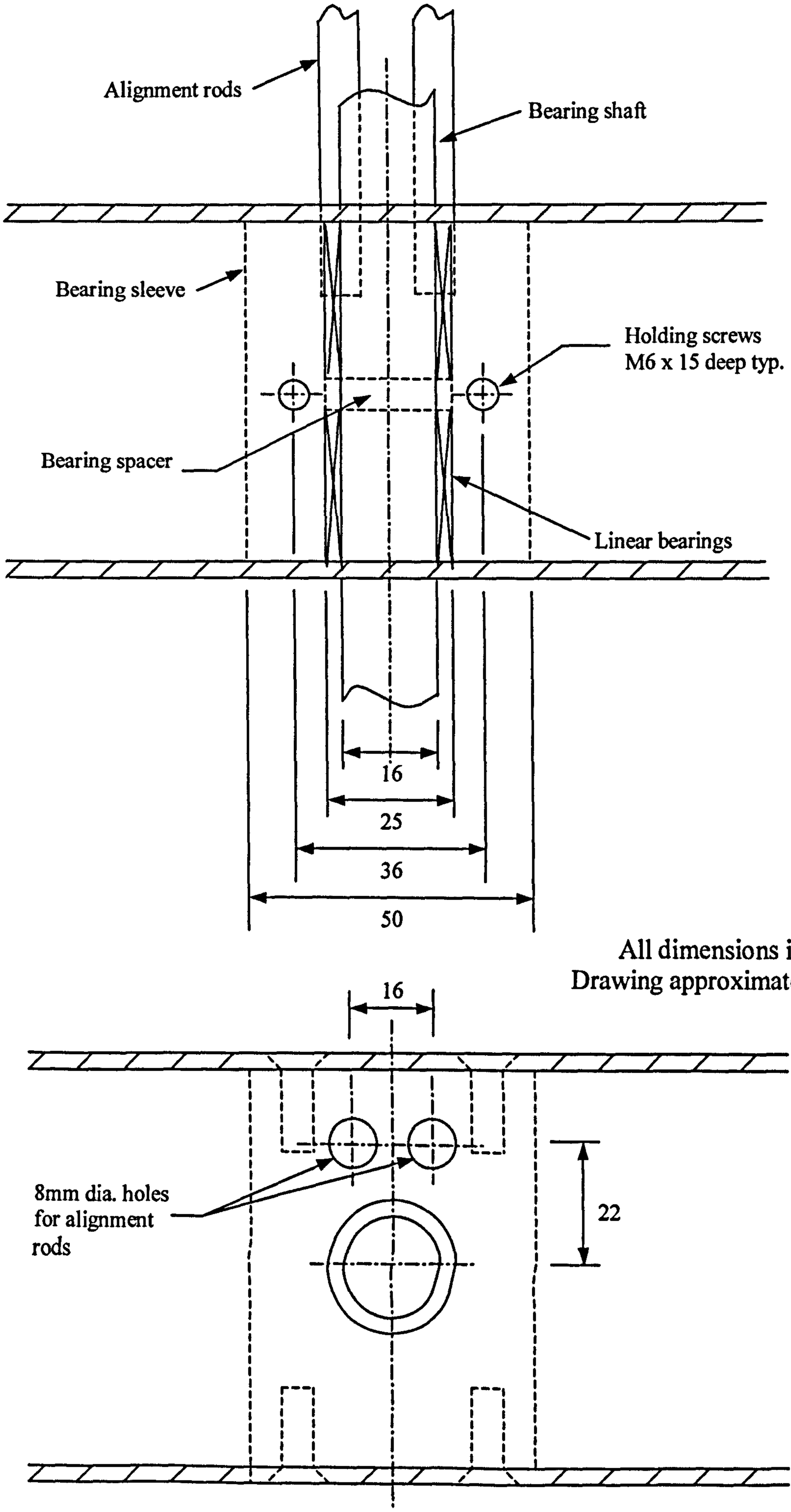

6. Alignment Rods and Brace

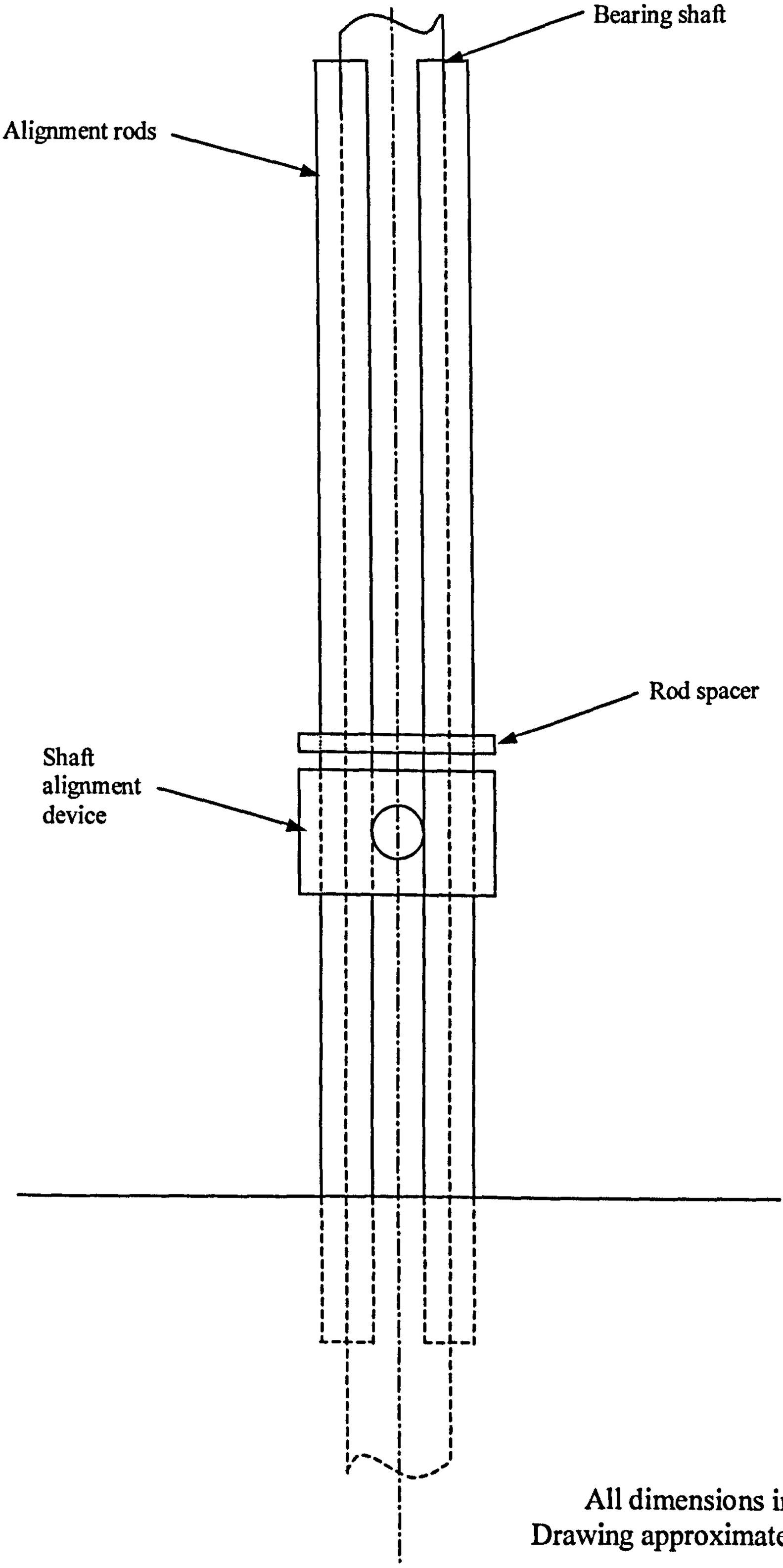

All dimensions in mm.
Drawing approximately to scale

7. Shaft Alignment Device and Rod Spacer

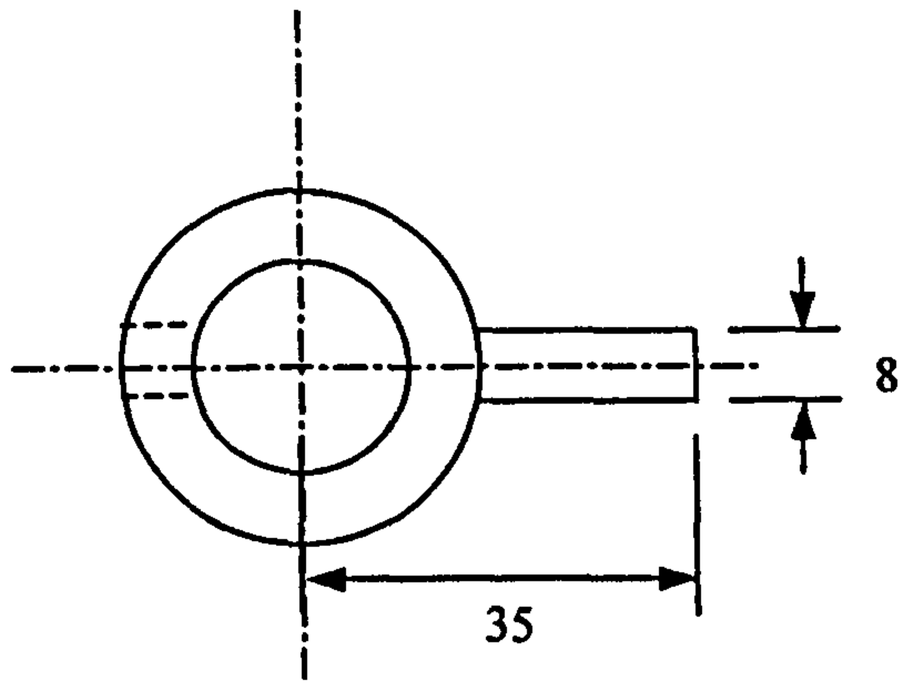

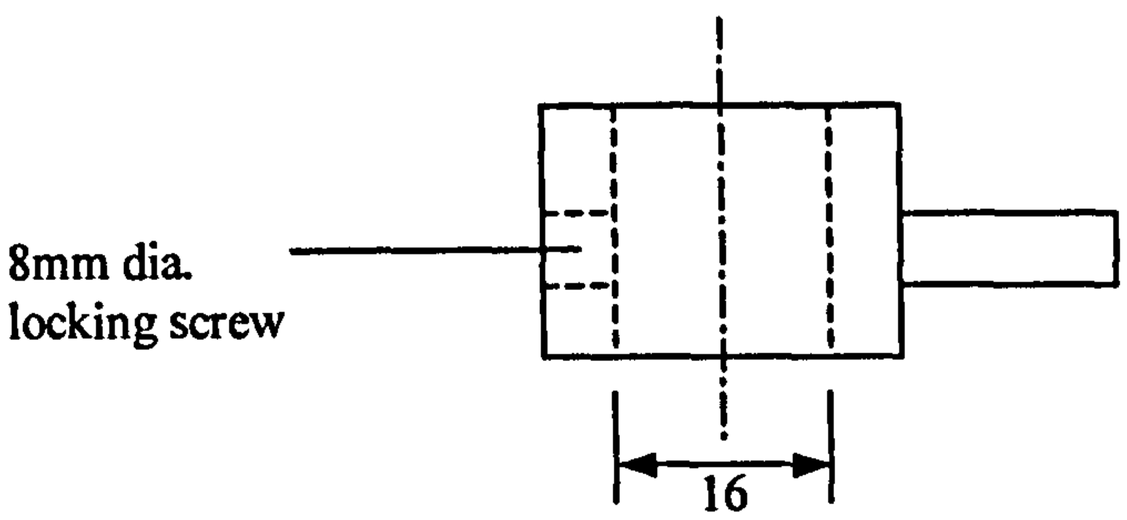

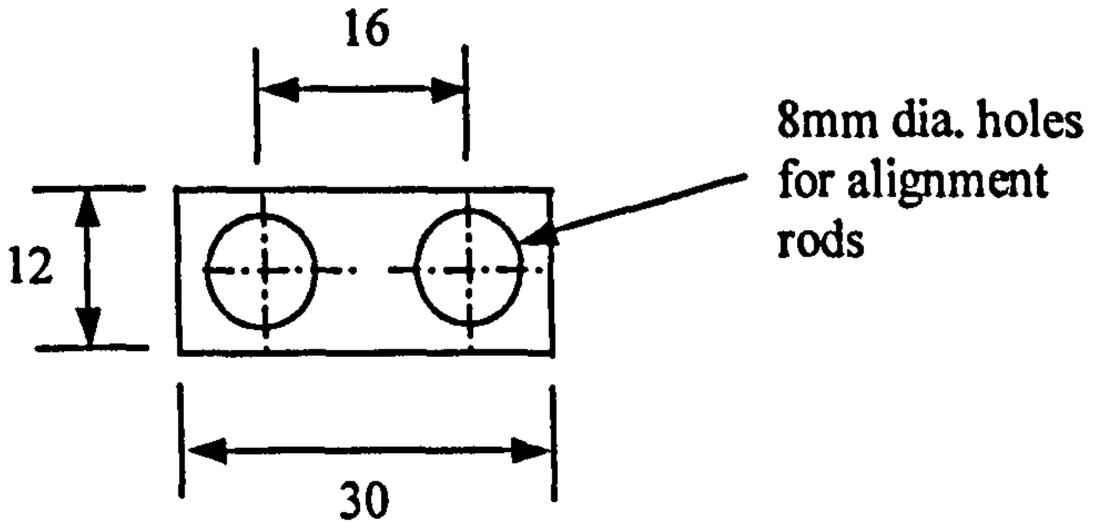

All dimensions in mm.
Drawings approximately to scale

Appendix II

Preliminary Experimental Results

Cleat Type	Vertical Load (kg)	Initial Sinkage (mm)	Sinkage (mm) Front	Sinkage (mm) Rear	Slip Distance (mm)	Horizontal Load (kg)
b × d × h (no taper)	10	22	45	43	47	5.5
b × d × h (no taper)	10	23	43	43	53	5.0
b × d × h (no taper)	10	23	43	45	49	4.5
b × d × h (no taper)	5	7	26	34	42	3.5
b × d × h (no taper)	5	7	42	40	49	4.0
b × d × h (no taper)	5	13	35	32	34	3.5
b × 3d × h (no taper)	20	1.5	25	23	24	5.5
b × 3d × h (no taper)	20	1.5	25	10	20	6.0
b × 3d × h (no taper)	20	1.5	25	16	20	6.0
b × 5d × h (no taper)	20	0.5	27	19	35	7.0
b × 5d × h (no taper)	20	0.5	16	17	21	6.0
b × 5d × h (no taper)	20	0.5	27	23	24	6.5

Table 1: Results of initial tests on unprepared sand (vertical shaft)

Cleat Type	Vertical Load (kg)	Initial Sinkage (mm)	Rear Sinkage (mm)		Front Sinkage (mm)		Slip Distance (mm)	horizontal Load (kg)
			actual	flow	actual	flow		
b × d × h (no taper)	20	27	43	45	44	46	43	6.5
b × d × h (no taper)	20	32	42	44	44	47	44	6.5
b × d × h (no taper)	20	32	43	46	45	48	43	6.0
b × d × h/2 (no taper)	20	18	35	35	32	38	37	7.0
b × d × h/2 (no taper)	20	2	32	38	39	42	40	8.0
b × d × h/2 (no taper)	20	2	45	41	42	44	45	8.0
b × 3d × h (no taper)	20	0.5	26	22	21	16	31	5.5
b × 3d × h (no taper)	20	0.5	30	32	24	17	49	6.4*
b × 3d × h (no taper)	20	0.5	24	25	19	22	49	6.8*
b × 5d × h (no taper)	20	0.5	20	26	24	32	84	10.0
b × 5d × h (no taper)	20	0.5	13	16	19	34	69	10.0
b × 5d × h (no taper)	20	0.5	18	19	18	30	70	9.5
b × d × h (taper)	20	26	36	39	40	44	29	7.0
b × d × h (taper)	20	29	41	43	45	47	22	8.0
b × d × h (taper)	20	28	42	44	43	47	33	8.0
b/2 × d × h (no taper)	20	43	54	61	54	59	33	10.5
b/2 × d × h (no taper)	20	43	58	64	58	63	34	10.0
b/2 × d × h (no taper)	20	43	45	55	46	52	32	10.5

*Density exceeding acceptable range

Table 2: Initial results of tests on prepared sand

Appendix III

Program Flow Chart For Interacting Quadrilateral Shear Zones

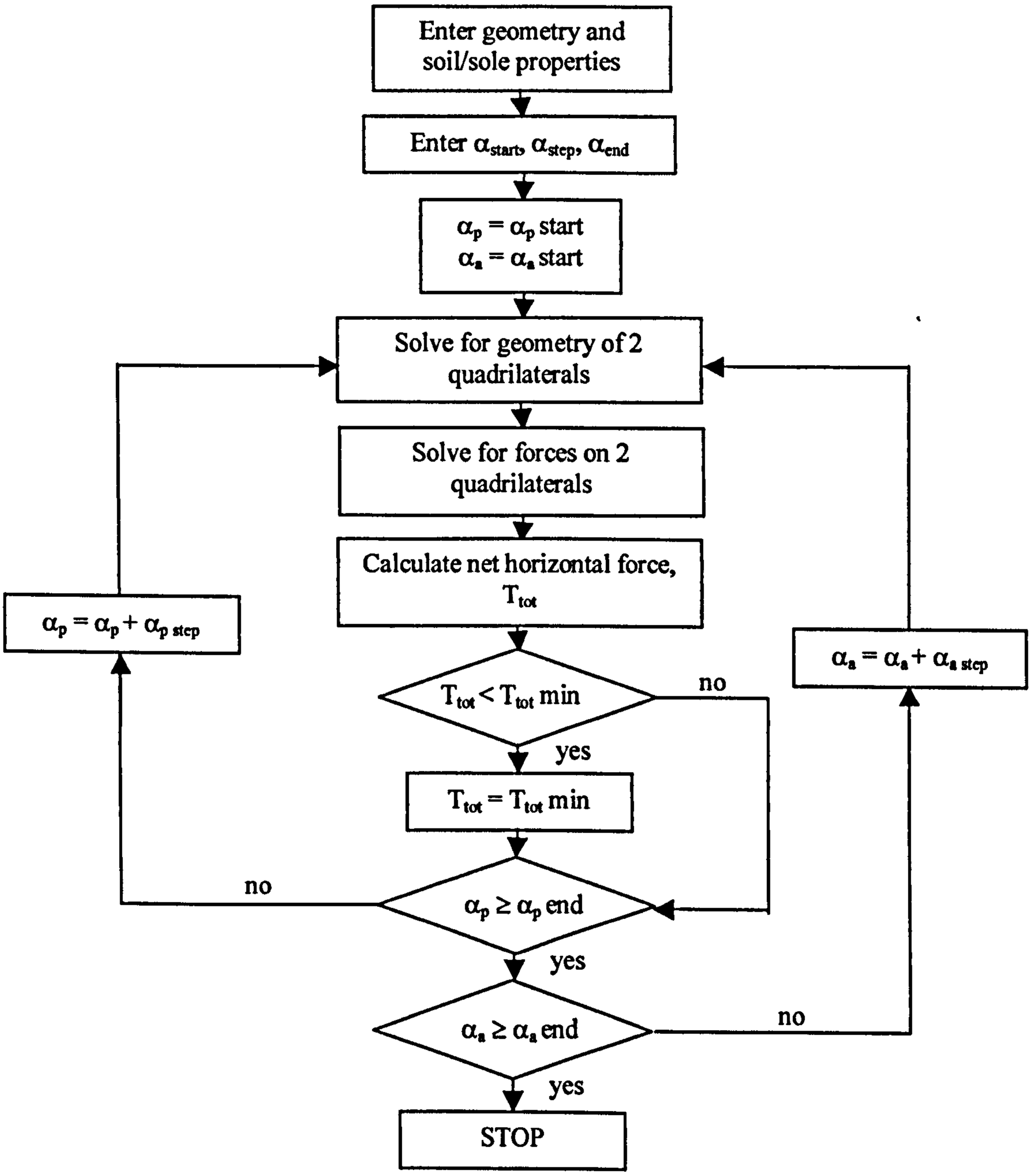

Appendix IV

F Table: $F_{.10}(f_1,f_2)$, 90% Confidence

f_1 = Number of degrees of freedom of numerator
f_2 = Number of degrees of freedom of denominator

f_2 \ f_1	1	2	3	4	5	6	7	8	9	10	12	15	20	24	30	40	60	120	∞
1	39.864	49.500	53.593	55.833	57.241	58.204	58.906	59.439	59.858	60.195	60.705	61.220	61.740	62.002	62.265	62.529	62.794	63.061	63.328
2	8.5263	9.0000	9.1618	9.2434	9.2926	9.3255	9.3491	9.3668	9.3805	9.3916	9.4081	9.4247	9.4413	9.4496	9.4579	9.4663	9.4746	9.4829	9.4913
3	5.5383	5.4624	5.3908	5.3427	5.3092	5.2847	5.2662	5.2517	5.2400	5.2304	5.2156	5.2003	5.1845	5.1764	5.1681	5.1597	5.1512	5.1425	5.1337
4	4.5448	4.3246	4.1908	4.1073	4.0506	4.0098	3.9790	3.9549	3.9357	3.9199	3.8955	3.8689	3.8443	3.8310	3.8174	3.8036	3.7986	3.7753	3.7607
5	4.0604	3.7797	3.6195	3.5202	3.4530	3.4045	3.3679	3.3393	3.3163	3.2974	3.2682	3.2380	3.2067	3.1905	3.1741	3.1573	3.1402	3.1228	3.1050
6	3.7760	3.4633	3.2888	3.1808	3.1075	3.0546	3.0145	2.9830	2.9577	2.9369	2.9047	2.8712	2.8363	2.8183	2.8000	2.7812	2.7620	2.7423	2.7222
7	3.5894	3.2574	3.0741	2.9605	2.8833	2.8274	2.7849	2.7516	2.7247	2.7025	2.6681	2.6322	2.5947	2.5723	2.5555	2.5351	2.5142	2.4928	2.4708
8	3.4579	3.1131	2.9238	2.8064	2.7265	2.6683	2.6241	2.5893	2.5612	2.5380	2.5020	2.4642	2.4246	2.4041	2.3830	2.3614	2.3391	2.3162	2.2926
9	3.3603	3.0065	2.8129	2.6927	2.6106	2.5509	2.5053	2.4694	2.4403	2.4163	2.3789	2.3396	2.2983	2.2768	2.2547	2.2320	2.2085	2.1843	2.1592
10	3.2850	2.9245	2.7277	2.6053	2.5216	2.4606	2.4140	2.3772	2.3473	2.3226	2.2841	2.2435	2.2007	2.1784	2.1554	2.1317	2.1072	2.0818	2.0554
11	3.2252	2.8595	2.6602	2.5362	2.4512	2.3981	2.3416	2.3040	2.2735	2.2482	2.2087	2.1671	2.1230	2.1000	2.0762	2.0516	2.0261	1.9997	1.9721
12	3.1765	2.8068	2.6055	2.4801	2.3940	2.3310	2.2828	2.2446	2.2135	2.1878	2.1474	2.1049	2.0597	2.0360	2.0115	1.9861	1.9597	1.9323	1.9036
13	3.1362	2.7632	2.5603	2.4337	2.3467	2.2830	2.2341	2.1953	2.1638	2.1376	2.0966	2.0532	2.0070	1.9827	1.9576	1.9315	1.9043	1.8759	1.8462
14	3.1022	2.7265	2.5222	2.3947	2.3059	2.2426	2.1931	2.1539	2.1220	2.0954	2.0537	2.0095	1.9625	1.9377	1.9119	1.8852	1.8572	1.8280	1.7973
15	3.0732	2.6952	2.4898	2.3614	2.2730	2.2081	2.1582	2.1185	2.0862	2.0593	2.0171	1.9722	1.9243	1.8990	1.8728	1.8454	1.8168	1.7867	1.7551
16	3.0481	2.6682	2.4618	2.3327	2.2438	2.1783	2.1280	2.0880	2.0553	2.0281	1.9854	1.9399	1.8913	1.8656	1.8388	1.8108	1.7816	1.7507	1.7182
17	3.0262	2.6446	2.4374	2.3077	2.2183	2.1524	2.1017	2.0613	2.0284	2.0009	1.9577	1.9117	1.8624	1.8362	1.8090	1.7805	1.7506	1.7191	1.6856
18	3.0070	2.6239	2.4160	2.2858	2.1958	2.1296	2.0785	2.0379	2.0047	1.9770	1.9333	1.8868	1.8368	1.8103	1.7827	1.7537	1.7232	1.6910	1.6567
19	2.9899	2.6056	2.3970	2.2663	2.1760	2.1094	2.0580	2.0171	1.9836	1.9557	1.9117	1.8647	1.8142	1.7873	1.7592	1.7298	1.6988	1.6659	1.6308
20	2.9747	2.5893	2.3801	2.2489	2.1582	2.0913	2.0397	1.9985	1.9649	1.9367	1.8924	1.8449	1.7938	1.7667	1.7382	1.7083	1.6769	1.6433	1.6074
21	2.9609	2.5746	2.3549	2.2333	2.1423	2.0751	2.0232	1.9819	1.9480	1.9197	1.8750	1.8272	1.7756	1.7481	1.7193	1.6890	1.6569	1.6228	1.5862
22	2.9486	2.5613	2.3512	2.2193	2.1279	2.0605	2.0084	1.9668	1.9327	1.9043	1.8503	1.8111	1.7590	1.7312	1.7021	1.6714	1.6389	1.6042	1.5668
23	2.9374	2.5493	2.3387	2.2065	2.1149	2.0472	1.9949	1.9531	1.9189	1.8903	1.8450	1.7964	1.7439	1.7159	1.6864	1.6554	1.6224	1.5871	1.5490
24	2.9271	2.5383	2.3274	2.1949	2.1030	2.0351	1.9826	1.9407	1.9063	1.8775	1.8319	1.7831	1.7302	1.7019	1.6721	1.6407	1.6073	1.5715	1.5327
25	2.9177	2.5283	2.3170	2.1843	2.0922	2.0241	1.9714	1.9292	1.8947	1.8548	1.8200	1.7708	1.7175	1.6890	1.6589	1.6272	1.5934	1.5570	1.5176
26	2.9091	2.5191	2.3075	2.1745	2.0822	2.0139	1.9610	1.9188	1.8841	1.8550	1.8090	1.7596	1.7059	1.6771	1.6468	1.6147	1.5805	1.5437	1.5036
27	2.9012	2.5106	2.2987	2.1655	2.0730	2.0045	1.9515	1.9091	1.8743	1.8451	1.7989	1.7492	1.6951	1.6662	1.6356	1.6032	1.5687	1.5313	1.4906
28	2.8939	2.5028	2.2906	2.1571	2.0645	1.9959	1.9427	1.9001	1.8652	1.8359	1.7895	1.7395	1.6852	1.6560	1.6252	1.5925	1.5575	1.5198	1.4784
29	2.8871	2.4955	2.2831	2.1494	2.0566	1.9678	1.9345	1.8918	1.8560	1.8274	1.7808	1.7306	1.6759	1.6465	1.6155	1.5825	1.5472	1.5090	1.4670
30	2.8807	2.4887	2.2761	2.1422	2.0492	1.9803	1.9269	1.8841	1.8498	1.8195	1.7727	1.7223	1.6673	1.6377	1.6065	1.5732	1.5376	1.4989	1.4564
40	2.8354	2.4404	2.2261	2.0909	1.9968	1.9269	1.8725	1.8289	1.7929	1.7627	1.7146	1.6624	1.6052	1.5741	1.5411	1.5056	1.4672	1.4248	1.3769
60	2.7914	2.3932	2.1774	2.0410	1.9457	1.8747	1.8194	1.7748	1.7380	1.7070	1.6574	1.6034	1.5435	1.5107	1.4755	1.4373	1.3952	1.3476	1.2915
120	2.7478	2.3473	2.1300	1.9923	1.8959	1.8238	1.7675	1.7220	1.6843	1.6524	1.6012	1.5450	1.4821	1.4472	1.4094	1.3676	1.3203	1.2646	1.1926
∞	2.7055	2.3026	2.0638	1.9449	1.8473	1.7741	1.7167	1.6702	1.6315	1.5987	1.5458	1.4871	1.4206	1.3832	1.3410	1.2951	1.2400	1.1686	1.0000

F Table: $F_{.01}(f_1,f_2)$, 99% Confidence

f_1 = Number of degrees of freedom of numerator
f_2 = Number of degrees of freedom of denominator

f_2 \ f_1	1	2	3	4	5	6	7	8	9	10	12	15	20	24	30	40	80	120	∞
1	4052.2	4999.5	5403.3	5624.6	5763.7	5859.0	5928.3	5981.6	6022.5	6055.8	6106.3	6157.3	6208.7	6234.6	6260.7	6286.8	6313.0	6339.4	6366.0
2	98.503	99.000	99.166	99.249	99.299	99.332	99.356	99.374	99.388	99.399	99.415	99.432	99.449	99.458	99.466	99.474	99.483	99.491	99.501
3	34.116	30.817	29.457	28.710	28.237	27.911	27.672	27.489	27.345	27.229	27.052	26.872	26.690	26.598	26.505	26.411	26.316	26.221	26.125
4	21.198	18.000	16.694	15.977	15.522	15.207	14.986	14.799	14.659	14.546	14.374	14.198	14.020	13.929	13.838	13.745	13.652	13.558	13.463
5	16.258	13.274	12.060	11.392	10.967	10.672	10.456	10.289	10.158	10.051	9.8883	9.7222	9.5527	9.4665	9.3793	9.2912	9.2020	9.1118	9.0204
6	13.745	10.925	9.7795	9.1483	8.7459	8.4661	8.2600	8.1016	7.9761	7.8741	7.7183	7.5590	7.3958	7.3127	7.2285	7.1432	7.0568	6.9690	6.8801
7	12.246	9.5466	8.4513	7.8467	7.4604	7.1914	6.9928	6.8401	6.7188	6.6201	6.4691	6.3143	6.1554	6.0743	5.9921	5.9084	5.8236	5.7372	5.6495
8	11.259	8.6491	7.5910	7.0060	6.6318	6.3707	6.1776	6.0289	5.9106	5.8143	5.6668	5.5151	5.3591	5.2793	5.1981	5.1156	5.0316	4.9460	4.8588
9	10.561	8.0215	6.9919	6.4221	6.0569	5.8018	5.6129	5.4671	5.3511	5.2565	5.1114	4.9621	4.8080	4.7290	4.6486	4.5667	4.4831	4.3978	4.3105
10	10.044	7.5584	6.5523	5.9943	5.6363	5.3858	5.2001	5.0567	4.9424	4.8402	4.7059	4.5582	4.4054	4.3269	4.2469	4.1653	4.0619	3.9965	3.9090
11	9.6460	7.2057	6.2167	5.6683	5.3160	5.0692	4.8861	4.7445	4.6315	4.5393	4.3974	4.2509	4.0990	4.0209	3.9411	3.8596	3.7761	3.6904	3.6025
12	9.3302	6.9266	5.9526	5.4119	5.0643	4.8206	4.6395	4.4994	4.3875	4.2961	4.1553	4.0096	3.8584	3.7805	3.7008	3.6192	3.5355	3.4494	3.3608
13	9.0738	6.7010	4.7394	5.2053	4.8616	4.6204	4.4410	4.3021	4.1911	4.1003	3.9603	3.8154	3.6646	3.5868	3.5070	3.4253	3.3413	3.2548	3.1654
14	8.8616	6.5149	5.5639	5.0354	4.6950	4.4558	4.2779	4.1399	4.0297	3.9394	3.8001	3.6557	3.5052	3.4274	3.3476	3.2656	3.1813	3.0942	3.0040
15	8.6831	6.3589	5.4170	4.8932	4.5556	4.3183	4.1415	4.0045	3.8948	3.8049	3.6662	3.5222	3.3719	3.2940	3.2141	3.1319	3.0471	2.9595	2.8684
16	8.5310	6.2262	4.2922	4.7726	4.4374	4.2016	4.0259	3.8896	3.7804	3.6909	3.5527	3.4089	3.2588	3.1808	3.1007	3.0182	2.9330	2.8447	2.7528
17	8.3997	6.1121	5.1850	4.5590	4.3359	4.1015	3.9267	3.7910	3.6822	3.5931	3.4552	3.3117	3.1615	3.0835	3.0032	2.9205	2.8348	2.7459	2.6530
18	8.2854	6.0129	4.0919	4.5790	4.2479	4.0146	3.8406	3.7054	3.5971	3.5082	3.3706	3.2273	3.0771	2.9990	2.9185	2.8354	2.7493	2.6597	2.5660
19	8.1850	5.9259	5.0103	4.5003	4.1708	3.9386	3.7653	3.6305	3.5225	3.4338	3.2965	3.1533	3.0031	2.9249	2.8442	2.7608	2.6742	2.5839	2.4893
20	8.0960	5.8489	4.9382	4.4307	4.1027	3.8714	3.6987	3.5644	3.4567	3.3682	3.2311	3.0880	2.9377	2.8594	2.7785	2.6947	2.6077	2.5168	2.4212
21	8.0166	5.7804	4.8740	4.3688	4.0421	3.8117	3.6396	3.5056	3.3981	3.3098	3.1729	3.0299	2.8976	2.8011	2.7200	2.6359	2.5484	2.4568	2.3603
22	7.9454	5.7190	4.8166	4.3134	3.9880	3.7583	3.5867	3.4530	3.3458	3.2576	3.1209	2.9780	2.8274	2.7488	2.6675	2.5831	2.4951	2.4029	2.3055
23	7.8811	5.6637	4.7649	4.2635	3.9392	3.7102	3.5390	3.4057	3.2986	3.2106	3.0740	2.9311	2.7805	2.7017	2.6202	2.5355	2.4471	2.3542	2.2559
24	7.8229	5.6136	4.7181	4.2184	3.8951	3.6667	3.4959	3.3629	3.2560	3.1681	3.0316	2.8887	2.7380	2.6591	2.5773	2.4923	2.4035	2.3099	2.2107
25	7.7698	55.680	4.6755	4.1774	3.8550	3.6272	3.4568	3.3239	3.2172	3.1294	2.9931	2.8502	2.6993	2.6203	2.5383	2.4530	2.3637	2.2695	2.1694
26	7.7213	5.5263	4.6366	4.1400	3.8183	3.5911	3.4210	3.2884	3.1818	3.0941	2.9579	2.8150	2.6640	2.5848	2.5026	2.4170	2.3273	2.2325	2.1315
27	7.6767	5.4881	4.6009	4.1056	3.7848	3.5580	3.3882	3.2558	3.1494	3.0618	2.9256	2.7827	2.6316	2.5522	2.4699	2.3840	2.2938	2.1984	2.0965
28	7.6356	5.4529	4.5681	4.0740	3.7539	3.5276	3.3581	3.2259	3.1195	3.0320	2.8959	2.7530	2.6017	2.5223	2.4397	2.3535	2.2529	2.1670	2.0642
29	7.5976	5.4205	4.5378	4.0449	3.7254	3.4995	3.3302	3.1982	3.0920	3.0045	2.8685	2.7256	2.5742	2.4946	2.4118	2.3253	2.2344	2.1378	2.0342
30	7.5625	5.3904	4.5097	4.0179	3.6990	3.4735	3.3045	3.1726	3.0665	2.9791	2.8431	2.7002	2.5487	2.4589	2.3860	2.2992	2.2079	2.1107	2.0062
40	7.3141	5.1785	4.3126	3.8283	3.5138	3.2910	3.1238	2.9930	2.8876	2.8005	2.6649	2.5216	2.3689	2.2880	2.2034	2.1142	2.0194	1.9172	1.8047
60	7.0771	4.9774	4.1259	3.6591	3.3389	3.1187	2.9530	2.8233	2.7185	2.6318	2.4961	2.3523	2.1978	2.1154	2.0285	1.9360	1.8363	1.7263	1.6006
120	6.8510	4.7865	3.9493	3.4706	3.1735	2.9559	2.7918	2.6629	2.5586	2.4721	2.3363	2.1915	2.0346	1.9500	1.8600	1.7629	1.6557	1.5330	1.3805
∞	6.6349	4.6052	3.7816	3.3192	3.0173	2.8020	2.6393	2.5113	2.4073	2.3209	2.1848	2.0385	1.8783	1.7908	1.6964	1.5923	1.4730	1.3246	1.0000

References

1. Inman, V.T., Ralston, H.J., & Todd, F. *Human Walking.* Baltimore: Williams & Wilkins (1981)

2. Rose, G. & Gamble, J.G. *Human Walking, 2nd Ed.* Baltimore: Williams & Wilkins (1984)

3. Whittle, M. W. *Gait Analysis: An introduction.* Butterworth-Helnemann Ltd. (1991)

4. Rodgers, M.M. Biomechanics of the foot. In *Current Issues in Biomechanics.* Edited by Grabiner, M.D. (1984)

5. Cavanagh, P.R. *The running shoe book.* Anderson World, Inc. (1980).

6. Frederick, E.C. *Sports shoes and playing surfaces.* Human Kinetics Publishers, Inc. (1984)

7. Nigg, B.M. *Biomechanics of running shoes.* Human Kinetics Publishers, Inc. (1986)

8. Craig, R.F. *Soil Mechanics*, 5th ed. Chapman & Hall, (1992)

9. Smith, G.N. & Smith, I.G.N. *Elements of soil mechanics,* 7th ed. Blackwell Science Ltd (1998)

10. Spangler, M.G. and Handy, L.H. *Soil Engineering*, 4th ed. Harper & Row, (1982)

11. Whitlow, R. *Basic Soil Mechanics*, Longman Scientific & Technical, (1990)

12. Zamparo, P., Perini, R., Sacher, M. & Ferretti, G. The energy cost of walking and running on sand. *Eur. J. Appl. Physiol.* Vol. 65, pp. 183-187 (1992)

13. Goldman, R.F. & Soule, R.G. Terrain coefficients for energy cost prediction. *J. Appl. Physiol.* Vol. 32 (5), pp. 706-708 (1972)

14. Pandolf, K.B., Haisman, M.F. & Goldman, R.F. Metabolic energy expenditure and terrain coefficients for walking on snow. *Ergonomics.* Vol. 19 (6), pp. 683-690 (1976)

15. Creagh, U., Reilly, T. and Lees, A. Kinematics of Running on Off-Road Terrain, *Erg.* Vol. 41 (7), pp. 1029-1033 (1998)

16. Manning, D.P., Jones, C. & Bruce, M. Improved slip resistance on oil from surface roughness of footwear. *Rubber Chemistry And Technology.* Vol. 56, pp. 703-717 (1983)

17. Nagy, P.V. Modelling walker/terrain interaction to achieve reliable, autonomous walking control. *Proc. IEEE Int. Conf. on Intelligent Control,* pp.202-207 (1993)

18. Caurin, G. & Tschichold-Gurman, N. The development of a robot terrain interaction system for walking machines. *Proc. IEEE Int. Conf. on Robotics and Automation,* pp.1013-1018 (1994)

19. Sakakibara, Y., Kan, K., Hosoda, Y., Hattori, M. & Fugie, M. Low-Impact foot trajectory for a quadruped walking machine. *Advanced Robotics,* Vol. 7 (4), pp. 343-360 (1993)

20. Brough, R., Malkin, F. & Harrison, R. Measurement of the coefficient of friction of floors. *J. Phys. D: Appl. Phys.* Vol. 12. pp. 517-528 (1979)

21. Malkin, F. & Harrison, R. A small mobile apparatus for measuring the coefficient of friction of floors. *J. Phys. D: Appl. Phys.* Vol. 13, pp. 77-79 (1980)

22. Childs, T.H.C. and Tabor, D. *Proc. Instn. Mech. Engrs.* Vol. 182 (3G), pp. 32. (1967)

23. Harper, F.C., Warlow, W.J. & Clarke, B.L. The forces applied to the floor by the foot in walking. (I. Walking on a level surface). *National Building Studies Research Paper 32.* (1961)

24. Harper, F.C., Warlow, W.J. & Clarke, B.L. The forces applied to the floor by the foot in walking. (II. Walking on a slope. III. Walking on stairs). *National Building Studies Research Paper 32.* (1967)

25. Wilson, M. Slip resistance performance of soling materials. *SATRA bulletin,* (May 1996)

26. Wilson, M. Slip resistance characteristics of footwear solings assessed using the SATRA friction tester. *American Society for Testing and Materials.* (1996)

27. Pooley, R.W. Measurement of frictional properties of footwear sole and heel materials. In *Walkway surfaces: Measurement of slip resistance.* ASTM STP 649 pp. 11-20 (1978)

28. Wilson, M. and Russel, B. Slip Resistance Assessment and Accident Prevention, *SATRA Bulletin,* (July/Aug. 1997)

29. Investigation Into the Effects of Sole Pattern on Wear Properties. *Schuh-Technik,* Vol. 10, pp. 1675-1681 (1970)

30. Perkins, P.J. Measurement of slip between the shoe and ground during walking. *Walkway Services: Measurement of slip resistance, Am. Soc. Testing Materials,* pp. 71-87 (1978)

31. Frederick, E.C. Optimal frictional properties for sports shoes and sports surfaces. *Proc. XI th Int. Soc. Biomechanics in Sports,* pp. 15-22 (1993)

32. Valiant, G.A. The effect of outsole pattern on basketball shoe traction. *III rd Int. Soc. Biomechanics in Sports,* pp. 29-37 (1987)

33. Rheinstein, D.J., Morehouse, C.A. & Niebel, B.W. Effects on traction of outsole composition and hardness of basketball shoes and three types of playing surfaces. *Med. Sci. Sports* Vol. 10 (4), pp. 282-288 (1978)

34. Nigg, B.M. & Segesser, B The influence of playing surfaces on the load on the load on the locomotor system and on football and tennis injuries. *Sports Medicine* Vol. 5 pp. 375-385 (1988)

35. Torg, J.S. & Quededfeld, T Effect of shoe type and cleat length on incidence and severity of knee injuries among high school football players. *Research Quarterly,* Vol. 42 pp. 203-211 (1971)

36. Van Gheluwe, B., Deporte, E. & Hebbelinck, M. Frictional forces and torques of soccer shoes on artificial turf. In: Nigg, B.M. & Kerr, B.A. (Eds.). Biomechanical aspects of sports shoes and playing surfaces. *Proc. Int. Symp. Biomechaincal Aspects of Sports Shoes and Playing Surfaces,* pp. 161-168 (1983)

37. Schlaepfer, F., Unold, E. & Nigg, B.M. The frictional characteristics of tennis shoes. In: Nigg, B.M. (Ed.): Biomechanics of Running Shoes, pp. 153-160, Human Kinetic Press (1986)

38. Bonstingl, R.W., Morehouse C.A. & Niebel, B.W. Torques developed by different types of shoes on various playing surfaces. *Med. Sci Sports,* Vol. 7 (2), pp. 127-131 (1975)

39. Nigg, B.M. & Yeadon, M.R. Biomechanical aspects of playing surfaces. *J. Sports Med.* Vol. 5, pp. 117-145 (1987)

40. Smith, N., Dyson, R. & Hale, T. The effects of sole configuration on ground reaction force measured on natural turf during soccer specific actions. *Science and Football VI,* pp. 44-49, Routledge (2002)

41. Valiant, G.A. Static friction characteristics of cleated outsole samples on Astroturf. *Med. Sci. Sports,* Vol. 17 (2), pp. 222-223 (1985)

42. Milburn, P.D. & Barry, E.B. Shoe-surface interaction and the reduction of injury in rugby union. *Sports Med.* Vol. 25 (5), pp. 319-327 (1998)

43. Frederick, E.C. Kinematically mediated effects of sports shoe design: A review. *J. Sports Sciences,* Vol. 4, pp. 169-184 (1986)

44. Ekstrand, J. & Nigg, B.M. Surface-related injuries in soccer. *Sports Med.* Vol. 8 (1), pp. 56-62 (1989)

45. Heidt Jr., R.S., Dormer, P.W., Cawley, P.W., Scranton, P.E., Losse, G. & Howard, M. Differences in friction and torsional resistances in athletic shoe-turf surface interfaces. *Am. J. Sports Med.* Vol. 24 (6), pp. 834-842 (1996)

46. Bowers Jr.,K.D. & Martin, R.B. Cleat-surface friction on new and old Astroturf. *Med. Sci. Sports,* Vol.7 (2), pp. 132-135 (1975)

47. Valiant. G.A. Ground reaction forces developed on artificial turf. In: Reilly, T. et al (Eds.) Science and Football, pp. 406-415 (1988)

48. Barry, E.B. & Milburn, P.D. A mechanism explaining traction of footwear on natural surfaces. *Proc. 4th Symp. Footwear Biomechanics,* pp. 22-23. (1999)

49. Barry, E.B. & Milburn, P.D. A footwear traction measuring device. *Proc. 4th Symp. Footwear Biomechanics,* pp. 20-21. (1999)

50. Wong, J.Y. *Terramechanics and off-road vehicles,* pp. 72-80. Elsevier (1989)

51. Barry, E.B. & Milburn, P.D. *Science and Football VI,* pp. 3-7, Routledge (2002)

52. Wong, J.Y. An introduction to terramechanics. *J. Terramechanics,* Vol. 21 (1), pp. 5-17, (1984)

53. Bekker, M.G. *Theory of land locomotion,* pp. 21-25. The university of Michigan Press (1956)

54. Bejune, D., David, J., Oullette, W., Zeilinski, B., Chen, N., Peura, B. & Norton, R.L. Design of a walking simulator. *Machine elements and machine dynamics,* 71, ASME Design Tech. Conf. (1994)

55. Wong, J.Y. Behaviour of soil beneath rigid wheels. *J. Agric. Engng. Res.*, Vol. 12 (4), pp. 257-269 (1967)

56. Wong, J.Y. & Reece, A.R. Soil failure beneath rigid wheels. *Proc.2nd Int. Conf. ISTV's,* pp. 425-445 (1966)

57. Wong, J.Y. Prediction of rigid wheel performance based on the analysis of soil-wheel stresses Part 1. Performance of driven rigid wheels." *J. Terramechanics,* Vol. 4 (1), pp. 81-98 (1967)

58. Onafeko, O. & Reece, A.R. Soil stresses and deformations beneath rigid wheels. *J. Terramechanics,* Vol. 4 (1), pp. 59-80 (1967)

59. Coulomb, C.A. Essai sur une Application des Regles des Maximis et Minimis a\ quelques Problemes de Statique Relatifis a\ l'Architecture, *Mem. acad. roy. pres. divers savants,* Paris, Vol. 7 (1776)

60. Terzaghi, K. *Theoretical soil mechanics*, New York (1943)

61. Terzaghi, K. Old earth pressure theories and new test results. *Engineering News Record*, Vol. 85, p. 632 (1920)

62. Terzaghi, K. and Peck, R.B. *Soil Mechanics in Engineering Practice*, 2nd Ed. Wiley, New York, (1967)

63. Muro, T. Tractive performance of a driven rigid wheel on soft ground based on the analysis of soil-wheel interaction. *J. Terramechanics,* Vol. 30 (5), pp. 351-369 (1993)

64. Foda, M. On the prediction of drawbar pull-normal slip relationship for a pneumatic tyre moving on soft soil. *J. Terramechaincs,* Vol. 28 (4), pp. 383-392 (1991)

65. Baladi, G.Y. & Rohani, B. Development of a soil-wheel interaction model, *Proc. 8th Int. Conf. ISTV's* (1984)

66. Mahmoud, M.M-A. & Dwyer, M.J. The effect of tyre-soil interface shape on the prediction of vehicle off-road performance. *Proc. 5th Euro. Conf. ISTV's* pp. 97-104 (1991)

67. Plackett, C.W. A review of force prediction methods for off-road wheels. *J. Agrig. Engng. Res.* Vol.31, pp. 1-29 (1985)

68. Shoop, S.A. *Terrain Characterisation for Trafficability*, U.S. Army Corps of Engs. (June 1993)

69. Dwyer, M.J., Okello, J.A. and Cottrell, F.B. The Effects of Various Design Parameters on the Tractive Performance of Rubber Tracks, *Proc. 5th Euro. Conf. ISTV's.* (1991)

70. Okello, J.A. A review and Selection of Soil Strength Characterisation techniques for the Prediction of Terrain Vehicle Performance, *J. Agric. Engng. Res.* Vol. 50 (2), (1991)

71. Bekker, M.G. *Off the road locomotion*, University of Michigan Press, (1960)

72. Caquot, A. and Kerisel, J. *Tables for the Calculation of Passive Pressure, Active Pressure and Bearing Capacity of Foundations*, Gauthier-Villars, Paris, 1948.

73. Sokolovski, V.V. *Statics of Granular Media*, Pergamon, Oxford, 1965.

74. Hansen, J.B. A revised extended formula for bearing capacity, *Danish Geotechnical Institute Bulletin*, No.28, 1968.

75. Meyerhof, G.G. Some recent research on the bearing capacity of foundations, *Canadian Geotechnical Journal*, Vol.1 (1), pp. 16-26, 1963.

76. Goriatchkin, B.P. et al, "*Teoria I proisvodstvo sielskohoziaynih mashin* (Theory and development of agricultural machinery), Moscow, (1936).

77. Burland, J.B. & Burbridge, M.C. Settlement foundations on sand and gravel. *Proc. Inst. Civil Engrs.* Vol. 78 (Dec), pp. 1325-81 (1985)

78. SATRA Footwear Technology Centre, *Physical Test Method PM144: Slip Resistance*, June 1992.

79. SATRA Footwear Technology Centre, *Notes On The Use of The SATRA Slip Resistance Test*, May 1997.

80. Bejune, B. et al, Design of a walking simulator, *Machine Elements and Machines Dynamics,* Vol. 71, pp. 463-468 (1994).

81. Pisani, R.M. & Howard, D., Foot-Ground Interaction, *Proc.Lower Limb Injuries 99,* pp. 33-38 (1999).

82. BS 1377: Part 8 (1990), *Methods of Test For Soils For Civil Engineering Purposes – Part 8: Shear strength tests (effective stress).*

83. BS 1377: Part 1 (1990), *Methods of Test For Soils For Civil Engineering Purposes – Part 1: General requirements and sample preparation.*

84. BS 1377: Part 4 (1990), *Methods of Test For Soils For Civil Engineering Purposes – Part 4: Compaction related tests.*

85. Ross, P.J. *Taguchi Techniques for Quality Engineering,* McGraw Hill (1988).

86. Roy, R.K. *A Primer on the Taguchi Method,* Van Nostrand Reinhold, New York, (1980).

Bibliography

Anon. *Code of practice for site investigation,* BS5930, British Standards Institution, London (1981).

Borowicka, H. Rearrangement of grains by shear tests with sand. *Proc. 8th Int. Conf. Soil Mech. Found. Engng. Moscow,* 1: pp71-77 (1973).

Casagrande, A. Classification and identification of soils, *Trans. A.S.C.E.,* Vol.113, pp901-992 (1948).

Conforth, D.H. Some experiments on the influence of strain conditions on the strength of sand, *Geotechnique,* 14: pp143-167 (1964).

Holtz, W.G. and Gibbs, H.J. Engineering properties of expansive clays. *Trans. A.S.C.E.,* 121: pp641-663 (1956).

Inman, V.T., Ralson, H.J. & Todd, F. (1981). *Human Walking.* Baltimore: Williams & Wilkins.

Nigg, B.M., Eberle, G., Frey, D., Luethi, S., Segesser, B. & Weber, B. (1978) Gait analysis and sports shoe construction. In Asmussen E, Jorgensen K (Eds.): *Biomechanics V1-A* pp303-309 Baltimore: University Park Press.

Rose, S. Footwear made for walking and hiking. *SATRA bulletin,* Sept. 1997.

Townsend, C. Fit for all seasons. *Gear.* (Date unknown).

Treibel, W. Mountaineering shoes-An overview. *Other athletic shoes,* pp 129-144.

Winter, D.A. Biomechanics of human movement. *John Wiley & Sons, Inc.* (1979)

Various information obtained from leading outdoor footwear manufacturers was also used.